THE PROCEEDINGS OF
THE PHYSICAL SOCIETY

Section B

VOL. 62, PART 11 1 November 1949 No. 359 B

# An Automatic Recording Apparatus for the Study of Flow and Recovery in Metals

BY E. N. DA C. ANDRADE AND A. J. KENNEDY
University College, London

*MS. received 7th July 1949*

*ABSTRACT.* An apparatus is described which records continuously on photographic paper the extension-against-time curve of a metal wire creeping under stress. The length and time scales are recorded on the paper at the same time as the extension, so that deformation of the paper during development and drying does not affect the accuracy of the record, which allows an extension of up to 10 cm. to be read to within 0·02 mm. The apparatus also automatically removes and restores, repeatedly if desired, the load at times which can be set before the start of the experiment.

## §1. INTRODUCTION

As part of the work on the flow of metals which is being carried out in this laboratory it has been decided to investigate the effect of periods of recovery, during which the metal is not exposed to external stress, these periods being of varied length and interpolated at various stages of the flow. In such experiments it is very convenient to be able to record automatically the progressive extension of the metal against time, both when the stress is continuously applied and when it is removed for specified periods and then reapplied. The apparatus here described was designed for such automatic recording and control and has now been sufficiently used to establish that it answers its purpose well.

## §2. GENERAL DESCRIPTION

The record is made on photographic paper wrapped round a drum which is driven at uniform speed by a phonic motor, suitably geared down. The same motor drives another shaft which carries a timing disc furnished with contact studs. This shaft and the drum shaft are provided with magnetic clutches. The phonic motor also actuates a cam and switch which flashes a lamp, at short regular intervals, to provide a time scale on the paper. Horizontal regularly spaced lines, providing a scale of length, are laid down by the projection of a vertical scale illuminated by a steady light source.

The wire is hung vertically and the load applied through the intermediacy of a vertical rod attached to its lower end. The wire can be relieved of stress by a device which grasps this rod and lifts it slightly, this device being actuated by the timing disc. At the same instant the lights which register the time and length scales and the instantaneous length of the wire are switched off and the drum is stopped.

After an interval, the timing disc actuates the device in such a way that it releases the loading rod and at the same time operates the relays which restart the drum and switch on all the lights. The timing disc and the arms which make contact with it are so arranged that the times at which unloading and reloading take place can be adjusted at will, and the process repeated a number of times if desired. The wire is surrounded by a thermostat and the load applied through an Andrade–Chalmers constant stress bar.

## § 3. MECHANICAL AND OPTICAL DETAILS

The recording apparatus is mounted on a steel base plate $60 \times 45$ cm. The Muirhead 220 v. phonic motor, controlled by a calibrated 50 c/s. fork, drives, through a 50,000 to 1 reduction gear, (1) the vertical shaft which carries the light-alloy recording drum D, 60 cm. high and 21 cm. in diameter, the photographic paper which is wrapped around it being shielded by a housing H pierced by a vertical slit to admit the operating beams of light, and (2) the horizontal shaft which carries the ebonite timing disc around which are disposed platinum studs. These studs make contact with brushes carried on two arms which can be rotated about an axis in line with that of the disc and can be clamped in positions read off on a circular scale taken from an old spectrograph. Of the contacts with these two arms, one serves to remove the load and the other to impose it again, by means of a device described later.

A plan of the optical system is shown in Figure 1. The periodic flash from the lamp A, which records the time scale on the paper, takes place every 16 seconds,

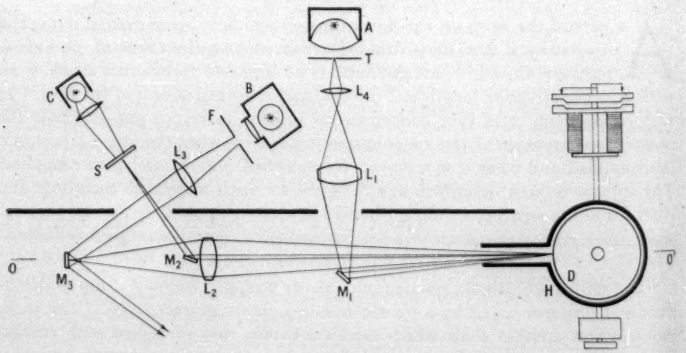


Figure 1.

a period dictated by the gears available. The light illuminates the slit T, an image of which is thrown on the drum through the intermediacy of a cylindrical lens $L_4$, a converging lens $L_1$ and a front-silvered mirror $M_1$. The horizontal length scale, providing lines spaced at about 3 mm. on the drum, is produced by an image of the scale S, reflected in the front-silvered plane mirror $M_2$. This scale is made up of lines 0·5 mm. apart, so that the magnification is 6.

To produce the trace that gives the length of the flowing wire a good point source attached to the lower end of the wire is required. This is provided by a

small steel sphere of diameter 0·4 mm. attached to a strip of mirror $M_3$, the movement of which is restrained to a vertical plane by means of guide rods arranged so as to give a minimum of friction. This mirror, being arranged to throw light from the source B, rendered parallel by the lens $L_3$, well away from the axis OO′, ensures a good dark background for the light proceeding to the drum from the minute image of the light source formed by the sphere. An aperture F confines the light to the mirror and so avoids scattered light. This arrangement gives a fine trace which, with the magnification used, enables the length of wire to be read to within 1/50 mm. if necessary. A total extension of the wire of 10 cm. can be recorded. To make examination of the resulting graphs easier, every tenth horizontal and vertical line is automatically made darker than the others.

The systems A to $L_1$, B to $L_3$, C to S and $L_2$ to $M_1$ are mounted on four optical benches which are attached to the girder system which carries the thermostat, the constant stress bar, the unloading device and associated equipment, and the support for the upper end of the wire. Ilford document paper has been found to be very suitable for the recording. Part of a record obtained from the apparatus is shown in Figure 5 (Plate).

The unloading device, shown in Figure 2, consists of two jaws J, J attached to

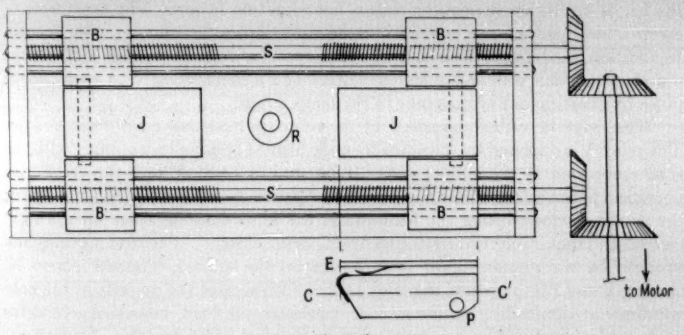


Figure 2.

blocks B, B which are threaded to take the screws S, S. These screws are right-handed and left-handed at the opposite ends respectively, so that rotation in one direction brings the blocks together and in the other direction takes them apart. The cross section of a jaw is shown at CC′: it is clear that a horizontal pressure on the edge E will cause the jaw to rotate about the rod P, the rotation being checked by the projection shown above the jaw. Thus, when the two jaws come together, they grasp the vertical rod R, which applies the load to the wire, and raise it slightly (about 0·5 mm.). When they are driven apart, the rod will be gently released and the load applied.

## §4. DETAILS OF ELECTRICAL OPERATION

The complete electrical circuit diagram is given in Figure 4, the diagram showing the units involved and the cabling between them.

The facilities which the apparatus provides may best be discussed by following through the processes involved, enlarging, where necessary, on those points where

alternatives are offered. The light supply is 230 v. A.C., the fork and motor supply is 230 v. D.C., the relays and clutches 130 v. D.C. and certain power relays and the timing lamp 24 v. D.C. All supplies are controlled in the first place by the power relay AP (Figure 4) which must be manually closed before any power can be put on to the equipment, the relay holding itself from the derived 24 v. supply. Should, for any reason, the power fail, this relay will release and will not remake when the power is re-established.

The 130 v. D.C. is provided by a bridge metal rectifier and a Variac transformer, this supply being common to relay and timing units and to the clutches. The 24 v. D.C. is provided through a mains rectifier set, the input being derived through the AP contacts. With AP closed and the fork set in vibration, the phonic motor may be started, and with the Variac output set at about 180 v., both clutches will operate. The closing, every 16 seconds, of the cam-operated contacts CM operates relay BS, which releases BP: this operates the large mercury relay MR, which closes the flash-lamp circuit. The cam-operated circuit also contains a 1,000-ohm counter which counts, when necessary, the number of pulses delivered. This circuit is used (*a*) to calibrate the timing against a standard clock, and (*b*) to record the duration of the "off-load" period, so that the accuracy with which the hands can be set against the scale is not a limiting factor. The exact time of creep under load can, of course, be read direct from the photographic record. In addition, the pulses delivered by the cam-operated contacts operate a P.O.-type uniselector which provides a higher voltage and a brighter flash at every tenth pulse by shorting out a resistance in the lamp circuit.

What may be called element 1 of the relay unit is shown in Figure 3 (*a*). The relay A is operated by the contact on the arm M coming into contact with the stud embedded in the timing disc. This stud is earthed, and the A contact operates a power relay CP (see Figure 4) which drives the unloading motor forward; the two jaws close, lifting the load and at the same time breaking all the light circuits and the circuit through the recording drum clutch. The stud is eventually brought by the phonic motor into contact on the second, "reload", arm N, causing B and BB to operate the relay DP, which reverses the polarity of the field windings in the loading motor so that it releases the load, continuing to drive back until its circuit is broken by another mechanical micro-switch. At the same time the lighting circuits are remade.

On the release of B, if only one interruption is to occur, the circuit is cut off and any further contacting, in rotation, has no effect. This is accomplished by a relay RA which operates when B and BB operate, and holds by one of its own contacts (see Figure 3 (*b*)). When B and BB release, the B contact falls back on to its rest position, but as RA has not had time to release, a pulse is provided through RB which holds through its own contact, preventing any further operation of the arm circuits. It may happen that, because of the geometry of the timing disc arrangement, the "reload" arm N is set in advance of the "unload" arm M. As a consequence, the operation of B and BB, and the cutting out of the circuits by RB, would mean that unloading would never occur. Hence R is introduced (see Figure 3 (*a*)) into the circuit, with the function of preventing the "load" circuit from operating unless A has operated and unloading has occurred. The effect is that the disc will drive past the load arm N to the unload arm M, and only operate "reload" on its next revolution.

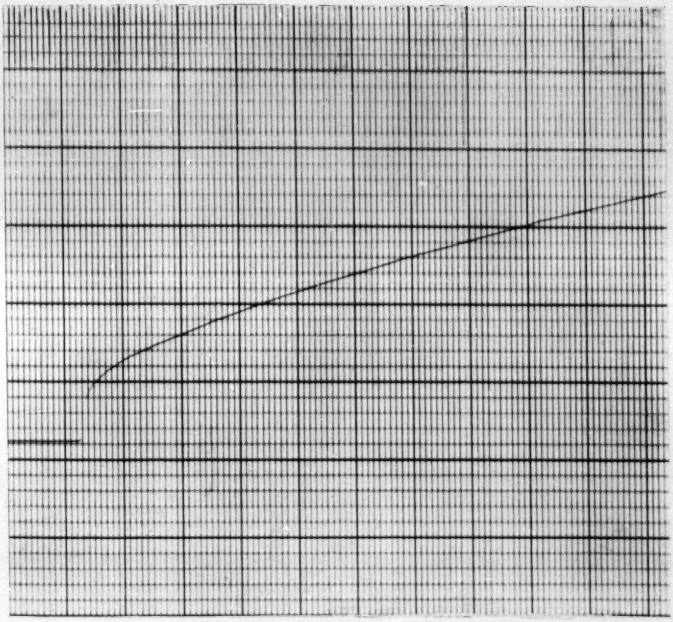

Figure 5.

Part of a record, showing the first few minutes of a creep curve.

*To face page 672*

*Repetition of the Unloading Operation*

If more than one unloading operation is required, then when the load has been replaced after the first operation, the timing system should return to the condition of the outset of the experiment, with the proviso that it retains a "memory" of one operation. As a consequence, if S in Figure 3(*c*) is switched to any of the positions 2 to 6 (representing the number of unloading events required) the operation of F, which is introduced in series with RB and operates whenever RB does (but has no influence in the single interruption arrangement), breaks the circuit through the timing clutch disc. This clutch is pulled out by springs—it is a friction cone type of drive—and the disc spins back under the force of the

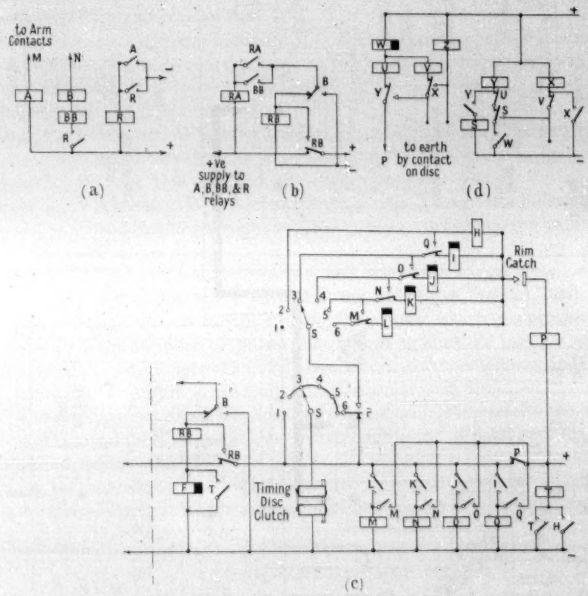


Figure 3.

spring mounted coaxially with the disc. A contact guided by a screw thread in the edge of the disc, in which it rides, moves back a conducting arm until the original, zero, position is reached, when the contact spindle snaps into a spring ("Rim Catch") at the edge of the disc, the clutch circuit is restored, and a pulse is delivered through the contact of switch S. If, for example, the switch S is set at 5, K operates, in turn operating N, which holds itself and steps the feed on to the next relay from K, i.e. J, ready for the next pulse. Simultaneously the pulse operates P, whose contacts break the power to all the relays concerned with the primary operations of loading and unloading, so that, as far as these are concerned, the circuits are as they were at the beginning of the experiment. The "memory" has been achieved by the operation of N, which remains held for the rest of the

experiment. This whole sequence is therefore repeated, the relays O, Q operating in turn until the feed is led direct to the relay H. This terminates the series, for the next pulse operates H direct, which, it will be seen, operates T. T holds itself through one of its contacts, the other contact short-circuiting the relay F, so that the next time an unloading operation is completed, only RB will operate, as at the

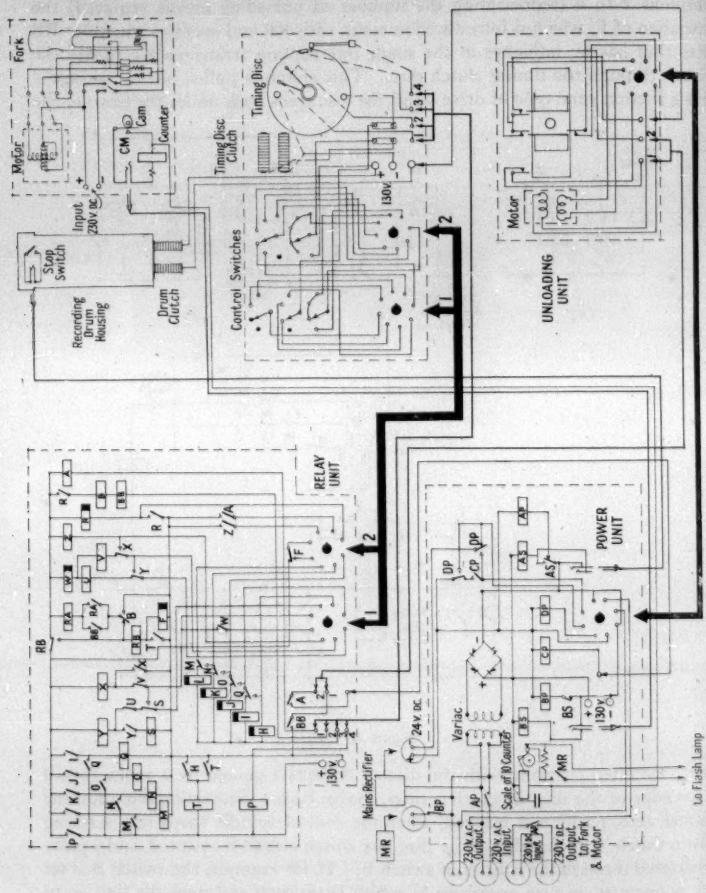


Figure 4.

Symbols are conventional, all contacts being shown "unoperated" and slow-to-release relays part blackened.

end of the single-interruption case; however long the disc continues to be driven, no further interruptions will take place. Hence a selectivity of 0–6 interruptions is at our disposal, with a choice of the settings of the hands anywhere within the 360°, the "off-load" period being variable, also, up to 360°, which corresponds to one revolution of the recording drum.

### *Additions of "Whole-revolutions" to the Off-load Period*

The off-load period has been made automatically controllable for a period longer than that represented by one revolution (i.e., approximately $1\frac{1}{2}$ or 3 hours, depending on the gear ratio used).

This has been effected by incorporating a second contact on the timing disc, diametrically opposite to the other contact, i.e., at the bottom of the disc in the zero position shown in Figure 4. Being at a greater radial distance from the centre, it does not contact the setting arms, but instead, a particular contact fixed to the base plate. The relay system which provided this facility may be represented as shown (Figure 3 (*d*)), in which the "barring" relay R to the B and BB relays (i.e., R must be operated, by A, before the B and BB relays can operate) is now operated, not by A, but by another relay Z.

Consider the circuit shown in Figure 3 (*d*) when the contact point P is connected to earth and then disconnected (that is, an earthed contact is driven across the arm) a number of times.

Make 1. W and U operate.

Break 1. U releases: W is slow to release, so that Y receives a pulse and operates and holds through S so that *both* S and Y are now held.

Make 2. Because Y is operated, this pulse operates V and W.

Break 2. V releases. W is slow to release, so that X receives a pulse, operates and holds through its own contact, switching the input from P on to Z.

Make 3. Z operates, which operates R and hence makes it possible for B and BB to operate on their next contact of the "reload" arm.

By introducing a switch into the circuits, the point at which this process starts, and, therefore, the number of pulses required to operate Z, may be selected. If a period of off-load longer than 12 hours, which is the maximum under automatic control, is required, it can be given by manual switching.

The two setting hands and the two switches, of which one selects the number of off-loadings and the other adds time increments to the off-load period, provide the required pre-set facilities.

When the experiment has been terminated by one complete revolution of the drum, a micro-switch in the drum-housing operates AS and hence releases AP, cutting off all the power supplies.

ACKNOWLEDGMENTS

We wish to acknowledge invaluable help rendered by Mr. L. Walden, Senior Technician, in the course of the building of the apparatus. The actual construction of all the mechanical parts, which have functioned admirably, was carried out in the workshops of the Physics Department at University College. To the head of the workshops, Mr. E. J. Faulkner, who personally executed much of the work, our best thanks are due.

Symbols are conventional, all contacts being shown "unoperated" and slow-to-release relays part blackened.

# An Investigation of the Mechanical Properties of Materials at very High Rates of Loading

By H. KOLSKY

Imperial Chemical Industries Limited, Butterwick Research Laboratories, Welwyn, Herts.

*MS. received* 21*st March* 1949; *read before the Society* 7*th October* 1949

*ABSTRACT.* A method of determining the stress–strain relation of materials when stresses are applied for times of the order of 20 microseconds is described. The apparatus employed was a modification of the Hopkinson pressure bar, and detonators were used to produce large transient stresses. Thin specimens of rubbers, plastics and metals were investigated and the compressions produced were as high as 20% with the softer materials. It was found that whilst Perspex recovered almost as soon as the stress was removed, rubbers and polythene showed delayed recovery, and copper and lead showed irrecoverable flow. The phenomenon of delayed recovery is discussed in terms of the theory of mechanical relaxation and *memory* effects in the material.

## §1. INTRODUCTION

THE mechanical behaviour of materials at high rates of loading is of interest from two points of view. Firstly, the engineer, who wishes to use the materials under conditions where they may have to withstand sudden impacts, requires to know how their mechanical properties depend on the rate at which stresses are applied. Secondly, since the variation of the stress–strain diagram with loading rate is related to relaxation processes taking place on a microscopic scale in the material, the results are of interest to the physicist who is studying the relation between physical problems and molecular structure.

The present investigation was undertaken largely from this second point of view and the first experiments were carried out with specimens of several rubbers and plastics. Earlier work (Naunton and Waring 1938, Alexandrov and Lazurkin 1940) has shown that the mechanical behaviour of these materials is highly dependent on the rate of application of stress, and it was considered of interest to investigate their mechanical properties when they are being submitted to large stresses which are maintained for only a few microseconds. Some experiments on the behaviour of copper and lead under these conditions have also been carried out.

Two problems are encountered in such an experimental investigation of the mechanical behaviour of materials at very high rates of loading. These are associated with inertia effects in the apparatus and with the recording of transient stresses and strains.

As the rate of loading is increased, the acceleration of any moving parts of the straining apparatus begins to require forces comparable with those necessary to deform the specimen. It is often impossible to separate these inertia effects from the effects due to the physical properties of the material under investigation, and at the highest rates of loading the inertia of the specimen itself will result in a non-uniform distribution of stress along its length. In the work described here these difficulties were overcome by the use of very thin specimens and the stresses were applied by a simple mechanical system for which the inertia effects could be calculated in terms of the propagation of stress waves.

The natural period of ordinary stress gauges is far too long for them to respond to forces which are applied for only a few microseconds, and special techniques must be used for recording such transient stresses. Hopkinson (1914) was the first to devise a satisfactory method of doing this and the technique was later developed by Landon and Quinney (1923). More recently R. M. Davies (1948) has made a critical study of the method and has described a modified form of the apparatus in which the measurements are made electrically. This overcomes many of the disadvantages associated with the earlier experimental work.

Hopkinson's original apparatus, which has become known as the *Hopkinson pressure bar*, consisted of a cylindrical steel bar suspended ballistically. The pressure to be measured was applied to one end of the bar whilst at the other end a cylindrical pellet, known as the *time piece*, was wrung on. These pellets were of the same diameter as the bar and of the same type of steel. The end of the bar and one surface of the pellet were ground flat so that the pellet could be attached to the end of the bar with very little grease.

The principle of the method is that when a pulse of compression travels down the bar it is transmitted through the greased joint without change of form. When it reaches the other face of the pellet, which is a free boundary, it is reflected as a pulse of tension. Since the greased joint is unable to withstand any appreciable tensile stress, the pellet flies off as soon as the reflected pulse builds up any tension across the interface. The momentum trapped in the pellet corresponds to a section of pulse the length of which is twice that of the pellet. If the experiment is repeated with pellets of different length, and the momentum measured in each case by capturing the pellet in a ballistic pendulum, the nature of the pressure–time relation for the pulse can be investigated.

Although Hopkinson's original method has the advantage of simplicity and has been used with success by the Research Department, Woolwich (Robertson 1921), for measuring the pressures set up by the detonation of various explosives, it suffers from several serious limitations. Firstly, it gives only a series of pressure–time integrals for different sections of the pulse. From these the maximum amplitude of the pressure, and the time for which any value of the pressure was exceeded may be deduced, but the actual pressure–time curve is not determined. Secondly, the force necessary to break the greased joint introduces an unknown variable into the experiments, and this precludes the use of the apparatus for the measurement of pulses of small amplitude. Finally, the method assumes that the pulse is propagated down the bar without appreciable change of form: this is true only for pulses which are long in comparison with the diameter of the bar and within which there are no sudden changes in pressure.

In the Davies method (Davies 1948) the first two of these difficulties are overcome by eliminating the pellet and greased joint and obtaining a continuous record of the very small displacement of the free end of the bar. This is done by making the free end of the bar the earthed conductor of a parallel-plate condenser which operates as a condenser microphone. The amplified output from this microphone is fed into a cathode-ray oscillograph and a photographic record made. From this record the displacement–time curve may be obtained and if the applied pressures do not exceed the elastic limit of the steel the pressure–time curve can be deduced. Davies has also investigated the theory of the propagation of pulses down cylindrical bars and shown under what conditions the distortions become too severe for the method to be used satisfactorily.

In the work described here an apparatus based on that designed by Davies has been used for making stress–strain measurements. The specimens, which were in the form of thin discs, were placed between the flat faces of two cylindrical steel bars. The transient pressure was applied by firing a detonator at the end of one of the bars and the displacement at the free end of the other bar was measured with a parallel-plate condenser microphone. From this the pressure on the specimen could be calculated. A cylindrical condenser microphone was also fitted around the bar between the detonator and the specimen; this was used to measure the amplitude of the pressure pulse arriving at the specimen, and the deformation of the specimen could then be deduced.

## § 2. APPARATUS

### (i) *General Description*

Figure 1 shows the general arrangement of the apparatus; this is similar to that described by Davies except that the bar is in two parts and a second condenser microphone and amplifier are introduced.

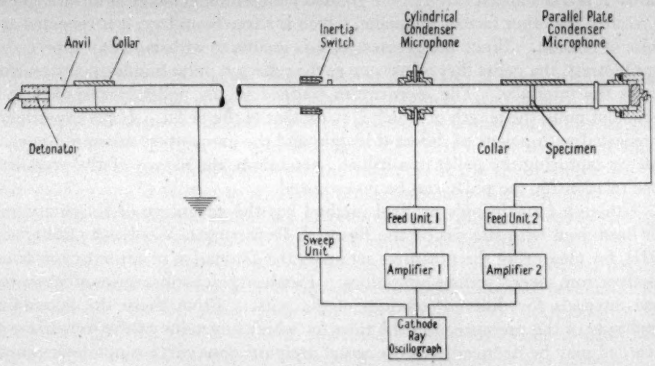


Figure 1. General arrangement of apparatus.

### (ii) *The Pressure Bar*

The bar and extensions were of silver steel (yield point 40 tons/in$^2$) 1 in. in diameter. The bar was 6 feet in length and extensions 4 in., 6 in. or 8 in. in length could be attached with a brass collar, the specimens being lubricated and placed between the flat faces of the bar inside the collar. The ends of both the main bar and the extensions were carefully ground and the collar was made to be a good sliding fit over both bars. In order to protect the pressure end of the bar, the detonators were fired against hardened steel anvils of the same diameter as the bar. These anvils, which were replaced frequently, were cylinders 1½ in. in length with their ends ground flat. A close-fitting steel collar held them against the end of the bar, a very small quantity of grease or heavy oil being used between the flat surfaces to ensure uniform contact.

The detonators, which could be fired electrically, were specially prepared by the Research Department of the Nobel Division of Imperial Chemical Industries Limited, and consisted of flat-based aluminium tubes 0·25 in. in diameter containing

0·5 gm. of tetryl loaded and pressed in increments of 0·1 gm., and primed with 0·35 gm. of a composition of lead azide and lead styphnate. The results obtained with these detonators were found to be consistent to one or two per cent.

The detonators were fitted to the anvils by means of cylindrical polythene holders down the axes of which holes of suitable diameter had been drilled. The holders were attached to the anvils with adhesive tape so that the flat base of the detonator was firmly in contact with the face of the anvil. The bar was suspended ballistically and the momentum communicated on firing the detonator was measured with a light metal pointer which gave the maximum amplitude of swing. The various electrical connections were made with thin flexible wire so that they did not hinder the motion of the bar.

### (iii) *The Condenser Microphones*

Figures 2 and 3 show the construction of the two condenser microphones used with the apparatus. The cylindrical microphone shown in Figure 2 consists

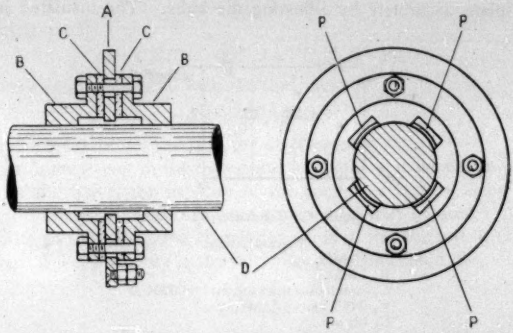


Figure 2. Cylindrical condenser microphone.

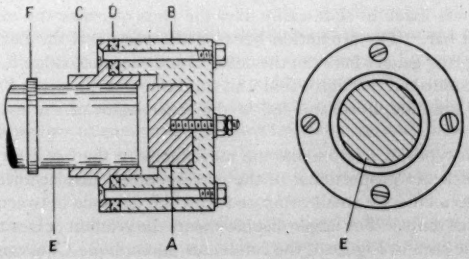


Figure 3. Parallel-plate condenser microphone.

of a circular disc of mild steel A $\frac{1}{8}$ in. thick, through which a concentric hole 1·020 in. in diameter has been drilled; this disc is held between two mild steel collars B by four bolts. Two Perspex washers C were used to insulate the disc

from the collars as this material was found to give good electrical insulation and mechanical rigidity. The collars were machined to slide easily over the bar D, the bore being slotted at four places P to allow feeler gauges to be inserted. The microphone was placed on the bar, the insulated ring was set concentrically by means of feeler gauges and the bolts were then tightened. This left an annular gap of 0·010 in. between the bar and the ring.

This condenser microphone was normally placed 7 in. from the end of the main bar and the insulated disc was charged to two or three hundred volts through a high resistance. The condenser feed-unit is shown in Figure 4. Whilst the compression pulse from the detonator was passing through the microphone, a lateral expansion of the bar took place, which caused a change in the capacity of the cylindrical condenser consisting of the bar and ring. This resulted in a small change in voltage across the condenser which was amplified and fed to one beam of a double-beam oscillograph as shown in Figure 1.

The parallel-plate condenser microphone shown in Figure 3 is similar to the one described by Davies (1948), except that provision has been made to set the insulated plate accurately by adjusting the bolts. The insulated metal plate

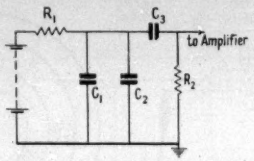


Figure 4. Condenser feed unit.

Typical values.
$R_1$ 50 MΩ.
$R_2$ 2 MΩ.
$C_1$ (condenser microphone) 0·00004 μF.
$C_2$ 0·001 μF.
$C_3$ 0·1 μF.

A is held in the cylindrical block of polythene B which is bolted to a mild steel collar C, a soft rubber disc D being placed between the polythene and the collar. The collar was made to slide easily over the ends of either the extension bar E or the main bar. The separation between the plate and the bar was adjusted by inserting ring gauges between the collar C and the small ridge F. The microphone was connected through a feed unit similar to that shown in Figure 4. The output was then amplified and fed to the other beam of the oscillograph (see Figure 1).

For both types of microphone the movements in the bar are converted into voltages which are proportional to the corresponding displacements so long as these displacements are small compared with the distance between the plates of the condenser units. For larger displacements the relation ceases to be linear.

As can be seen in Figure 4, the condenser microphone $C_1$ is connected across a much larger capacity $C_2$ and these are both charged through a high resistance $R_1$, $C_3$ being a large isolating condenser between the feed unit and the amplifier. The value of $R_1$ is sufficiently large for the charge across the two condensers in parallel to remain constant whilst the value of $C_1$ is being changed by the pressure pulse. Thus, if we write $C$ for $C_1+C_2$, and $c_1$ is the change in capacity of $C_1$,

$V$ the original potential difference across the condensers and $v$ the change in potential difference, we have

$$Q = VC = (V - v)(C + c_1), \qquad \ldots\ldots(1)$$

and if $c_1$ is small compared with $C$ (as it was with both condenser units), we may write

$$v = c_1 V/C. \qquad \ldots\ldots(2)$$

For the parallel-plate condenser unit the capacity $C_1$ is given by

$$C_1 = A(1 + \phi)/4\pi D, \qquad \ldots\ldots(3)$$

where $A$ is the area of the plates, $D$ the initial distance between them and $\phi$ a correction term to allow for edge effects. This term is small when $D$ is small compared with the radius of the plates. If we take $C_1 = B/D$ where $B = A(1 + \phi)/4\pi$, $B$ will remain appreciably constant for small changes in $D$.

If the end face of the bar moves a distance $x$ to produce the change in capacity $c_1$, we have $C_1 + c_1 = B/(D - x)$, so that

$$c_1 = Bx/(D - x)D, \qquad \ldots\ldots(4)$$

or substituting in (2)

$$v = VBx/(D - x)CD = VC_1 x/(D - x)C. \qquad \ldots\ldots(5)$$

If $x$ is very small compared with the separation $D$

$$v = VC_1 x/CD, \qquad \ldots\ldots(6)$$

so that the voltage is proportional to the displacement.

Since the annular gap in the cylindrical microphone is small compared with the radius of the bar $r$, the capacity of the condenser is here again inversely proportional to the width of this gap and equation (5) may be used. $D$ is in this case the width of the gap, $x$ the change in radius of the bar and, if edge effects are neglected, $B = rl/2$ where $l$ is the thickness of the insulated disc.

### (iv) *Amplifiers*

The output obtained from both types of condenser microphone described above will be proportional to the voltage applied across them, but even if this is increased to 1,000 v. the output resulting from the small movements of the bar produced by the pressure pulse will still be only a small fraction of a volt. In order to use this to produce a measurable deflection of the beam of a cathode-ray oscillograph a high-gain amplifier is therefore necessary. The design of such an amplifier which will give undistorted amplification of short transient pulses is a matter of some difficulty since stray capacities result in poor high-frequency response and attempts to compensate for this by using partially inductive loads in the anode circuits may easily lead to the setting up of parasitic oscillations. Fortunately, satisfactory wide-band amplifiers of high gain have been designed recently (Valley and Wallman 1948) and one of these, the No. 234 Pulse Amplifier, developed by the Telecommunications Research Establishment, was used in the present investigation. This amplifier gives an even voltage amplification from audio frequencies up to frequencies of several megacycles per second and has a maximum gain of about 30,000.

The amplifier is designed to work only with pulses of one sign but this did not matter with the parallel-plate microphone as the displacement of the bar resulting from a pressure pulse is always in one direction. With the cylindrical unit,

oscillations in the displacement are found to occur and in order to observe these a wide-band amplifier of smaller gain, which did not suffer from this limitation, was employed.

The connections between the feed units and the amplifiers were made with low-capacity coaxial cable and this was also used for connecting the outputs of the amplifiers to the Y plates of the double-beam oscillograph.

### (v) *Cathode-ray Oscillograph*

A Cossor oscillograph Unit Model 3402, employing a 3259J double-beam tube, was used in these experiments. This tube can be run at a maximum anode voltage of 3,000 v. and was found to give an adequate writing speed for the experiments when fast photographic plates and a large aperture camera lens were employed.

The output from each amplifier was connected to the Y deflector plates of one of the beams, the other deflector plate in each case being at earth potential. Provision was made to substitute an oscillator of accurately known frequency on to one of the Y plates, and this was used as a time calibration for the records.

The X plates were connected across a balanced time-sweep unit which, when triggered, resulted in a single traverse of the two beams across the screen. At the same time it applied a transient positive potential to the modulating grid of the cathode-ray tube, which brought the beam to maximum brightness during the sweep.

The camera lens used had an aperture of f/2·9 and was of 8 in. focal length, a magnification of 0·5 was generally employed. In order to ensure that no distortion was being introduced by the camera, a graduated grid was placed in the plane of the cathode-ray tube screen and photographed; the plate was then measured with a travelling microscope. Ilford H.P.3 quarter plates were used and these were found to give a considerably higher writing speed than other plates with the J screen tube. The plates were measured with a Beck travelling microscope which gave traverses in two directions at right angles.

In carrying out the experiments the brilliancy control of the cathode-ray oscillograph was adjusted so that the spots just disappeared, the room was then placed in darkness and the camera shutter opened. When the detonator was fired it actuated an inertia switch on the bar which triggered the sweep unit giving a single traverse of the two beams.

### (vi) *Sweep Unit*

The circuit of the sweep unit, together with the values of the resistances and condensers normally used, is shown in Figure 5. The sweep unit is designed to give a large transient voltage between X1 and X2 when a positive pulse is applied to terminal T. To prevent defocusing of the beam this voltage is balanced about earth potential. As soon as the unit is triggered it also applies a positive voltage to the modulating grid of the cathode-ray tube from terminal M, and this voltage is maintained positive for the duration of the sweep; it then falls back through zero to a small negative value and then asymptotically back to zero again. V1 is a rectifying valve and V2 a gas-filled or mercury vapour relay valve. For sweep voltages up to 500 v. a GT1C Osram valve with indirectly heated cathode was used. To obtain larger sweeps a BT19 mercury vapour thyratron working at 1,000 v. was employed.

The potentiometer R6 could be set so that the sweep unit triggered itself and gave a repeating stroke. It was used in this position whilst the other controls were being adjusted.

In order to apply a triggering voltage to terminal T some microseconds before the pressure pulse reached the cylindrical microphone, an inertia switch was fitted to the bar 6 in. from the microphone (see Figure 1). Several types of inertia switch were tried in attempts to effect triggering at a reproducible time before the head of the pressure pulse reached the specimen. With all mechanical types an uncertainty of 2 or 3 microseconds was found to occur and a simple *ring switch* similar to that described by Davies was finally employed. This is shown diagrammatically in Figure 1 and consists of a metal tube pressed round a plastic insulating collar which slides easily on the bar.

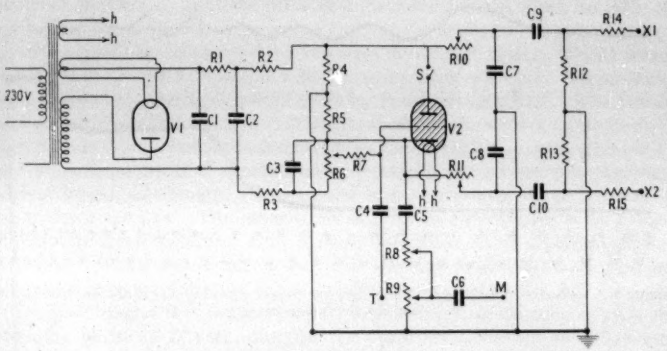


Figure 5. Sweep unit.

| | | | |
|---|---|---|---|
| R1, 14, 15 | 30,000 Ω. | C1 | 0·5 μF. |
| R2, 3 | 0·5 MΩ. | C2 | 10 μF. |
| R4, 5 | 2 MΩ. | C3 | 50 μF. |
| R6, 7, 8, 9 | 100,000 Ω. | C4, 6, 7, 8, 9, 10 | 0·01 μF. |
| R10, 11 | 20,000 Ω. | C5 | 0·001 μF. |
| R12, 13 | 1 MΩ. | | |

It was found that the flash from the explosion of the detonator could be used to trigger the sweep unit satisfactorily by letting the light fall on a photoelectric cell with a one-valve amplifier. By this means results reproducible to within one microsecond were obtainable and this method was employed for some of the experiments.

Figure 6 shows a photograph of the traces obtained in an experiment when the bar and extension were wrung together with a thin layer of grease between them. The top and middle traces are the amplified outputs from the cylindrical and parallel-plate microphones respectively. The bottom trace is a timing wave of 5·30 μsec. period.

### (vii) *Static Stress–Strain Apparatus*

Figure 7 shows a diagrammatic representation of the apparatus used to obtain stress–strain curves for the materials under static loading conditions. These were carried out for comparison with the results obtained for the Hopkinson bar apparatus. The specimens were placed in the hydraulic ram between the flat

end of the piston which was 1 in. in diameter and a stop of the same diameter, the faces of the specimen being lubricated to allow free lateral movement. The stress was measured with the pressure gauge which gave the oil pressure on the piston. The change in thickness of the specimen was measured with a travelling microscope which read directly to 0·01 mm. The pressure was built up with the pump, the booster being used as a fine control.

## § 3. THEORY OF THE METHOD

If a plane compression pulse is propagated along a cylindrical bar and the pressure does not exceed the elastic limit of the material, the velocity of propagation will be $c$ where $c=\sqrt{(E/\rho)}$, $E$ being Young's modulus for the material and $\rho$ its

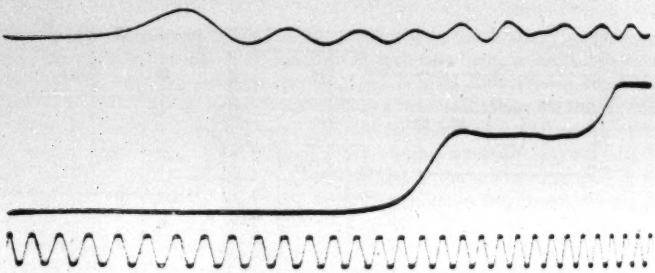

Figure 6. Cathode-ray oscillograph traces showing outputs from the two condenser microphones and 5·3 $\mu$sec timing wave.

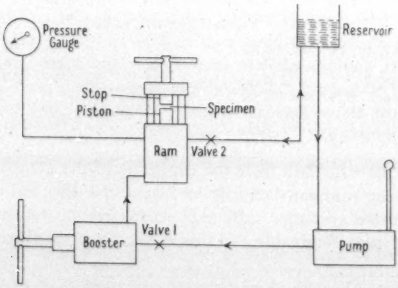


Figure 7. Static stress–strain apparatus.

density. Also if the particle velocity at any point is $u$ and the amplitude of the pressure is $p$, we have $p=\rho cu$. (These relations assume that the pulse is propagated without distortion, the pressure being uniform over any given cross section; this is true only for pulses which are long in duration compared with the time taken for the pulse to travel a distance equal to the radius of the bar.)

At the free end of the bar the compression pulse will be reflected as a pulse of tension. This is of the same form as the outgoing pressure pulse, and the velocity of the end of the bar is therefore twice the corresponding particle velocity associated

with the pulse travelling along the bar. Thus, if we denote the displacement of the end of the bar, at time $t$, by $\xi$ we have

$$p = \tfrac{1}{2}\rho c \frac{d\xi}{dt}. \qquad \ldots\ldots (7)$$

The output from the parallel-plate microphone gives the relation between $\xi$ and $t$ and by differentiating this curve the pressure–time relation for the pulse may be derived.

The radial displacement of the bar $\zeta$ is given by

$$\zeta = \sigma r p/E, \qquad \ldots\ldots (8)$$

where $\sigma$ is Poisson's ratio and $r$ is the radius of the bar. Thus the cylindrical condenser microphone gives the pressure–time curve directly, when the value of $\sigma r/E$ for the bar is known.

Davies (1948) has considered the two ways in which distortion appears when the pulse is of a length comparable with the cross section of the bar. He has done this in terms of the elastic equations given by Pochhammer (1876), Chree (1889) and Love (1927) for the propagation of longitudinal vibrations of a circular cylinder. This treatment shows that for such short pulses considerable dispersion takes place, the Fourier components of short wavelength travelling with lower velocities than those of longer wavelength. This results in a lengthening of the pulse as it travels down the bar. The other form that the distortion takes is in a non-uniformity of the distribution of the pressure and displacement across any section of the bar. When measurements are made with the parallel-plate microphone this results in an amplification of the high-frequency components.

Davies estimates that when a bar 2 ft. long and 1 in. in diameter is used for measuring pulses of 20 $\mu$sec. duration the distortion causes errors of between 2 and 3% in the values obtained. He also describes experiments which confirm that this is the order of the error observed. The distortion results in larger errors when a cylindrical condenser microphone is used and Davies suggests that this method can only be used profitably with pulses which are very long compared with the diameter of the bar.

In the method described here for obtaining stress–strain measurements, any distortion introduced by the main bar does not affect the validity of the results, but only changes the form of the stress cycle to which the specimen is subjected.

If a sufficiently thin specimen is inserted in the split Hopkinson bar, described in the previous section, the pressure is effectively the same throughout the specimen during the passage of the compression pulse, and this will be true so long as the thickness of the specimen is small compared with the wavelength of the shortest operative wave in the Fourier spectrum of the pulse. This pressure is communicated along the extension bar to the parallel-plate condenser microphone. On differentiating the displacement–time curve, which is obtained from this microphone, the stress–time relation for the specimen may be derived using equation (7).

If the displacement–time relation for the initial pulse travelling down the main bar is also known, the strain–time relation may be determined and the stress–strain curve can then be derived. Let the pressure of the incident pulse at any time $t$ be $p_I$, of the transmitted pressure pulse which acts on the specimen

$p_T$, and of the reflected pulse, which is a pulse of tension travelling back along the bar $-p_R$, then

$$p_I = p_R + p_T. \qquad \ldots\ldots(9)$$

If we denote the displacement of the face of the main bar in contact with the specimen at time $t$ by $\xi_1$ we have

$$\xi_1 = \frac{1}{\rho c}\int_0^t (p_I + p_R)dt, \qquad \ldots\ldots(10)$$

and if the displacement of the face of the extension bar in contact with the specimen is $\xi_2$,

$$\xi_2 = \frac{1}{\rho c}\int_0^t p_T dt. \qquad \ldots\ldots(11)$$

Now if the thickness of the specimen is $z$, the fractional strain $s$ is given by $(\xi_1 - \xi_2)/z$, hence from (9), (10) and (11) we have

$$s = \frac{2}{\rho c z}\int_0^t (p_I - p_T)dt. \qquad \ldots\ldots(12)$$

Now
$$\frac{2}{\rho c}\int_0^t p_T dt = \xi_T$$

is the displacement measured by the parallel-plate microphone with the specimen between the bar and the extension, and

$$\frac{2}{\rho c}\int_0^t p_I dt = \xi_I,$$

the displacement produced by the pulse when no specimen is present, the two bars being in contact. Thus

$$s = (\xi_I - \xi_T)/z, \qquad \ldots\ldots(13)$$

so that if we know the displacement–time relations for $\xi_I$ and $\xi_T$ we can obtain the strain–time curve and, since the gradient of the $\xi_T$ curve gives us the stress–time curve, we can derive the stress–strain relation for the material under the conditions of the experiment.

As mentioned above, the distortion introduced by the bar causes the values of the pressure amplitude obtained with the cylindrical microphone to be rather unreliable. Nevertheless, the experimental results showed that the pressure–time integral, which is all that is required to determine the strain in the specimen, agreed closely with the values obtained directly with the parallel-plate microphone.

In the stress–strain determinations described here, however, it was generally found most convenient to determine $\xi_I$ and $\xi_T$ in separate experiments with similar detonators, the two bars being wrung together with a little grease in the first case, and the specimen lubricated and inserted between the bars in the second case. The cylindrical-condenser microphone, did, however, serve two useful purposes. Firstly, it gave a convenient method of fixing the same zero in time for the two experiments, since measurements along the time scale could be made from the first intercept of the cylindrical microphone trace on the horizontal axis (Figure 6, top trace). This could be done with considerable accuracy whereas, since the displacement begins rising very slowly (Figure 6, middle trace), the arrival of the

pressure pulse cannot be fixed at all accurately. Secondly, the trace from the cylindrical microphone gave an accurate check that the pressure pulses obtained with different detonators were of the same shape and amplitude.

The forward acceleration of the specimen is proportional to the difference in pressure between the two faces and, so long as the specimen is sufficiently thin, the inertia of the specimen may be neglected from this point of view in determining its stress–strain behaviour. The radial motion, however, depends on the time rate of change of the longitudinal strain and a correction must be applied for the radial kinetic energy however thin the specimen may be.

If we take $p_s$ as the stress required to produce a fractional strain $s$ when no kinetic energy is given to the specimen, $p_m$ to be the measured pressure with the specimen in the split Hopkinson bar apparatus, and $G$ to be the radial kinetic energy, we have

$$Az\int_0^s (p_m - p_s)ds = G, \qquad \ldots\ldots(14)$$

where $A$ is the cross-sectional area and $z$ is the thickness of the specimen.

Differentiating with respect to $s$ we obtain

$$p_m - p_s = \frac{dG}{ds}\Big/ Az. \qquad \ldots\ldots(15)$$

Now if the specimen is expanding uniformly and friction between it and the bars is neglected, the radial kinetic energy may be obtained by integration and is given by

$$G = \tfrac{1}{4}A\rho_s z V_r^2, \qquad \ldots\ldots(16)$$

where $\rho_s$ is the density of the specimen and $V_r$ is the radial velocity of a point on the circumference.

If $\sigma_s$ is Poisson's ratio for the specimen and $r$ its radius, we have

$$V_r = \sigma_s r\frac{ds}{dt},$$

and substituting in (16) and differentiating we obtain

$$\frac{dG}{ds} = \tfrac{1}{2}\sigma_s^2 r^2 A\rho_s z\frac{d^2s}{dt^2}; \qquad \ldots\ldots(17)$$

hence from (15)

$$p_m - p_s = \tfrac{1}{2}\sigma_s^2 r^2\rho_s\frac{d^2s}{dt^2}. \qquad \ldots\ldots(18)$$

This correction was found to be not more than a few per cent in most of the experiments and is only important when the rate of straining is changing rapidly, which, in these experiments, was at the beginning of the stress cycle. Nevertheless, having to use this correction does introduce a certain amount of error into the results, in that the value of $\sigma_s$ at these very high rates of loading is not known accurately, and the assumption that the expansion is uniform with no frictional effects is not necessarily justified. The double differentiation of the strain–time curve may also result in appreciable errors when the correction term is comparable with the actual applied stress.

The value of the correction term is proportional to the square of the radius of the specimen and if the method is to be used at higher rates of straining, smaller specimens would have to be employed.

## §4. CALIBRATION OF THE APPARATUS

The foregoing treatment to the experimental method assumes that the apparatus fulfils the following conditions: (*a*) the extension bar does not introduce any further distortion to the stress pulses transmitted through it; (*b*) the pulse is transmitted across a greased joint between the bars without distortion; (*c*) the brass collar connecting the two bars does not transmit any appreciable stress-wave from the main bar to the extension bar.

A series of experiments were carried out to test the extent to which these conditions were fulfilled by the apparatus. To investigate conditions (*a*) and (*b*) the collar and extension bar were removed and the parallel-plate microphone was set up at the end of the main bar. Records were then taken of the pulses from detonators, and the results compared with those obtained when the microphone was at the end of an extension bar wrung on to the main bar with a little grease. It was found that the results obtained with 4 in., 6 in. and 8 in. extension bars all gave the same displacement–time curve as that found when the microphone was at the end of the main bar.

Thus conditions (*a*) and (*b*) were fulfilled for the pressure pulse which had arrived at the end of the main bar. The method also assumes, however, that the modified pulse, produced when a specimen of some other material is inserted between the bars, travels down the extension bar without distortion. In the experiments it was found that these pulses were longer than the original pulse from the detonator and that the changes in pressure were generally more gradual. From Davies' treatment one would therefore expect that these pulses would travel down the extension bars with even less distortion than the pulse from the detonator. This could not be tested directly, but it was found that here again identical results were obtained whichever length of extension bar was employed.

It is perhaps worth mentioning that the results obtained when the microphone was used with extension bars differed in two minor respects from those obtained with the microphone at the end of the main bar. The middle trace of Figure 6 shows the trace from the parallel-plate microphone when it was placed at the end of a 6 in. extension wrung on to the main bar. It may be seen that the displacement rises to an approximately constant value at which it stays for about 35 $\mu$sec., after which it begins to rise again.

This second rise results from the reflected pulse travelling back along the extension bar, being reflected at the greased joint as a pulse of compression, and finally arriving at the condenser microphone as a pulse similar in form to the initial one. (The whole of the second pulse was not obtained in the experiment shown in Figure 6, as the amplifier was overloaded before the maximum displacement had been reached.)

When the microphone was placed at the end of the main bar no such second rise could be observed since it would arrive after the pulse had twice travelled the full 6 ft. length of the bar; it would thus be well outside the duration of the trace. The other difference between the traces obtained when the microphone was at the end of the main bar, and when an extension bar was used, is that in the former case instead of the trace being approximately flat after the main pulse had passed, it showed a series of oscillations. Such oscillations have been observed by Davies and shown by him to be due to the distortion introduced by the bar; this distortion results in a lagging behind of the high-frequency components of the pulse.

These oscillations may also be seen in the top trace of Figure 6 which corresponds to the radial displacements of the surface of the main bar when the pulse is passing. The theoretical treatment shows that these will be more marked than the corresponding longitudinal vibrations in the bar and it can be seen from the Figure that in this case the vibrations are comparable with the main pulse.

The reason these oscillations do not appear when an extension bar is used is that the greased joint does not transmit tensile stresses. The bars consequently separate slightly as soon as the first oscillation in the stress pulse builds up an appreciable tension across the greased joint; this joint thus acts as a *mechanical rectifier*.

To test whether condition (*c*) was fulfilled, the two bars were separated in the collar by an air gap of 0·020 inches (this gap being several times larger than the calculated maximum displacement of the end of the bar produced by the pulse). The amplifier of the parallel-plate microphone was then set at maximum gain and a polarizing voltage of 360 v. was used across the microphone. The sensitivity of the microphone was then about 30 times as great as it was in the stress–strain determinations. A detonator was fired at the end of the bar and the cathode-ray oscillograph traces photographed. The trace from the parallel-plate condenser microphone was perfectly flat, showing that no appreciable motion had been communicated to the extension bar through the brass collar.

Before the apparatus could be used for stress–strain measurements the relation between the values of the deflections on the cathode-ray oscillograph records and the corresponding displacements of the end of the bar had to be determined. In addition, as may be seen from equation (7), in order to calculate the pressure from the gradient of the displacement–time curve, the value of $\rho c$ for the material of the bar had to be ascertained.

The relation between the voltage output of the condenser microphone system and the displacement at the end of the bar is given in equation (5) and this equation may be rewritten

$$x = \frac{Dv}{C_1V/C + v}. \qquad \text{.....(19)}$$

If unit deflection on the photographic plate corresponds to an output of $N$ volts from the condenser microphone and feed unit, we have

$$x = \frac{y}{C_1V/CND + y/D} = \frac{y}{K + y/D}, \qquad \text{.....(20)}$$

where $y$ is the deflection on the photographic plate corresponding to a displacement $x$ at the end of the pressure bar. Now $N$ may be determined if the gain of the amplifier, the sensitivity of the cathode-ray oscillograph and the photographic reduction are known. If the capacity of the parallel-plate condenser unit, $C_1$, can also be determined for a known value of $D$, either by calculation or with a capacity bridge, equation (20) may be used to calculate the displacements from the measurements of the cathode-ray oscillograph records.

As this method involves the accurate determination of all the above constants, it was considered both simpler and more accurate to determine the quantity $C_1V/CND = K$, experimentally. From this value of $K$, and $D$ as measured with gauges, equation (20) could be used to convert the values of $y$ into displacements.

If the value of $y$ for one known displacement $x$ can be measured the value of

$K$ may be derived. Now, by integrating equation (7) it can be seen that when a pressure pulse is reflected at the end of the bar the maximum displacement $\bar{x}$ is given by

$$\bar{x} = \frac{2}{\rho c} \int p dt. \qquad \ldots\ldots(21)$$

But if $M$ is the momentum associated with the pulse, and $A$ is the cross-sectional area of the bar, we have

$$M = A \int p dt. \qquad \ldots\ldots(22)$$

nus from (21) and (22)

$$\bar{x} = 2M/A\rho c. \qquad \ldots\ldots(23)$$

Hence, if the momentum $M$ associated with a pressure pulse is known, the maximum displacement of the end of the bar when the pulse is reflected may be calculated.

Relation (23) can thus be used to determine the value of $\bar{x}$ for one known value of $y$, and $K$ can hence be determined. To do this a detonator was fired at the end of the bar, the maximum amplitude of swing was determined, the cathode-ray oscillograph traces were photographed and the gain of the amplifiers measured. From the amplitude of swing, the mass of the bar and its period of oscillation the value of $M$ was calculated. Hence the value of $\bar{x}$ was derived using the values of $\rho$ and $c$, which, as described later in this section, had to be determined for the pressure measurements.

Substituting $\bar{x}$ and the corresponding value of $y$ (measured on the cathode-ray oscillograph record) in equation (20), the value of $K$ was determined. Since $K$ is proportional to the gain of the amplifier, which may vary with time, in the later work the gain was measured in each experiment and the value of $K$ changed accordingly.

To ensure that the momentum was entirely that of the short pressure pulse and that the amplitude of swing of the bar had not been increased by the general rush of gas following the explosion, the following experiments were carried out. The condenser microphone and the extension bar were removed and time pieces of different lengths, similar to the ones used by Hopkinson (1914) were wrung on to the bar. Detonators were then fired at the other end of the bar and the amplitude of swing measured. It was found that with a time piece $2\frac{1}{2}$ in. long there was no measurable deflection of the bar, the entire momentum having been trapped in the time piece.

It may be seen from equation (20) that in order to convert the values of $y$ into displacements, the value of $D$ is required as well as the value of $K$. $D$ was determined with mechanical gauges and there may have been an inaccuracy of one or two per cent in the value taken. $y/D$ was, however, always small compared with $K$ and the error introduced into the values of $x$ by this factor was consequently negligible.

As was mentioned earlier, the value of $\rho c$ of the material of the bar is required to convert the displacement measurements into pressures. The density $\rho$ of the steel was measured by weighing a section of known dimensions and was found to be 7·89 gm/cm$^3$. The velocity of propagation $c$ of the pressure pulses was measured by comparing the interval of time between the arrival of the pulse at the end of

the main bar, and at the ends of extension bars of different lengths. Records were taken with the parallel-plate condenser microphone first at the end of the main bar and then at the end of an extension bar, the cylindrical microphone being kept at the same position for all the experiments. The velocity of propagation $c$ could then be calculated from the difference in separation between the pulses from the two microphones with and without the extension bar (cf. Figure 6). The mean value obtained for the velocity was 5,320 metres/sec. This value was checked by setting a length of magnetized bar in longitudinal resonance by means of an oscillator and energizing coil, and measuring the frequency, and it was found that the velocity of sound measured in this way agreed closely with the velocity of the pulses.

## § 5. EXPERIMENTAL RESULTS

### (i) *General Procedure*

The specimens used for the experiments with the pressure bar were in the form of circular discs of uniform thickness. In order to allow for the lateral expansion of the specimens when they were being compressed, their initial diameters were made slightly less than that of the bar, the maximum permissible diameter in each case being determined by preliminary experiments. To reduce friction between the specimens and the bars both surfaces of each specimen were lubricated before it was placed in the apparatus. A thin layer of grease was generally used except with the rubber specimens, when glycerol was used. A number of different oils and greases were first tried in order to ensure that the viscosity of the lubricant did not materially influence the results. Similar results were obtained with all the lubricants used; when, however, no lubricant was used, it was found that larger stresses were required to obtain a given strain, which indicated that there was then a considerable amount of friction between the specimen and the bars.

For each group of experiments the gains of the amplifiers were measured, and in addition one or two experiments were included in which the main bar and the extension bar were wrung together with no specimen between them. The traces obtained under these conditions were useful as a calibration of the microphones and as a check that the apparatus as a whole was operating satisfactorily.

The results of the ballistic calibration of the pressure bar, described in the previous section, showed that when the pressure pulse from one of the detonators used was reflected at the free end of the main bar, this end surface moved forward a distance of 0·12 mm. In the limiting case of a very soft specimen the movement of the end face would be very nearly as much as for a free end. The other face of the specimen in contact with the extension bar would remain almost fixed, and the maximum fractional strain would then be given by the ratio of 0·12 mm. to the initial thickness of the specimen (cf. equation (13)).

With harder materials both surfaces of the specimen move and the strains are consequently smaller; nevertheless, by using specimens of different thicknesses, the rate of straining and the maximum fractional strain can be varied within certain limits. These limits are set on the one hand by the fact that, for very thin specimens, there is not sufficient difference between the cathode-ray oscillograph traces obtained when the specimen is present and when the bars are wrung together for accurate values of the strain to be determined. On the other hand, if the specimens are too thick, the assumption that the pressures on both sides of the specimen are sensibly the same is no longer valid.

The method of determining the stress–strain curve from the photographic records is described in the section dealing with the theory of the method. The procedure after the plates had been measured was first to convert the measurements into displacement–time curves, using equation (20). The displacement–time curve obtained from the experiment when the specimen was present was then differentiated numerically, and this gave the pressure–time curve, as may be seen from equation (7). The strain–time curve was derived from the difference between the corresponding values of the two displacement–time curves, using equation (13). All measurements of time were made from the same point on the trace from the cylindrical microphone; as this microphone was in the same position along the bar in both experiments, this ensured that the values of stress and strain corresponded to the same instants of time.

Before deriving the stress–strain curve from these results, the stresses had to be corrected for the radial kinetic energy effect, as described in an earlier section, and where the strains were large the change in the cross-sectional area of the specimen during straining had to be allowed for to obtain the true values of the stress.

The experiments were all carried out at room temperature and calculation showed that the heating produced by the compression of the specimens never amounted to more than 1·5° c. in these experiments.

(ii) *Polythene*

Figure 8 shows the stress–strain curves obtained with four different thicknesses of polythene (polymerized ethylene) of a type known as grade 20. The specimens were prepared from cast sheet which was carefully annealed to ensure that there was no preferred molecular orientation. The points on each curve correspond to 2 $\mu$sec. intervals in the stress–strain cycle, so that the rates of stressing and straining may be derived from the curves. This same convention has been used in the dynamic stress–strain curves for other materials shown in the later figures. To avoid confusion around the origin in Figure 8 the first two or three points on each curve have been omitted. The broken curve on this figure shows the results obtained for the static stress- strain relation, using the apparatus shown in Figure 7.

It may be seen that the effective elastic modulus for the dynamic tests is very much higher than that observed statically, and that in all four experiments the strain continues to increase after the stress has passed its maximum and has decreased to a fraction of its maximum value. Since there was no permanent plastic flow in the material, the specimens being of exactly the same dimensions after the experiment, this increase of strain with decreasing stress may appear at first sight rather surprising. The interpretation of this effect in terms of a memory function of the type first suggested by Boltzmann is discussed in detail in the next section.

(iii) *Rubber*

Experiments were carried out with specimens of natural and synthetic rubbers, and the results obtained were somewhat similar to those observed with polythene. The delayed recovery effect with these materials was even more pronounced than for polythene, the strain continuing to increase rapidly after the stress had passed its maximum value.

The specimens of the three synthetic rubbers investigated, neoprene GN, Perbunan and GR-S were closely similar in their static mechanical behaviour to

the specimen of natural rubber used, and it was found that their dynamic behaviour was also very similar to that of the natural rubber. For all these materials no permanent deformation could be observed after the dynamic tests.

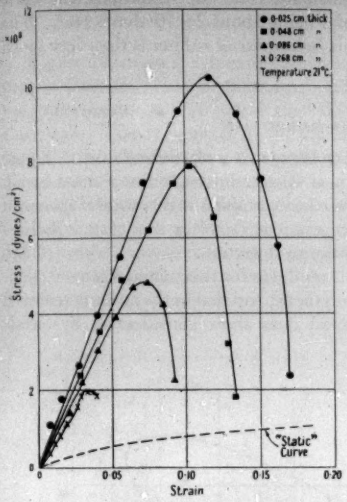


Figure 8. Dynamic stress–strain curves for polythene.

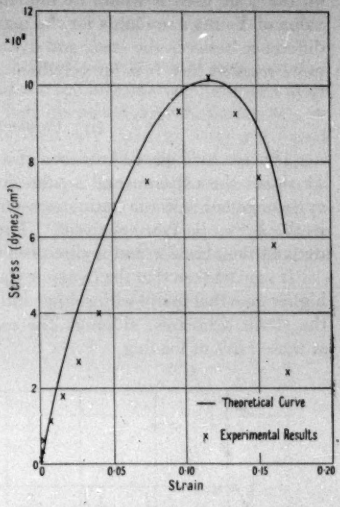


Figure 9. Theoretical curve for polythene.

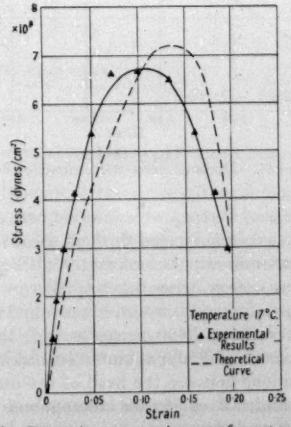


Figure 10. Dynamic stress–strain curve for natural rubber.

Figure 10 shows a typical dynamic stress–strain curve obtained with natural rubber. The specimen used for this experiment was initially 0·03 cm. in thickness,

and the maximum strain observed was about 20%. The broken curve shown on the same figure was one derived theoretically in terms of a *memory* function, and is discussed in the next section. No static stress–strain curve is shown, since on the scale used it would be indistinguishable from the strain axis, the static value of Young's modulus for the material being about $2 \times 10^7$ dynes/cm$^2$. The difference between the static and dynamic behaviour of rubber is thus very much more marked than it is for polythene.

### (iv) *Polymethyl-methacrylate*

This is a hard glass-like plastic of which Perspex is a plasticized form. Figure 11 shows the experimental results given at 2 $\mu$sec. intervals for a stress–strain cycle, together with the static stress–strain curve obtained with a similar specimen in the hydraulic ram apparatus. The continuous curve in this case is the one derived theoretically and is discussed in the next section.

It may be seen that the dynamic elastic modulus for this material is very much higher than that found with rubber and polythene, and that as the stress is removed the strain decreases, although the material does show considerable hysteresis at these rates of loading.

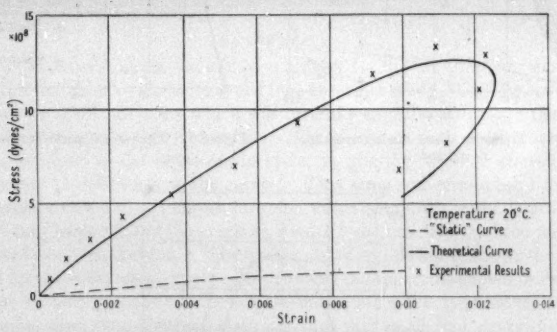


Figure 11. Dynamic stress–strain curve for Perspex.

When thick specimens of Perspex were inserted between the bars it was found that a pressure pulse was communicated through them from the main bar to the extension bar. The transmitted pulse was flatter in shape and of longer duration than the initial pulse, as well as being much smaller in amplitude. By using a series of specimens of up to 2 in. in thickness, it was found that the head of the pulse was propagated with a velocity of 2,400 metres/second; this corresponds to a value of Young's modulus of $6{\cdot}8 \times 10^{10}$ dynes/cm$^2$. In making this determination of the velocity, the separations between the head of the pulse and a fixed point on the trace from the cylindrical condenser microphone were measured on the cathode-ray oscillograph records.

When comparable thicknesses of either rubber or polythene were tried no well-defined pulse was transmitted through them. This is to be expected from the dynamic stress–strain curves shown in Figures 8 and 10. From these it can

be seen that the layers of material will not recover immediately the stress is removed, so that a continued lengthening of the pulse with a corresponding drop in the pressure amplitude will take place as the pulse travels through the material.

### (v) *Copper*

Figure 12 shows the dynamic and static curves for specimens of pure annealed copper sheet 0·05 cm. in thickness. When the specimens were measured after the experiments it was found that they had decreased approximately 4% in thickness. The behaviour of the metal is thus very different from that found with polythene and rubber, although the appearance of the curves is rather similar. The material is here flowing under the influence of the applied stress, the only recoverable part of the deformation being the very small strain corresponding to the initial steep rise in the stress–strain curve. The difference between the static and dynamic behaviour for copper is not nearly so marked as it was found to be with the other materials investigated.

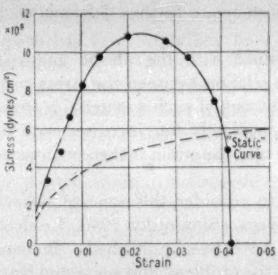


Figure 12. Dynamic stress–strain curve for copper.

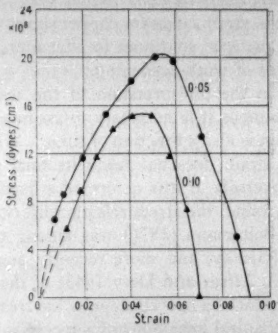


Figure 13. Dynamic stress–strain curve for lead.

### (vi) *Lead*

Figure 13 shows the dynamic stress–strain curves obtained with lead specimens 0·05 and 0·10 cm. thick. As in the case of copper, it was found that after the tests the specimens were thinner by the fraction indicated by the curves. As a result of the comparatively small stress required to start deforming the specimens and the high density of lead, the radial kinetic energy correction was found to be large, and the values of the stress in the region near the origin were consequently rather uncertain. The results did, however, show that the yield point was very small compared with the order of magnitude of the maximum stress applied in these experiments.

It was found that for this material the values of the stress were approximately proportional to the rate of straining; this indicates that the lead is behaving like a viscous liquid under these dynamic conditions.

As in the case of rubber the stresses required to deform the material statically were found to be too small to be shown on the same scale as the dynamic results.

## § 6. DISCUSSION OF RESULTS

The experimental results described in the previous section have shown three types of mechanical behaviour that may occur when materials are submitted to rapidly changing stresses. Under these conditions, polythene and rubber only begin to recover after the stress has fallen back to zero, but the recovery is complete and no permanent deformation can be observed after the experiments. Polymethyl–methacrylate shows a hysteresis loop at these high rates of loading, but with this material a considerable fraction of the strain disappears within a few microseconds of the stress passing its maximum. Here again, after the experiments, there is no permanent deformation and, when the specimens were examined through crossed nicols, they showed no optical strain.

Copper and lead, unlike the plastics and rubbers, were permanently deformed and showed no recovery either immediately the stress began to fall or subsequently. The difference in behaviour between copper and lead results from the much higher yield point of the former metal, which has a definite elastic region in its stress–strain curve. The yield point of lead on the other hand is so low that in these experiments its behaviour is very much like that of a viscous fluid. The static stress–strain curve for copper shows that even after the yield point has been passed the material continues to offer increasing resistance to further deformation as a result of work-hardening.

In the interpretation of the results obtained with the plastic and rubber specimens it is necessary to assume that the relation between the stress and the strain is also a function of time. When a specimen of such a material is stressed, the strain does not reach its final value immediately but increases with time. Conversely, if it is deformed a fixed amount and the strain is then maintained at this value, the stress relaxes with time.

Boltzmann (1876) was among the first to consider this type of behaviour analytically, and more recently several surveys (Slonimsky 1940, Leaderman 1943, Alfrey and Doty 1945) of the subject have been published. Boltzmann introduced a new concept in his treatment of the problem, and suggested that the mechanical behaviour of a specimen was a function of its entire previous history. He further assumed that when a specimen had undergone a series of deformations, the effect of each deformation was independent of the others, and the behaviour of the specimen could be calculated by a simple addition of the effects that would occur when the deformations took place singly. This assumption has become known as the Principle of Superposition.

In considering the behaviour of a specimen in which both the stress and the strain are varying simultaneously, we may consider the strains produced by known stresses, and the problem is then one of *creep*. Alternatively we may calculate the stresses produced when the specimen is deformed a known amount and treat the problem in terms of the *relaxation of stress*. It has been shown (Gross 1947) that the two treatments are equivalent, and it is generally a matter of convenience which of them is followed.

In Boltzmann's original treatment he considered the problem in terms of the relaxation of stress and postulated that the stresses produced by dilatational and shear strains may relax in different ways. The case of uniaxial compression or tension involves both shear and dilatational deformations, and if two separate relaxation phenomena have to be taken into account the problem becomes rather complex. Boltzmann, however, suggested that it was unlikely that many materials

would show dilatational relaxation phenomena and in fact there is no experimental evidence to show that such phenomena occur. Recent work (Pinkerton 1947, Mason *et al.* 1948) on liquids has shown that when such relaxation does occur, the times involved are very much shorter than those with which we are concerned here.

Boltzmann considered the past strain history of the specimen as divided into a number of infinitesimal time elements. At time $t$ the residual stress due to a strain $\epsilon(\tau)$ which took place at time $\tau$ and was maintained for an element of time $\delta\tau$ is expressed as $-\phi(t-\tau)\epsilon(\tau)$ where $\phi(t-\tau)$ is called a *memory* function. If at time $t$ the value of the strain is $\epsilon(t)$ there will be a stress $\psi[\epsilon(t)]$ due to this, together with the residual stresses due to all the previous deformations. Thus, the resultant value of the stress $\sigma(t,\epsilon)$ will be given by

$$\sigma(t,\epsilon)=\psi[\epsilon(t)]-\int_{-\infty}^{t}\phi(t-\tau)\epsilon(\tau)d\tau. \qquad \ldots\ldots(24)$$

In interpreting the delayed recovery effects observed in the present work on plastic and rubber specimens, it has been found convenient to use a slightly different treatment from that suggested by Boltzmann. This treatment is similar to that used by G. I. Taylor and E. Volterra (Taylor 1946) in their work on the mechanical behaviour of polythene at lower rates of loading, and an analogous approach has been described by Leaderman (1943) in his treatment of creep phenomena.

In this treatment, instead of considering the total strains to be maintained for short elements of time, we consider the small changes in strain which have occurred in the past history of the specimen and sum the residual elements of stress produced by them. Thus, if between the times $\tau$ and $\tau+\delta\tau$ the strain changes from $\epsilon$ to $\epsilon+\delta\epsilon$, this will result in a change of stress $\delta\sigma$ which will relax with time. If we call the final value of the stress when relaxation is complete $F(\delta\epsilon)$, then at time $t$ the residual value of the element of stress will be given by

$$\delta\sigma=F(\delta\epsilon)+f(t-\tau)\delta\epsilon, \qquad \ldots\ldots(25)$$

where $f(t-\tau)$ is a memory function which approaches zero as $t$ increases.

The resultant value of the stress $\sigma$ at time $t$ when the strain is $\epsilon$, is then given by

$$\sigma=F(\epsilon)+\int_{-\infty}^{t}f(t-\tau)\frac{d\epsilon}{d\tau}d\tau. \qquad \ldots\ldots(26)$$

A material whose mechanical behaviour is represented by (26) will not show any permanent strain but may show delayed recovery.

If when the strains are maintained for a sufficiently long time the material obeys Hooke's law, $F(\epsilon)$ will be given by $E\epsilon$ where $E$ is the value of the appropriate elastic modulus. Taylor (1946) has indicated how the function $f(t-\tau)$ can be determined from experimental results, but it was found that when this method was applied to the results of the present experiments the scatter was too large for a satisfactory determination of the function to be made. Instead, it was assumed that $f(t-\tau)$ was of the form $A\exp[-(t-\tau)/\alpha]$ and the values of $A$ and $\alpha$ which gave the best fit were then determined.

This assumption is equivalent to regarding the mechanical behaviour of the material as being similar to that of a system consisting of two springs in series, with a dashpot connected across one of the springs. The springs are assumed to obey Hooke's law and the dashpot is assumed to obey Newton's law of viscosity,

i.e. the viscous force is proportional to the velocity with which it moves. $E$ is then the effective elastic modulus of the two springs in series, and $(E+A)$ is the effective modulus for the spring which has no dashpot across it. The time of relaxation of the system is governed by the ratio of the magnitude of the viscous and elastic elements of the dashpot and spring in parallel.

In deriving the theoretical curves which are shown in the figures the relation used has been

$$\sigma = E\epsilon + A\int_0^t \exp[-(t-\tau)/\alpha]\frac{d\epsilon}{d\tau}d\tau, \qquad \ldots\ldots(27)$$

the values of $E$, $A$ and $\alpha$ having been chosen to give the best fit with the experimental results. It would appear possible to determine the value of $E$ experimentally, since it should correspond to the value of Young's modulus for strains which have taken place very slowly. Unfortunately, it is found (Alexandrov and Lazurkin 1940, Hillier and Kolsky 1949) that the value obtained for $E$ with many of these plastic materials depends on whether the forces are applied in times of the order of minutes, seconds or milliseconds, and it is consequently difficult to determine the appropriate value experimentally. In theory, the value to be taken should be that for strains which have been maintained for an infinitely long time, but since experimental evidence shows that irrecoverable plastic flow as well as relaxation phenomena of very much longer period take place, the exact experimental significance of $E$ in equation (27) is not so well defined, and it must be considered as an average value of the modulus for times long compared with the duration of the *dynamic* experiments but short compared with those of the *static* tests.

The assumption that with these materials there is only a single relaxation time is a considerable over-simplification of the problem. The assumption that Hooke's Law is obeyed exactly with stresses which have been applied slowly is also not altogether justified. Nevertheless, fairly good agreement with the experimental results was obtained for polythene and polymethyl–methacrylate on these assumptions. With rubber the agreement was less satisfactory and it seems clear that the model assumed will give only qualitative agreement with the actual behaviour of rubber at these rates of loading.

Figure 9 shows a plot of equation (27) with $A = 4{\cdot}6 \times 10^{10}$, $E = 10^9$, in dynes/cm$^2$, and $\alpha = 2\,\mu$sec.; the values of $\epsilon$ and $d\epsilon/d\tau$ were obtained from the experimental results with polythene and the observed values of stress are also shown in the figure. Using a similar treatment for results obtained with polythene, the stresses having been applied for times of the order of ten milliseconds, Taylor (1946) obtained lower values of $A$ and $E$ and the value given for $\alpha$ is 1·7 milliseconds. Thus, it would appear that relaxation phenomena are exhibited over a range of times, but that in a given experiment the relaxation times of the order of the duration of the experiment are the only ones that are of importance.

Figure 10 gives the theoretical curve for rubber, with $A = 2{\cdot}4 \times 10^{10}$, $E = 10^8$, and $\alpha$ is again taken as $2\,\mu$sec. The value of $E$ in this case is too small to affect the shape of the theoretical curve appreciably, and this value was chosen as one that corresponds to the modulus for stresses applied for times of the order of a few milliseconds. Although the values of $A$ and $\alpha$ used were the ones which gave the best agreement with the experimental results, it can be seen that quantitatively the agreement is not very good and a more complicated model must be considered to account for the exact shape of the stress–strain curve.

Figure 11 gives the curve for $A = 14{\cdot}5 \times 10^{11}$, $E = 8 \times 10^{10}$ and $\alpha = 0{\cdot}5\,\mu$sec. The agreement with the experimental results obtained with polymethyl–methacrylate is here quite close and the difference in the behaviour of this material and that of polythene and rubber thus appears to be due to the shorter effective relaxation time. This results in the term $E\epsilon$ becoming very much more important in determining the instantaneous values of the stress than it was with either polythene or rubber.

## § 7. CONCLUSION

The experimental method described in this paper has enabled measurements to be made of the stress–strain behaviour of materials in times of the order of $20\,\mu$sec. The main disadvantage of the method lies in the fact that the specimens have to be compressed between two parallel surfaces, and that even when lubricants are used, there is some uncertainty whether there is free lateral movement of the specimen, and whether the effects of friction between the specimen and the bar are not introducing large errors. Since, however, the use of different lubricants did not affect the results, and where permanent deformations were obtained they were fairly uniform with no evidence of *barrelling*, friction effects would not appear to be large. In the experiments, it was attempted to maintain two thin lubricant layers between the surfaces of the specimen and the faces of the bars, and since there was not sufficient time for the lubricant to be squeezed out, the conditions are in this respect more favourable from the point of view of eliminating friction than in comparable static experiments where the lubricant layers may become very thin.

The interpretation of the results has shown that very marked relaxation phenomena occur in plastics and rubber in the microsecond region, and that their mechanical properties under these rapid conditions of loading are very different from those observed when forces are applied more slowly. Although the assumption of a single relaxation time has led to reasonable agreement with the experimental results, the complicated molecular structure of these materials would indicate that a large number of different relaxation phenomena take place simultaneously and a more complicated memory function is applicable. Work at lower rates of loading (Alexandrov and Lazurkin 1940, Nolle 1947) has indicated that the dynamic behaviour of materials composed of macromolecules is very sensitive to temperature, and it would therefore seem desirable to continue these experiments over a wide range of temperatures.

The theoretical interpretation of rubber-like elasticity in terms of molecular processes, which has been put forward by several workers (Guth and Mark 1934, Kuhn 1936), shows that the high extension and low elastic modulus of rubber-like materials may be accounted for in terms of the uncurling of molecular chains under the influence of the applied stress; this involves the rotation of segments of the chains around single carbon–carbon bonds. Two other molecular processes associated with very much higher elastic moduli may also occur in these materials; these are changes in the values of the angles between the bonds and changes in the distances between adjacent carbon atoms. Since the increase of interatomic distances will require very large forces, it seems reasonable to correlate the two components of the elastic behaviour given in equation (27) with the changing of bond angles and the uncurling of chains. $E$ is then the modulus corresponding to the latter process and the integral involving the memory function corresponds

to the fact that the uncurling process requires times comparable with the time of application of the stress. Thus, when the stress is first applied, the initial deformation corresponds to only a change in the bond angles.

ACKNOWLEDGMENTS

The author wishes to thank Miss D. E. Spear for her help both with the experiments and with the often tedious calculations, and Mrs. M. J. Moore and Dr. K. W. Hillier for very useful discussions. He would also like to express his thanks to Professor R. M. Davies for encouragement and advice.

REFERENCES

ALEXANDROV, A. P., and LAZURKIN, J. S., 1940, *Acta Physicochimica U.R.S.S.*, **12**, 648, 669.
ALFREY, T., and DOTY, P., 1945, *J. Appl. Phys.*, **16**, 700.
BOLTZMANN, L., 1876, *Pogg. Ann. Erg.*, **7**, 624.
CHREE, C., 1889, *Proc. Camb. Phil. Soc.*, **14**, 250.
DAVIES, R. M., 1948, *Phil. Trans.* A, **240**, 375.
GROSS, B., 1947, *J. Appl. Phys.*, **18**, 212.
GUTH, E., and MARK, H., 1934, *Monat. Chem.*, **65**, 93.
HILLIER, K. W., and KOLSKY, H., 1949, *Proc. Phys. Soc.* B, **62**, 111.
HOPKINSON, B., 1914, *Phil. Trans.* A, **213**, 437.
KUHN, W., 1936, *Kolloidzschr.*, **76**, 258.
LANDON, J. W., and QUINNEY, H., 1923, *Proc. Roy. Soc.* A, **103**, 622.
LEADERMAN, H., 1943, *Elastic and Creep Properties of Filamentous Materials* (Washington : Textile Foundation).
LOVE, A. E. H., 1927, *Mathematical Theory of Elasticity* (Cambridge : University Press).
MASON, W. P., *et al.*, 1948, *Phys. Rev.*, **73**, 1074.
NAUNTON, W. J. S., and WARING, J. R. S., 1938, *Trans. Inst. Rubber Ind.*, **12**, 845.
NOLLE, A. W., 1947, *J. Acoust. Soc. Amer.*, **19**, 194.
PINKERTON, J. M. M., 1947, *Nature, Lond.*, **160**, 128.
POCHHAMMER, L., 1876, *J. reine angew. Math.*, **81**, 324.
ROBERTSON, R., 1921, *Trans. Chem. Soc.*, **119**, 1.
SLONIMSKY, G. L., 1940, *Acta Physicochimica U.R.S.S.*, **12**, 99.
TAYLOR, G. I., 1946, *J. Instn. Civ. Engrs.*, **8**, 486.
VALLEY, G. E., and WALLMAN, H., 1948, *Vacuum Tube Amplifiers* (New York : McGraw-Hill).

# A Method of Measuring some Dynamic Elastic Constants and its Application to the Study of High Polymers

By K. W. HILLIER
Imperial Chemical Industries Limited, Butterwick Research Laboratories, Welwyn, Herts.

*MS. received* 16*th May* 1949; *read before the Society* 7*th October* 1949

*ABSTRACT.* The preliminary work on the measurement of velocity of propagation and attenuation of longitudinal sound oscillations in high polymer filaments already described by Hillier and Kolsky has been continued. It was concluded in that paper that temperature control would be advantageous, and that by varying the temperature and the frequency of oscillations more useful information could be acquired. An apparatus is described whereby the velocity of propagation and the attenuation of longitudinal oscillations throughout the range 0° to 50° C. and 500 c/s. to 30 kc/s. can be measured. The results obtained with one material, polythene, are discussed in terms of several theories of the elasticity of high polymers, and the constants of the several equations considered are calculated from the data.

## § 1. INTRODUCTION

The aim of the investigation was to study the mechanical behaviour of some long chain polymers when subjected to small, rapidly changing forces, in order to separate the elastic and plastic components of strain. The method employed was to send a sonic or ultrasonic longitudinal wave along a filament of the material, and to measure the velocity of propagation $V$ and the attenuation per unit length $\alpha$. The theory of the method used has been reported previously (Hillier and Kolsky 1949). The values of $V$ and $\alpha$ were obtained for several frequencies between 500 c/s. and 30 kc/s., and for temperatures between 0° and 40° C. From the results obtained for polythene it has been possible to obtain values for an equivalent mechanical model in the manner described by Alfrey (1948), and to discuss other methods of expressing the results, (*a*) in terms of a complex compliance by analogy with the dielectric equations given by Fuoss and Kirkwood (1941) and others, and (*b*) in terms of Maxwell's equation, derived from a definition of viscosity (Maxwell 1868).

## § 2. DESCRIPTION OF APPARATUS

The apparatus can be conveniently considered in two parts: (*a*) the constant temperature enclosure containing the filament, and (*b*) the velocity and attenuation measuring equipment.

The constant temperature enclosure (Figure 1) consisted of a copper tube 10 S.W.G., six inches in diameter and twelve feet long. This length was required so that measurements could be made on filaments whilst they were drawn to four or five times their original length. On to the outside of this tube was wound, and fixed by spot welding, a spiral of 16 S.W.G. wire with a pitch of three inches per turn. Over this was slid a second copper tube slightly shorter than the first, thus enclosing an annular space. The wire diameter was such as to seal the gap between the two tubes so that when oil was pumped into one end of the annular

gap it was spiralled round the tube before emerging at the far end. The heat transfer was thus high, and by using a large, well-lagged reservoir tank and a high-speed oil pump the inside of the tube oven could be maintained at any constant temperature within the range. To reduce heat loss and avoid local air pockets the copper tubes were mounted in a sealed wooden box of square cross section, so constructed that the tube rested in the centre with adequate air space all round. A centrifugal fan was coupled to the apparatus with flexible hose couplings, and air was driven along the outside of the tubes and returned to the fan via the inside space. The air system was closed so that both sides of the fan were used, and the pressure was nowhere very far from atmospheric. The oil pumped between the copper tubes was stored in a tank equipped with an immersion heater and refrigerating coil, and was lagged with 3 in. thick cork slabs. Suitable thermostats kept the oil temperature at a constant value in the tank, and the thermostats were sufficiently sensitive to maintain the air temperature in the oven constant to within 1° c. throughout the range 0° to 60° c. The temperature could be measured to 0·5° c. continually by means of a calibrated thermocouple.

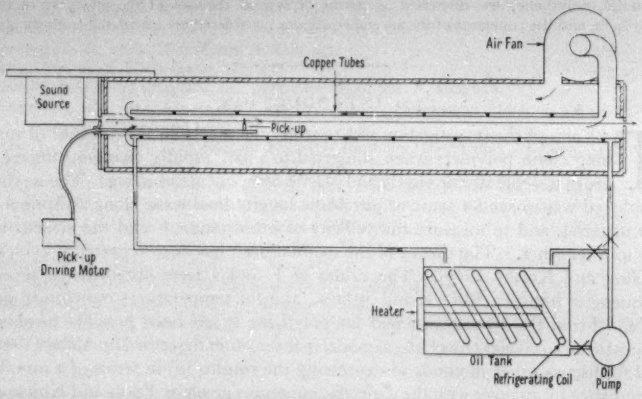


Figure 1.

The measurement apparatus consisted of a crystal pick-up mounted on a carriage sliding on two long parallel cylindrical steel rods rigidly clamped together. This part of the apparatus was mounted in the constant temperature oven. The carriage was driven along the rods by means of a lead screw mounted between them and rotated from outside by a small reversing electric motor through a reduction gear and flexible drive. Provision was made for ascertaining the position of the carriage by using a flexible steel tape fixed at one end to the carriage and sliding past a fixed mark on the outside of the oven (Figure 2). The sound source was either a modified moving-coil mains energized speaker as described previously (Hillier and Kolsky 1949), used for frequencies up to 10 kc/s., or a magnetostriction transducer, used up to 30 kc/s. This transducer consisted of a nickel tube sealed at one end by a small pin chuck used to hold the filament coaxially, and with water-cooling tubes at the other end as shown in Figure 3.

The nickel tube was held in a ring clamp on which was mounted the energizing coil. Although no effort was made to drive the nickel tube at its resonant frequency, provision was made for altering the effective length to increase the response at selected frequencies.

The crystal pick-up was connected to the main amplifier by a coaxial cable with insulated outer screen so that the pick-up, insulated from the oven, could be kept at the amplifier earth. The amplifier was a three-stage, wide band-pass unit with negative voltage feedback to stabilize it and was used with a Cossor 339 double beam oscilloscope as previously. The sound source was fed from an R-C wide range oscillator (Dawe Instruments, Type 400B) through a suitable power amplifier. A valve voltmeter was used to measure the r.m.s. voltage on the $Y_1$ plates so that a measure of the amplitude variation along the filament

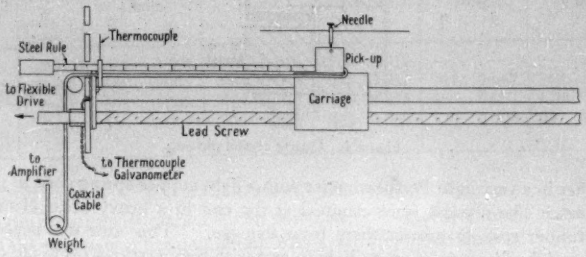


Figure 2. Pick-up carriage and drive.

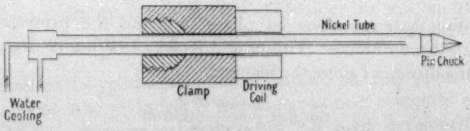


Figure 3. Magnetostriction oscillator.

could be made. To obtain the velocity of sound from the measurements of phase shift the frequency of the oscillator must be known. A quartz crystal oscillator and frequency dividing unit were built so that 100 kc/s. and 25 kc/s. signals were available to calibrate the wide-band driving oscillator. The quartz crystal used was of special low temperature coefficient cut, and it was considered that the frequency of 25 kc/s. was accurate to within 0·5%. As in the previous work, equipment was available to extend the filament at a constant rate, and to measure the tension in the filament at the same time as velocity measurements were being made. The apparatus for this is shown in Figure 6.

For all the work at frequencies up to 10 kc/s. and for temperatures up to 40° c. an ordinary piezo-electric gramophone pick-up cartridge was employed together with the type of needle described previously (Hillier and Kolsky 1949). For higher temperatures and for frequencies above 10 kc/s. at all temperatures, a quartz crystal unit was designed so that the inertia effects, which reduced the output of the ordinary type of unit above that frequency, and the temperature effect, which rendered Rochelle salt useless above 45° c., could be eliminated.

The unit is shown in Figure 4. For simplicity and ruggedness a simple bending system was employed; two rectangular silvered quartz plates 1 mm. thick and $\frac{5}{8}$ in. $\times \frac{1}{4}$ in. in dimensions, cut with X axes perpendicular to the face, were cemented

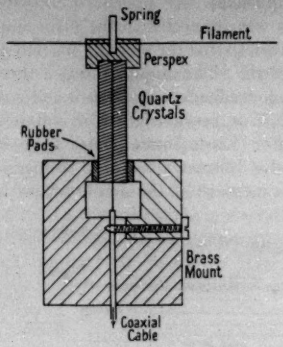


Figure 4. Quartz crystal pick-up.

together in a very light Perspex holder with a light copper spring used to grip the filament. The crystals were clamped at the end in a heavy brass clamp with thin rubber pads to protect them from damage. This unit was successfully employed for frequencies up to 30 kc/s. and with temperatures up to 60° C.

## § 3. RESULTS

The relation between observed phase shift and the propagation constants has previously been obtained (Hillier and Kolsky 1949), and if $\theta$ is the value of phase shift at a distance $l$ along the filament

$$\tan\theta = \frac{1+me^{-\alpha l}}{1-me^{-\alpha l}}\tan kl$$

where $m$ is the reflection coefficient at the pick-up, $k$ is equal to $2\pi/\lambda$, $\alpha$ the attenuation factor and $\lambda$ is the wavelength of sound oscillations in the material. The amplitude ratio $B/A$ is

$$B/A = (1-m)e^{-\alpha l}/(1-2me^{-\alpha l}\cos 2kl + m^2e^{-4\alpha l})^{\frac{1}{2}}.$$

For large values of $l$, $\theta = kl$, and accurate values can be obtained from the slope of the graph of $\theta$ against $l$. Similarly for large values of $l$ and $\alpha$, $B/A = Ke^{-\alpha l}$, and hence plotting $\log(B/A)$ against $l$ resulted in a line whose slope gave the value of $\alpha$. For intermediate values of $\alpha$ a different method was employed which was not so accurate (Hillier and Kolsky 1949). Another approximation is given by Ballou and Smith (1949).

The method gave results of the same general accuracy as those described previously. The frequency, however, was known to a greater accuracy and the temperature maintained more constant, so that more consistent results were obtained. Experiments were carried out on a variety of materials throughout the range of temperature and frequency. The most comprehensive results were obtained on a sample of polythene supplied by I.C.I. Alkali Division, Alkathene grade 20. Annealed filaments approximately 0·025 in. diameter and 150 cm.

long were used. Table 1 gives the values for velocity of propagation and the attenuation per unit length for this material. The results represent the mean of several experiments having a variation of less than 3% for the velocity measurements and 10% for the attenuation. It is hoped to publish later further results with other materials and also the results for experiments when the material was drawn during measurements. 'Static' values, $E_S$, of Young's modulus calculated from these stretching experiments with polythene are, however, included in Table 1.

Table 1. Values of $V$ (m/s.), $\alpha$ ($cm^{-1}$) and $E_S$ ($\times 10^8$ dynes/$cm^2$) for Polythene.

| Temp. (° c) | $E_S$ | Frequency | | | | | | | | | |
|---|---|---|---|---|---|---|---|---|---|---|---|
| | | 1 kc/s. | | 2 kc/s. | | 5 kc/s. | | 10 kc/s. | | 16 kc/s. | |
| | | $V$ | $\alpha$ | $V$ | $\alpha$ | $V$ | $\alpha$ | $V$ | $\alpha$ | $V$ | $\alpha$ |
| 0 | 26·0 | 1041 | 0·005 | 1066 | 0·010 | 1108 | 0·019 | — | — | — | — |
| 10 | 10·92 | 866 | 0·005 | 903 | 0·013 | 926 | 0·032 | 944 | 0·047 | 960 | 0·086 |
| 30 | 5·30 | 608 | 0·008 | 615 | 0·017 | 639 | 0·035 | 650 | 0·077 | 670 | 0·114 |
| 40 | 4·60 | 510 | 0·007 | 520 | 0·022 | 535 | 0·068 | 538 | 0·105 | 547 | 0·138 |

## §4. DISCUSSION OF RESULTS

In the experiments carried out on polythene, the velocity of phase propagation $V$ and the attenuation per unit length $\alpha$ for small amplitude sinusoidal oscillations along the filament have been measured.

In order to correlate these measurements with physical constants of the material, such as elasticity, it is necessary to consider the relation between stress, strain and time for the material, and then to derive the wave propagation constants $V$ and $\alpha$.

The fundamental hypothesis put forward as a starting point in a study of the deformation of real materials is the superposition principle enunciated by Boltzmann (1876). A more general theory has been developed by Volterra (1912), which includes Boltzmann's theory as a special case. This theory, of considerable mathematical complexity, is based on the theory of functionals (Volterra 1931). These are discussed in a recent paper by Kolsky (1949).

From time to time equations have been proposed relating stress, strain and time for the deformation of certain materials, which should have a limited use. Such equations are not intended to apply universally, but to be related to some specific conditions of material, stress or time (duration of stress). Maxwell (1868) suggested a differential equation to include both elastic and viscous behaviour, and since this equation has had very wide application and has formed the basis of much subsequent work, it is worth quoting.

If $\sigma$ is the elastic force acting and $\epsilon$ is the strain produced, then, for a material obeying Hooke's law, $\sigma = E\epsilon$ where $E$ is the elastic modulus. If viscosity is present then $\sigma$ will vary with time at a rate dependent on $\sigma$ and the nature of the body. Consider this rate proportional to $\sigma$, then

$$\frac{d\sigma}{dt} = E\frac{d\epsilon}{dt} - \frac{\sigma}{\tau}, \qquad \ldots\ldots (3)$$

$1/\tau$ being the constant of proportionality.

If $d\epsilon/dt$ is constant, $\sigma = E\tau(d\epsilon/dt) + Ce^{-t/\tau}$. Then $E\tau$ is the coefficient of viscosity and $\tau$ is a time called the time of relaxation. A perfectly elastic body has an infinite relaxation time, and for a purely viscous fluid $\tau = 0$. Equation (3) does not hold for many materials or over a wide range of stress and time intervals, but the idea of relaxation time has been extended and has proved very useful.

The concept of separating the elastic and viscous components of strain has given rise to the use of models to represent the mechanical behaviour of materials and to allow for calculation of the results of specific applied stresses. The simplest such model is based on Maxwell's treatment, where an elastic component and a viscous component are joined in series. Such models can consist of either mechanical or electrical components (Alfrey 1948, Gemant 1936). Either the behaviour of the material is calculated by analysing a system of springs (pure elastic elements) and dashpots (viscous elements) linked in some manner (mechanical analogue) or by computing the current or E.M.F. in an electrical circuit containing capacity and resistance (electrical analogue). Simha (1942) has given a generalized model theory.

Frenkel and Obrastov (1940) have published a generalization of Maxwell's equation using tensor notation and the postulate of 'volume viscosity'. Their final complete equation contains seven constants. The results of any ordinary tests made on real materials are very difficult to put into this very complicated equation, so that the evaluation of the constants and a verification of the equation are both difficult and tedious.

Tobolsky, Powell and Eyring (1943) have published an account of a physical theory based on Eyring's rate process conception and certain free energy hypotheses. In this theory a deformation is considered as affecting a kinematic unit of molecular dimensions, and for a macro-body the stress–strain–time equation is the sum of all such small unit deformation processes. Thermal agitation will result in an oscillation of the unit about its mean position in some form of 'energy well'. If a potential gradient is formed by the application of stress, such that work is done when a unit moves in a specific direction, then the net velocity of units in the direction of the gradient can be evaluated by summation. When certain assumptions are made as to the kinetic units and the type of energy well in which they oscillate, this theory can be shown to be akin to the model theory. The treatment is of interest in that it incorporates temperature as a further variable and enables thermodynamic relationships to be developed.

It is proposed now to consider three equations connecting stress, strain and time: first, Maxwell's equation, secondly, one based on a model in which a spring of elasticity $E$ and a dashpot of constant $\eta^*$ are connected in parallel, as in Figure 5($a$), and thirdly, a composite model akin to the second, but with an added spring in series with the spring–dashpot unit (Figure 5($b$)). For each of these equations the constant of elasticity and relaxation time will be derived in terms of the velocity of phase propagation $V$ and the attenuation $\alpha$.

In all cases $u$ is the displacement along the $x$ axis, i.e. along the filament, and $\sigma$, the applied stress, is of the form $\sigma = \sigma_0 \sin \omega t$ at $x = 0$.

(1) *Maxwell's equation.*

From equation (3), $E\dfrac{d\epsilon}{dt} = \dfrac{\sigma}{\tau} + \dfrac{d\sigma}{dt}$, and $\epsilon = \dfrac{du}{dx}$.

Thus
$$E\frac{d^2u}{dx\,dt} = \frac{\sigma}{\tau} + \frac{d\sigma}{dt}. \qquad \ldots\ldots (4)$$

By Newton's laws, since acceleration is $d^2u/dt^2$ and increment of force is $d\sigma/dx$,

$$\rho d^2u/dt^2 = d\sigma/dx \qquad \ldots\ldots (5)$$

where $\rho$ is the mass per unit length of filament.

A solution of these two equations of the form

$$u = u_0 \exp i\omega(t - x/c); \quad \sigma = \sigma_0 \exp i\omega(t - x/c)$$

satisfies the condition $\sigma = \sigma_0 \sin \omega t$ at $x = 0$.

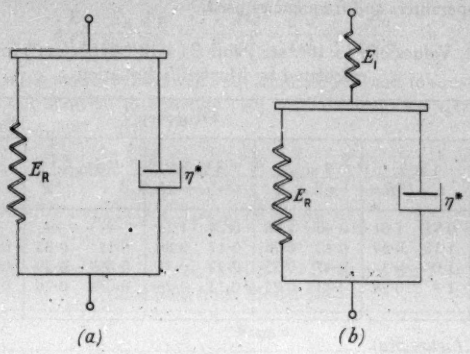


Figure 5.

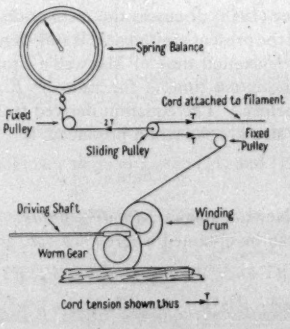


Figure 6.

The equation $u = u_0 \exp i\omega(t - x/c)$ is a form of the wave equation with frequency $\omega/2\pi$ and with complex propagation constant $c = a + ib$. Then

$$u = u_0 \exp -b\omega x/(a^2 + b^2) \exp i\omega\{t - ax/(a^2 + b^2)\} \qquad \ldots\ldots (6)$$

A damped wave propagated in the direction of $x$ with frequency $\omega/2\pi$ will give rise to a particle displacement $u$ given by

$$u = u_0 \exp(-\alpha x) \exp i\omega(t - x/V).$$

Thus the attenuation factor $\alpha = b\omega/(a^2 + b^2)$ and the velocity $V = (a^2 + b^2)/a$.

From equations (4), (5) and (6)

$$a^2 = \tfrac{1}{2}(E/\rho)\{\omega\tau/(1+\omega^2\tau^2)\}\{(1+\omega^2\tau^2)^{\frac{1}{2}}+\omega\tau\}$$

and

$$b^2 = \tfrac{1}{2}(E/\rho)\{\omega\tau/(1+\omega^2\tau^2)\}\{(1+\omega^2\tau^2)^{\frac{1}{2}}-\omega\tau\}.$$

whence

$$\left.\begin{aligned}\tau &= (\omega^2 - V^2\alpha^2)/2V\alpha\omega^2,\\ E &= V^2\omega^2\rho/(\omega^2 - V^2\alpha^2).\end{aligned}\right\} \quad \ldots\ldots (7)$$

Table 2 gives values of $\tau$ and $E$ corresponding to the values of $V$ and $\alpha$ at the various temperatures and frequencies used.

Table 2. Values of $\tau$ ($\times 10^{-3}$ sec.) and $E$ ($\times 10^{10}$ dynes/cm$^2$) for Polythene calculated by Maxwell's Equation

| Temp. (° c.) | Frequency | | | | | | | | | |
|---|---|---|---|---|---|---|---|---|---|---|
| | 1 kc/s. | | 2 kc/s. | | 5 kc/s. | | 10 kc/s. | | 16 kc/s. | |
| | $\tau$ | $E$ | $\tau$ | $E$ | $\tau$ | $E$ | $\tau$ | $E$ | $\tau$ | $E$ |
| 0 | 0·95 | 1·01 | 0·46 | 1·06 | 0·24 | 1·14 | — | — | — | — |
| 10 | 1·15 | 0·69 | 0·42 | 0·76 | 0·17 | 0·80 | 0·11 | 0·83 | 0·060 | 0·86 |
| 30 | 1·0 | 0·3 | 0·47 | 0·35 | 0·22 | 0·37 | 0·099 | 0·39 | 0·065 | 0·41 |
| 40 | 1·4 | 0·24 | 0·43 | 0·25 | 0·14 | 0·26 | 0·088 | 0·26 | 0·066 | 0·27 |

(ii) *Model, Figure* 5(*a*).

This model represents a system exhibiting a *retarded* elasticity and is different from the Maxwell treatment where two separate mechanisms of response to stress are postulated. Alfrey (1948) discusses the distinction between the two systems in some detail, but for the present argument it is sufficient to note that a time factor corresponding to the relaxation time of Maxwell's equation can be obtained for the model. This *retardation* time is the ratio $\eta^*/E$ and can conveniently be represented by $\tau$ as before. The equation derived from the model, where $\sigma$, as before, is the applied stress, $\epsilon$ the strain produced, is

$$\sigma = E\epsilon + \eta^* \frac{d\epsilon}{dt}, \quad \ldots\ldots (8)$$

and, as before, by Newton's laws $\rho d^2u/dt^2 = d\sigma/dx$. A solution of the form $u = u_0 \exp i\omega(t - x/c)$ can be obtained where $c = a + ib$, and

$$a^2 = \tfrac{1}{2}(E/\rho)\{(1+\omega^2\tau^2)^{\frac{1}{2}}+1\}; \quad b^2 = \tfrac{1}{2}(E/\rho)\{(1+\omega^2\tau^2)^{\frac{1}{2}}-1\},$$

whence

$$\tau = 2V\alpha/(\omega^2 - V^2\alpha^2); \quad E = \rho V^2\omega^2(\omega^2 - V^2\alpha^2)/(\omega^2 + V^2\alpha^2)^2 \ldots\ldots (9)$$

Table 3 gives values of $\tau$ and $E$ for this system. It can be seen from equations (7) and (9) that the product of the relaxation and the retardation time is equal to $1/\omega^2$, which furnishes a check on the computations.

(iii) *Model, Figure* 5 (*b*).

The model shown in Figure 5(*b*) gives an explanation of the behaviour attributed to a retarded elasticity. It cannot explain the instantaneous elastic response or the fact that the velocity of sound at very high frequencies is still finite. In order to improve on this model a component to represent the residual elasticity, effective at high frequencies, has been included. To the system illustrated by Figure 5 (*a*) a second spring has been added in series. This leads

to the following equations where, as before, $\sigma$ and $\epsilon$ are the stress and strain of the total system and $E$, $E_R$ and $\eta^*$ are the constants of the springs and dashpots. If $\epsilon_1$ and $\epsilon_R$ are the strains in each part separately so that $\epsilon=\epsilon_1+\epsilon_R$, then

$$\sigma=E_1\epsilon_1=E_R\epsilon_R+\eta^*(d\epsilon_R/dt)$$

and, as before, $\rho(d^2u/dt^2)=d\sigma/dx$ and $\tau=\eta^*/E_R$. The following differential equation connecting the displacement $u$ and the constants of the system can be obtained:

$$\rho\frac{E_1+E_R}{E_1E_R}\frac{d^2u}{dt^2}+\rho\frac{\tau}{E_1}\frac{d^3u}{dt^3}=\frac{d^2u}{dx^2}+\tau\frac{d^3u}{dx^2dt} \qquad \ldots\ldots(10)$$

This equation must reduce to Maxwell's equation if $E_R=0$ and to equations (8) and (9) if $E_1=\infty$. A solution to equation (10) is of the form $u=u_0\exp i\omega(t-x/c)$ where $c$ is complex, and is given by

$$\frac{1}{c^2}=\frac{\rho(E_1+E_R)+\rho E_R\omega^2\tau^2}{E_1E_R(1+\omega^2\tau^2)}-\frac{i\rho E_1\omega\tau}{E_1E_R(1+\omega^2\tau^2)}. \qquad \ldots\ldots(11)$$

Now
$$1/c^2=(\omega^2-V^2\alpha^2)/V^2\omega^2-i2\alpha/V\omega. \qquad \ldots\ldots(12)$$

Table 3. Values for $\tau'(\times10^{-3}$ sec.) and $E'$ $(\times10^9$ dynes/cm$^2)$ for Polythene calculated from Model 5*a*.

| Temp. (° c.) | Frequency | | | | | | | | | |
|---|---|---|---|---|---|---|---|---|---|---|
| | 1 kc/s. | | 2 kc/s. | | 5 kc/s. | | 10 kc/s. | | 16 kc/s. | |
| | $\tau'$ | $E'$ | $\tau'$ | $E'$ | $\tau'$ | $E'$ | $\tau'$ | $E'$ | $\tau'$ | $E'$ |
| 0 | 0·03 | 9·9 | 0·014 | 10·4 | 0·004 | 11·2 | — | — | — | — |
| 10 | 0·02 | 6·8 | 0·015 | 7·3 | 0·006 | 7·7 | 0·002 | 8·1 | 0·002 | 8·3 |
| 30 | 0·03 | 3·3 | 0·013 | 3·4 | 0·005 | 3·7 | 0·003 | 3·8 | 0·002 | 4·0 |
| 40 | 0·02 | 2·3 | 0·015 | 2·3 | 0·007 | 2·5 | 0·003 | 2·6 | 0·001 | 2·7 |

Equating the real and imaginary parts of $1/c^2$ in (11) and (12),

$$\frac{2\alpha}{V\omega}=\frac{\rho\omega\tau}{E_R(1+\omega^2\tau^2)} \qquad \ldots\ldots(13)$$

and
$$\frac{\omega^2-V^2\alpha^2}{V^2\omega^2}=\frac{\rho(E_1+E_R)+\rho E_R\omega^2\tau^2}{E_1E_R(1+\omega^2\tau^2)}. \qquad \ldots\ldots(14)$$

For very long times, so-called 'static' loading, the response of the system will be given by the elastic response of the two springs in series, i.e. the 'static' modulus $E_S$ is given by $1/E_S=1/E_1+1/E_R$. This modulus was measured in the course of the experiments carried out to investigate the change in velocity of sound on stretching the material, and values of this 'static' modulus at each temperature are given in Table 1. Then from equations (13) and (14), replacing $E_1$ and $E_R$ by $E_S$,

$$\tau=\frac{V}{2\alpha E_S}-\frac{\omega^2-V^2\alpha^2}{2V\alpha\omega^2}. \qquad \ldots\ldots(15)$$

Table 4 gives the values of $\tau$ calculated by equation (15) at the various frequencies and temperatures used.

As can be seen from Tables 2, 3 and 4, the values of $E$ and $\tau$ are not constant with respect to frequency, and this can be regarded as showing the existence of a spread of relaxation or retardation times over the time scale. Experiments at much lower frequencies carried out on high polymer materials of similar long chain structure, e.g. rubber (Alexandrov and Lazurkin 1940), have demonstrated the existence of relaxation times of the order 0·1 sec. to 0·01 sec.; long term creep experiments (Leaderman 1943) have indicated that some relaxation processes may have characteristic times of the order of minutes or days, and very recently Kolsky (1949) has shown that at very high rates of loading, relaxation effects in times of the order of microseconds occur. Consideration of the molecular processes that can occur in a material consisting of long chain molecules very slightly cross linked or, as in the case of polythene, held by regions of crystallization (Bunn and Alcock 1945), is consistent with such a spectrum of relaxation times.

Table 4. Values of $\tau$ ($\times 10^{-3}$ sec.) for Polythene calculated from Model 5*b*.

| Temp. (° c) | Frequency | | | | |
|---|---|---|---|---|---|
| | 1 kc/s. | 2 kc/s. | 5 kc/s. | 10 kc/s. | 16 kc/s. |
| 0 | 2·78 | 1·4 | 0·8 | — | — |
| 10 | 6·0 | 2·5 | 1·06 | 0·73 | 0·412 |
| 30 | 5·5 | 2·6 | 1·4 | 0·626 | 0·439 |
| 40 | 6·0 | 1·9 | 0·64 | 0·415 | 0·323 |

It was mentioned previously that Tobolsky, Powell and Eyring had considered a system based on molecular forces which introduced temperature as a variable. A brief summary of a simple system of this kind is given below, together with its application, to give an approximate estimate of the energy of activation of the process responsible for the retarded elasticity effect in polythene at the frequencies and temperatures given in Table 3.

The molecular unit is assumed to exist in a potential well, of form $F=\frac{1}{2}\Delta F(1-\cos 2\pi x/\lambda)$, where $\lambda$ is the distance between minima, $x$ is the distance from the unit and $\Delta F$ is the free energy of activation, that is the height of the barrier. The effect of an imposed stress field will be to add a linear term $-\sigma Ax$ where $\sigma$ is the stress and $A$ the effective area of the unit.

The total free energy as a function of $x$ is $F=\frac{1}{2}\Delta F(1-\cos 2\pi x/\lambda)-\sigma Ax$. Tobolsky, Powell and Eyring have shown that when $\sigma A\lambda \ll 2\boldsymbol{k}T$ and $\sigma A\lambda \gg F$, then

$$\frac{d\epsilon}{dt}=\frac{\lambda^2 A}{\lambda_1 2\pi^2\Delta F}\frac{d\sigma}{dt}+\frac{\lambda^2 A\sigma}{\lambda_1 \boldsymbol{h}}\exp(-\Delta F/\boldsymbol{k}T.)$$

This can be identified with $$\frac{d\epsilon}{dt}=\frac{1}{E}\frac{d\sigma}{dt}+\frac{1}{\eta^*}\sigma$$

where $$\frac{1}{E}=\frac{\lambda^2 A}{\lambda_1 2\pi^2\Delta F}\,;\quad \frac{1}{\eta^*}=\frac{\lambda^2 A}{\lambda_1 \boldsymbol{h}}\exp-\frac{\Delta F}{\boldsymbol{k}T}$$

or, if $\eta^*/E=\tau$, $$\frac{d\sigma}{dt}=E\frac{d\epsilon}{dt}-\frac{\sigma}{\tau}\quad \text{(cf. equation (3)).}$$

Then $$\tau=\frac{\eta^*}{E}=\frac{\boldsymbol{h}}{2\pi^2}\frac{1}{\Delta F}\exp\Delta F/\boldsymbol{k}T, \qquad \text{i.e., } \ln\tau=K+\Delta F/\boldsymbol{R}T$$

Hence, if one molecular process is involved in the retarded elasticity effect, $\ln \tau$ plotted against $1/T$ should give a straight line of slope $\Delta F/k$.

From the results can be obtained the order of the activation energy for the process involved in this high rate low amplitude deformation. The value obtained for activation energy is approximately 200 cal/gr. mol. at 2 kc/s.

It has been suggested that a different method of expressing the results might lead to a more useful theoretical treatment. In the case of a dielectric exhibiting a frequency variation of dielectric constant and power factor the results of experi-

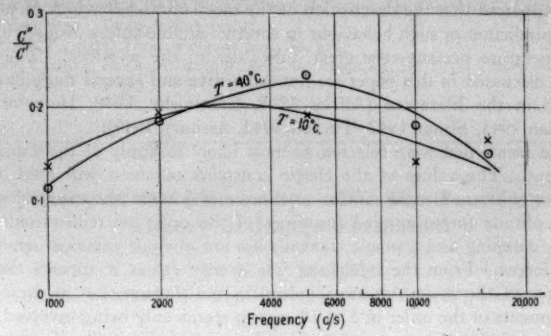


Figure 7. Values of the ratio of the imaginary to the real parts of the complex compliance against log frequency.

Table 5. Values of $C'$ ($\times 10^{-10}$ cm$^2$/dyne) and $C''$ ($\times 10^{-11}$ cm$^2$/dyne)*

| Temp. (° c). | Frequency | | | | | | | | | |
|---|---|---|---|---|---|---|---|---|---|---|
| | 1 kc/s. | | 2 kc/s. | | 5 kc/s. | | 10 kc/s. | | 16 kc/s. | |
| | $C'$ | $C''$ | $C'$ | $C''$ | $C'$ | $C''$ | $C'$ | $C''$ | $C'$ | $C''$ |
| 0 | 0·988 | 1·65 | 0·941 | 1·61 | 0·874 | 1·18 | — | — | — | — |
| 10 | 1·44 | 1·99 | 1·32 | 2·48 | 1·25 | 2·38 | 1·21 | 1·72 | 1·17 | 1·93 |
| 30 | 2·95 | 4·60 | 2·88 | 4·8 | 2·68 | 3·84 | 2·58 | 4·14 | 2·43 | 3·73 |
| 40 | 4·24 | 4·84 | 4·06 | 7·46 | 3·82 | 8·96 | 3·80 | 6·88 | 3·68 | 5·56 |

* $C'$ and $C''$ are the real and imaginary parts of the complex compliance for polythene.

ments can be considered in terms of a complex dielectric constant (Fuoss and Kirkwood 1941). By analogy it is possible to consider a complex compliance (reciprocal of elastic modulus) on a similar basis (M.I.T. Acoustics Laboratory 1947).

In a simple material $\rho c^2 = 1/C$, where $c$ is the propagation constant and $C$ is the compliance. Then if $C = C' + iC''$, we have $\rho(C' + iC'') = 1/c^2$.

Now if particle displacement $u$ is given by

$$u = u_0 \exp i\omega(t - x/c),$$

where $c = a + ib$, it can be shown that

$$\rho C' = (\omega^2 - V^2\alpha^2)/V^2\omega^2; \quad \rho C'' = -2\alpha/V\omega,$$

where, as before, $V$, $\alpha$ and $\omega$ are velocity of propagation, attenuation factor and pulsatance respectively. In the case of dielectrics, the ratio of imaginary to real parts of the complex constant is equal to $\tan\delta$, the loss in the dielectric. Then $C''/C'$ can be regarded as representing the mechanical loss in the material. Table 5 gives values for two quantities $C'$ and $C''$, and Figure 7 shows the variation of $C''/C'$ with frequency for one temperature.

## § 5. CONCLUSIONS

It is apparent that the description of the mechanical behaviour of polymers and the prediction of such behaviour in specific circumstances of load, load rate and temperature present very great difficulties to the physicist. The several methods discussed in this paper are not exhaustive and several more have been discussed in the literature (Alfrey 1948, Slonimsky 1940, Houwink 1937, Leaderman 1943, Simha 1942, Tuckett 1942, Astbury 1949).

Those mentioned were selected as most likely to apply to the experiments carried out. The values of the elastic constants obtained will hold only for conditions of stress loading similar to those met with in the experiments, i.e., small amplitude forces applied for times of the order of milliseconds; both vibration damping and acoustic transmission are obvious practical applications of such forces. From the calculated free energy values it appears that quite small units of the molecules are involved in the transmission of these forces, chain segments of the order of 5 to 10 carbon atoms only being involved. This conclusion is, however, very suspect, since the results indicate that the supposition of a single operative relaxation process is unjustified. Any experiment can only select relaxation effects that have constants in its immediate time scale, so that altering the temperature will merely select a different set of relaxation processes for study. To regard the results as implying that the processes involved at temperature A respond differently at temperature B is inaccurate. Until more details are known about the spread of relaxation effects, calculations of activation energies for the processes involved will give very low values.

The general conclusion must be made that an elucidation of the problems of high polymer molecular physics requires that very wide ranges of both time and temperature should be investigated before a solution can be reached.

## ACKNOWLEDGMENTS

The author wishes to express his thanks to Dr. H. Kolsky for his help and advice in many discussions during this work, to Mr. W. T. Moore for the engineering design and construction of the apparatus, and to Mr. D. A. Gray for his help in the experimental measurements.

## REFERENCES

ALEXANDROV, A. P., and LAZURKIN, J. S., 1940, *Acta Physicochimica U.R.S.S.*, **12**, 648.
ALFREY, T., 1948, *Mechanical Behaviour of High Polymers* (New York : Interscience).
ASTBURY, N. F., 1949, *Proc. Roy. Soc.* A, **196**, 92.
BALLOU, J. W., and SMITH, J. C., 1949, *J. Appl. Phys.*, **20**, 493.
BOLTZMANN, L., 1876, *Pogg. Ann. Erg.*, **7**, 624.
BUNN, C. W., and ALCOCK, T. C., 1945, *Trans. Faraday Soc.*, **41**, 317.
FRENKEL, J., and OBRASTOV, J., 1940, *J. Phys. U.R.S.S.*, **2**, 131.
FUOSS, R. M., and KIRKWOOD, J. G., 1941, *J. Amer. Chem. Soc.*, **63**, 385.
GEMANT, A., 1936, *Physics*, **7**, 311.

HILLIER, K. W., and KOLSKY, H., 1949, *Proc. Phys. Soc.* B, **62**, 111.
HOUWINK, R., 1937, *Elasticity, Plasticity and the Structure of Matter* (Cambridge: University Press).
KOLSKY, H., 1949, *Proc. Phys. Soc.* B, **62**, 676.
LEADERMAN, H., 1943, *Elastic and Creep Properties of Filamentous Materials* (Washington: Textile Foundation).
MAXWELL, C., 1868, *Phil. Mag.*, Ser. 4, **35**.
M.I.T. Acoustics Laboratory, 1947, *Quarterly Progress Report*, April, p. 16.
SIMHA, R., 1942, *J. Appl. Phys.*, **13**, 201.
SLONIMSKY, G. L., 1940, *Acta Physicochimica U.R.S.S.*, **12**, 99.
TOBOLSKY, A. V., POWELL, R. E., and EYRING, H., 1943, *The Chemistry of Large Molecules* (New York: Interscience), p. 125.
TUCKETT, R. F., 1942, *Trans. Faraday Soc.*, **38**, 310.
VOLTERRA, V., 1912, *Rendiconti della R. Acad. dei Lincei*, **21**, II; 1931, *Theory of Functionals* (London: Blackie).

---

# The Theory of the Microscope—IV: The Boundary-Wave Theory of Image Formation

BY L. C. MARTIN
Technical Optics Department, Imperial College of Science and Technology, London

*MS. received* 1*st April* 1949; *read before the Optical Group* 11*th June* 1948

*ABSTRACT.* The theory of boundary waves (Young, Rubinowicz, and others) is developed for the two-dimensional case and applied to discuss image formation for small apertures, obstacles and phase-retarding laminae. The theoretical predictions are illustrated by diffraction photographs. It is hoped thus to contribute towards a fuller understanding of microscope images for bright-field, dark-field and phase-contrast conditions.

## §1. INTRODUCTION

IN 1917, A. Rubinowicz, starting with the well-known Kirchhoff scalar diffraction theory, showed that the effects of diffraction by an aperture in a thin screen could be written down as the sum of (*a*) the amplitude which could be predicted if the domain of the direct light were strictly limited by rectilinear propagation from the source, plus (*b*) the integral of certain amplitude contributions derived from the boundary of the aperture.

This theory can be applied simply to explain the edge-diffraction effects which occur in important types of image formation, especially dark-ground illumination and phase-contrast. Though quantitative calculations are convenient only in simplified cases, the idea of the "boundary waves" gives a more comprehensible account of the phenomena than can be obtained from the usual discussions given by Rayleigh and others in terms of sine and cosine integrals.

The equation given by Rubinowicz for the amplitude $u$ is as follows:

$$u = u_E + u_B = u_E + \frac{1}{4\pi}\int_B \frac{\exp(ik\rho_s)}{\rho_s}\,\frac{\exp(ikr_s)}{r_s}\,\frac{\cos(n,r_s)}{1+\cos(r_s,\rho_s)}\sin(\rho_s,ds)\,ds, \qquad \ldots\ldots(1)$$

where $u_E$ is the amplitude of the "direct", and $u_B$ that of the diffracted light; the symbols in the integral expression may be understood by reference to Figure 1

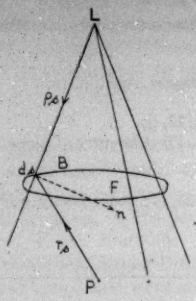


Figure 1.

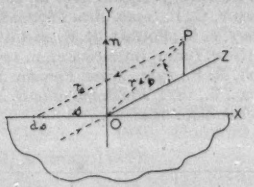


Figure 2.

where L is the source, F is the diffracting aperture and B the boundary; P is the point at which the amplitude is taken. The element $ds$ of the boundary is at a distance $\rho_s$ from L and $r_s$ from P, i.e.

$$\overrightarrow{L\,ds}=\rho_s, \qquad \overrightarrow{P\,ds}=r_s,$$

and, finally, $n$ is the inward directed normal (at $ds$) with reference to the cone defined by rays from L which touch the elements of the boundary.

## § 2. SEMI-INFINITE SCREEN

Referring to Figure 2, the direction of the incident parallel light is the Z axis of Cartesian coordinates, while the opaque screen occupies the X, Y plane below the X axis; thus the direction $n$ is represented by OY. We consider a point P in the Y, Z plane defined by the polar coordinates $r$, $\phi$ (positive as shown by the arrows). Then

$$(\rho_s, ds)=\pi/2, \quad \cos(n, r_s)=-\frac{r\sin\phi}{r_s} \quad \text{and} \quad \cos(r_s, \rho_s)=-\frac{r\cos\phi}{r_s}.$$

The Rubinowicz integral therefore becomes in our case

$$u=u_E+\frac{A}{4\pi}\int_{-\infty}^{+\infty}\frac{\exp(ikr_s)}{r_s}\frac{r\sin\phi}{r\cos\phi-r_s}\,ds, \qquad \ldots\ldots(2)$$

where $A$ is written for the amplitude of the plane wave in the XY plane.

Approximate numerical evaluation of this integral has been carried out. It leads to results similar to those obtained by the usual discussion of the Fresnel integrals and the associated phase-vector diagram (Cornu spiral), except in the immediate neighbourhood of the shadow, where complex considerations are required. We shall therefore now confine the discussion to the two-dimensional case. It will be seen below that the expression of the resultant amplitude as the sum of "direct illumination amplitude" *plus* "boundary wave amplitude" characteristic of the Rubinowicz expression is applicable in the more familiar treatment. This view was explained in a previous paper (Martin 1943), and a more detailed numerical discussion will now be given.

## §3. THE DARK-GROUND IMAGE OF A STRAIGHT-EDGE

The amplitude and phase in a plane surface S at a distance $l$ from the diffracting edge E (Figure 3) and perpendicular to the incident parallel light is represented by the length and direction of a line such as $G_2F_2$ (Figure 4) joining a point in the spiral curve to the focus. The coordinates $C$ and $S$ of points in the spiral are given by

$$C=\int\cos(\pi v^2/2)\,dv \quad \text{and} \quad S=\int\sin(\pi v^2/2)\,dv, \qquad \ldots\ldots(3)$$

where

$$\pi v^2/2=\pi y^2/\lambda l, \qquad \ldots\ldots(4)$$

and $y$ is the distance of the point (represented by the value of $v$) within the geometrical shadow. The coordinates of the focus are $C=S=\frac{1}{2}$.

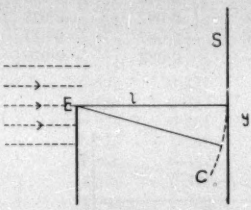


Figure 3.

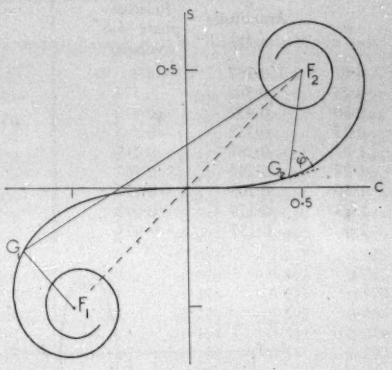


Figure 4.

Now since the gap between the circular locus $C$ centred in E (Figure 3) and the plane surface $S$ is (for small values of $y$) given by $y^2/2l$, the associated phase difference is $\pi y^2/\lambda l$, that is, $\pi v^2/2$. Hence the phase $\phi$ in the circle $C$ at the point having the same value of $y$ is

$$\phi=\arctan\{(\tfrac{1}{2}-S)/(\tfrac{1}{2}-C)\}-\pi v^2/2, \qquad \ldots\ldots(5a)$$

and the amplitude $A$ is given by

$$A^2=(\tfrac{1}{2}-S)^2+(\tfrac{1}{2}-C)^2. \qquad \ldots\ldots(5b)$$

Since the angle of slope of the spiral curve is $\pi v^2/2$, the value of $\phi$ is the angle between the element of the curve and the line joining that element to the focus. Starting from a value of $\pi/4$ when $v=0$, it will asymptotically approach $\pi/2$ as $v$ increases. Thus, subtracting a constant amount, $\pi/2$, from these values, we may exhibit the relative phase angles as starting with a value of $-\pi/4$ and approaching a constant value of zero. Table 1 is calculated with the aid of the known Fresnel integrals.

Apart from the region where $v$ is small, the change of phase becomes slow; and we may regard the disturbances as approximating to waves (the boundary waves) centred near the diffracting edge. If then the disturbance passes into an

image-forming system of small aperture, the above amplitude and phase distribution can be regarded as transferred to a corresponding locus, APR (Figure 5), centred in the geometrical image point E′ in the image plane.* $A_P$ and $\phi_P$ are the amplitude and phase respectively at P, and $\alpha'$ is the angle AE′P. Then the components of the amplitude at Q due to an element of the wave front at P are proportional (within well-understood limits of accuracy) to

$$A_P \cos\{\phi_P + (2\pi h'/\lambda)\sin\alpha'\} \quad \text{and} \quad A_P \sin\{\phi_P + (2\pi h'/\lambda)\sin\alpha'\},$$

where $h' = \text{E'Q}$, being very small. However, these expressions can be simplified for numerical computation. If R is the extreme point of the transmitted wave

Table 1

| $v$ | Amplitude ($A_P$) | Relative phase ($\phi_P$) (radians) | $v$ | Amplitude ($A_P$) | Relative phase ($\phi_P$) (radians) |
|---|---|---|---|---|---|
| 0·0 | 0·707 | $-\pi/4$ | 2·25 | 0·140 | −0·060 |
| 0·25 | 0·560 | −0·571 | 2·50 | 0·126 | −0·048 |
| 0·50 | 0·437 | −0·410 | 2·75 | 0·115 | −0·042 |
| 0·75 | 0·352 | −0·297 | 3·0 | 0·106 | −0·035 |
| 1·0 | 0·287 | −0·218 | 2·25 | 0·098 | −0·030 |
| 1·25 | 0·243 | −0·167 | 3·50 | 0·092 | −0·025 |
| 1·50 | 0·208 | −0·122 | 3·75 | 0·087 | −0·023 |
| 1·75 | 0·178 | −0·092 | 4·0 | 0·082 | −0·020 |
| 2·0 | 0·157 | −0·075 | | | |

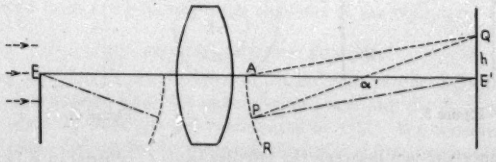


Figure 5.

front, and the angle AE′R is $\alpha'_m$, let us write (assuming radian units for $W_R$)

$$W_R = (2\pi h'/\lambda)\sin\alpha'_m; \qquad \ldots\ldots(6)$$

then

$$W_P = (2\pi h'/\lambda)\sin\alpha' \simeq W_R(v_P/v_R), \qquad \ldots\ldots(7)$$

where $v_P$ and $v_R$ are the $v$ values corresponding to the elements of the entrant wave front associated with P and R. Note that $W_R$ will change in sign for points Q above and below the axis.

The intensity $I$ due to the wave AR is obtained from the equation

$$I = C^2 + S^2, \qquad \ldots\ldots(8)$$

where

$$\begin{matrix} C \\ S \end{matrix} = k\int_0^v A_P \begin{matrix} \cos \\ \sin \end{matrix}\{\phi_P + W_R(v_P/v_R)\}\,dv, \qquad \ldots\ldots(9)$$

$k$ being a constant. The phase of the resultant is $\arctan S/C$.

* The assumptions are of an obvious character, and need not be discussed in a treatment of the present kind.

*Numerical case.*

In order to illustrate the procedure, the range of $v$ is taken from 0 to 4, and numerical integrations are carried out with the extension of Simpson's rule which is expressed by

$$\int = \frac{2x}{45}(7y_0 + 32y_1 + 12y_2 + 32y_3 + 7y_4),$$

where $x$ is the common interval between the ordinates $y_0, y_1, \ldots y_4$. The effect is to find the area under a curve of the fourth degree laid through five points on the true curve which have equal increments $x$ of their abscissae. This rule is, however, applied four times in the whole interval. If the ordinates were all unity the total area would be given as 16. It is therefore convenient to take $x$ as 10/16, so that the full sum with unit ordinates should be 10.

Table 2. Relative Displacements due to Lower Part of Boundary Wave only

| $W$ | $C$ | $S$ | $C^2+S^2$ | $W$ | $C$ | $S$ | $C^2+S^2$ |
|---|---|---|---|---|---|---|---|
| 14 | 0·384 | 0·216 | 0·194 | − 1 | 1·809 | −1·270 | 4·885 |
| 13 | 0·372 | 0·178 | 0·170 | − 2 | 1·268 | −1·666 | 4·384 |
| 12 | 0·353 | 0·173 | 0·155 | − 3 | 0·676 | −1·721 | 3·422 |
| 11 | 0·326 | 0·268 | 0·178 | − 4 | 0·237 | −1·513 | 2·345 |
| 10 | 0·393 | 0·349 | 0·276 | − 5 | 0·040 | −1·223 | 1·498 |
| 9 | 0·512 | 0·371 | 0·400 | − 6 | 0·022 | −1·015 | 1·030 |
| 8 | 0·614 | 0·316 | 0·477 | − 7 | 0·052 | −0·939 | 0·844 |
| 7 | 0·632 | 0·237 | 0·455 | − 8 | 0·021 | −0·943 | 0·889 |
| 6 | 0·584 | 0·237 | 0·397 | − 9 | −0·083 | −0·931 | 0·873 |
| 5 | 0·575 | 0·361 | 0·460 | −10 | −0·196 | −0·847 | 0·755 |
| 4 | 0·726 | 0·555 | 0·835 | −11 | −0·253 | −0·711 | 0·570 |
| 3 | 1·092 | 0·662 | 1·630 | −12 | −0·229 | −0·593 | 0·404 |
| 2 | 1·578 | 0·511 | 2·751 | −13 | −0·174 | −0·542 | 0·324 |
| 1 | 1·992 | 0·046 | 3·970 | −14 | −0·145 | −0·541 | 0·292 |
| 0 | 2·077 | −0·626 | 4·706 | | | | |

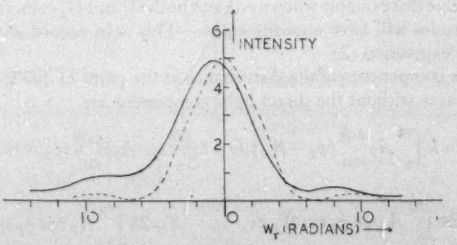


Figure 6.

The result of the computation is given in Table 2 and Figure 6, in which the intensity distribution characteristic of the edge-diffraction is represented. It is the halo, or dark-ground image, which would be obtained if a screen (suggested by $S_1$, Figure 7) could intercept the direct light while allowing all the diffracted light to enter the objective. There are important differences between this result and that which would be found (suggested by the broken curve, Figure 6) if the edge were self-luminous. The maximum intensity does not coincide with the

geometrical image position, and the darker bands which border the central maximum are not well developed. However, if the image-forming system is arranged so as to admit no light except that diffracted at reasonably large angles, the dark-ground "halo" image will approximate more closely to the type of the "self-luminous" one.

## §4. DIFFRACTION DUE TO BOTH PARTS OF THE BOUNDARY WAVE

If, instead of producing the dark-ground effect by the screen $S_1$, in front of the objective, we remove the direct light by a small screen, $S_2$ (Figure 7), in the back principal focus, the boundary wave which spreads from the diffracting edge into the *directly illuminated region* can also take part in the formation of the final image. Referring to the vector diagram of Figure 4, the total effect at a point in the region above the geometrical shadow is typified by $G_1F_2$, which can be regarded as the resultant of $G_1F_1$ and $F_1F_2$; that is, of the boundary wave represented by $G_1F_1$ and the direct light $F_1F_2$. This is identical with the Rubinowicz principle. This new boundary wave $G_1F_1$ has the same values of the phase for the same numerical values of $v$* but has the opposite sign for the

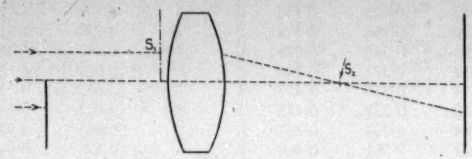


Figure 7.

amplitude. In the previous section we were dealing with the boundary wave $\overrightarrow{G_2F_2}$; we now deal with $\overrightarrow{G_1F_1}$, and it is obvious that when $v$ is given any particular numerical value (for example when $v=0$, and both $G_1$ and $G_2$ coincide at the origin), these amplitudes will have opposite signs. This is in accord with the modified Rubinowicz expression (2).

Thus the components of the disturbance at the point Q due to the sum of the boundary waves without the direct light component are

$$\begin{matrix} C \\ S \end{matrix} = k\int_0^{v_R} A_P \begin{matrix} \cos \\ \sin \end{matrix} \{\phi_P + W_P\}\, dv + k\int_0^{v_R} (-A_P) \begin{matrix} \cos \\ \sin \end{matrix} \{\phi_P - W_P\}\, dv,$$

that is

$$C = -2k\int_0^{v_R} A_P \sin\phi_P \sin W_P\, dv, \ldots \qquad S = 2k\int_0^{v_R} A_P \cos\phi_P \sin W_P\, dv. \qquad \ldots\ldots(10)$$

Each of these integrals will thus have a numerical value which is equal but of opposite sign for points in the focal plane at equal distances above and below the axis. The relative resultant amplitudes, i.e., $(C^2+S^2)^{\frac{1}{2}}$, are shown in Table 3, and in curve 1 of Figure 8; the relevant phase angles $\omega$ appear in curve 2, and the

* $v$ represents the numerical distance of a point in the Cornu spiral, measured from the origin along the curve; thus symmetrically placed points have the same $v$ values.

intensities in curve 3. The image of the edge should show a perfectly black line bordered by bright fringes if the image-forming light is limited to that of the boundary waves; this is easily observed in practice if a very narrow stop is placed in the principal focus of the lens in a system similar to that specified above. Plate I, A, shows the normal image of a straight-edge, and also the dark-ground image. The latter shows the centre dark fringe, bordered by bright fringes, as predicted above. Details of the system for the experiment are given below.

Table 3

Relative Displacements due to both Parts of Boundary Wave only; $v = 0$ to $\pm 4{\cdot}0$

| $W$ (radians) | $C$ | $S$ | $C^2+S^2$ | $(C^2+S^2)^{\frac{1}{2}}$ | $\omega$ (deg.) | $W$ (radians) | $C$ | $S$ | $C^2+S^2$ | $(C^2+S^2)^{\frac{1}{2}}$ | $\omega$ (deg.) |
|---|---|---|---|---|---|---|---|---|---|---|---|
| 16·0 | 0·503 | 0·782 | 0·865 | 0·930 | 57·2 | 6·0 | 0·562 | 1·252 | 1·883 | 1·372 | 65·8 |
| 15·0 | 0·515 | 0·805 | 0·913 | 0·956 | 57·4 | 5·0 | 0·535 | 1·584 | 2·795 | 1·672 | 71·3 |
| 14·0 | 0·529 | 0·757 | 0·853 | 0·924 | 55·1 | 4·0 | 0·489 | 2·068 | 4·516 | 2·125 | 76·6 |
| 13·0 | 0·546 | 0·720 | 0·817 | 0·904 | 52·7 | 3·0 | 0·415 | 2·383 | 5·851 | 2·419 | 80·25 |
| 12·0 | 0·582 | 0·766 | 0·925 | 0·962 | 52·7 | 2·0 | 0·310 | 2·177 | 4·835 | 2·199 | 81·9 |
| 11·0 | 0·579 | 0·979 | 1·294 | 1·137 | 59·4 | 1·0 | 0·183 | 1·316 | 1·765 | 1·329 | 82·8 |
| 10·0 | 0·589 | 1·196 | 1·777 | 1·333 | 63·8 | 0·5 | 0·082 | 0·687 | 0·479 | 0·692 | 83·2 |
| 9·0 | 0·595 | 1·302 | 2·049 | 1·432 | 65·4 | 0·25 | 0·042 | 0·352 | 0·126 | 0·354 | 83·25 |
| 8·0 | 0·593 | 1·259 | 1·937 | 1·392 | 64·8 | 0·0 | 0·0 | 0·0 | 0·0 | 0·0 | — |
| 7·0 | 0·580 | 1·176 | 1·719 | 1·311 | 63·7 | | | | | | |

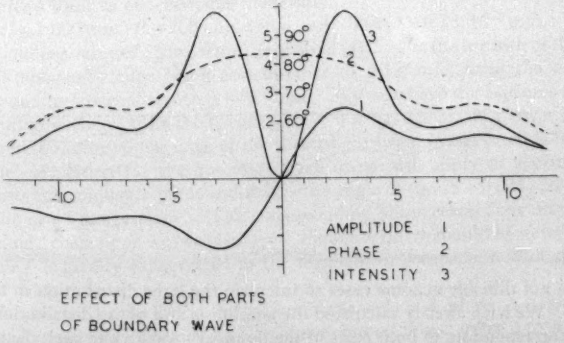


Figure 8.

## § 5. IMAGE OF A SMALL APERTURE

Consider a small aperture $G_1G_2$ (Figure 9), axially symmetrical with regard to the image-forming system, and illuminated by a parallel beam of coherent light; the amplitude in the plane surface containing the pupil of the system is now given in terms of the Cornu spiral by the vector, $G_1G_2$ say (Figure 4), representing the total interval $v$ corresponding to the aperture. When we consider the central point of the pupil, the points $G_1$ and $G_2$ are symmetrical with regard to the origin, but they travel along the curve (maintaining a constant interval) when we estimate

the amplitude at points further and further from the centre. We can distinguish three cases:

(*a*) $G_1$ and $G_2$ both in upper part of the spiral: then put $G_1G_2 = G_1F_2 + F_2G_2$;
(*b*) the origin lies between $G_1$ and $G_2$: then put $G_1G_2 = G_1F_1 + F_1F_2 + F_2G_2$*;
(*c*) $G_1$ and $G_2$ both in lower part of spiral: then put $G_1G_2 = G_1F_1 + F_1G_2$.

The components of the light entering an aperture of the objective system may therefore be described thus:

(i) both parts of the boundary wave corresponding to $G_1$;
(ii) both parts of the boundary wave corresponding to $G_2$ (opposite sign);
(iii) the direct-light component entering an aperture of the objective equal to the aperture in the diaphragm.

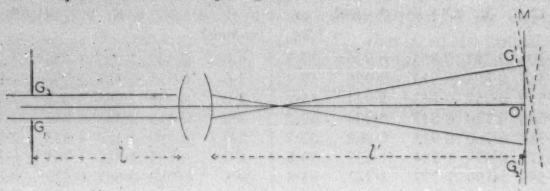


Figure 9.

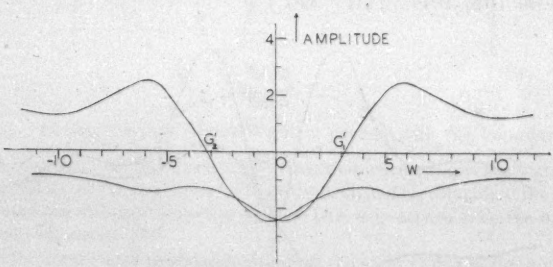


Figure 10.

It is not difficult in some cases to calculate the light distribution in the final image. We have already calculated the amplitude and phase distribution in the image corresponding to both parts of the boundary wave; one such distribution is now centred in the image of $G_1$ while another, with opposite sign, is centred in the image of $G_2$ as suggested in Figure 10. We must further calculate the displacement in the image plane due to the direct light and then combine all three components with due regard to phase.

In order to deal with any particular case a relation must be established between the above scale of distance ($W_R$) in the image plane and distances $h$ perpendicular to the axis in the object plane.

Assuming that the pupils of the objective coincide with the principal planes, and that $h, h'$ are the object and image heights, while the conjugate distances

* The discontinuities in both direct-light and boundary-wave contributions to the amplitude at the geometric shadow-edge, noted by Rubinowicz (1917), are manifest in this formulation.

are $l$ and $l'$, we have $h/l = h'/l'$ provided that the system has object and image in air. Now $W_R = (2\pi/\lambda)\, h' y_m / l'$, where $y_m$ is the semidiameter of the pupil; then, since, from (4), $l = 2y_m^2/\lambda v_m^2$, we find

$$W_R = \pi h v_m^2 / y_m. \qquad \ldots\ldots (11)$$

There is the complication that the distribution of phase calculated for both parts of the boundary wave does not apply immediately to the normal image plane; this will be obvious from Figure 9. The calculated phase applies to an image surface inclined at an angle $\tan^{-1}(h+h')/l'$. The relevant correction must be made. We may, however, ignore the correction to the numerical value of the amplitude and also ignore for a first calculation the fact that the boundary wave calculations made above for an axial "edge" should really be corrected for an object position off the axis. Both these corrections are likely to be very small in our case.

With reference to the direct light, its phase in the entrance pupil is uniform; therefore its advance over the phase of a wave centred in the axial point of the object plane is $\pi v^2/2$. On transmission through the optical system this wave (of uniform amplitude) will maintain the same phase-lead over a convergent wave centred in the axial point of the image. It is therefore simple to carry out integrations for any numerical case provided the phase changes concerned are not large.

These principles can now be applied in a numerical case, and the one chosen should lend itself to experimental observation.

Let $l = 1{,}000$ mm., $l' = 200$ mm. and $v_m = 4$. Take $\lambda = 0{\cdot}5 \times 10^{-3}$ mm.; then the corresponding value of $y_m$ is 2·0 mm. (equation (4)). Let the breadth of the object be 0·25 mm., each edge being at a distance of 0·125 mm. from the axis; the corresponding image distance is 0·025 mm. We now have the $\omega_R$ corresponding to the image distance from the equation (11); it is $\pi$ radians. Moreover the value of $v$ corresponding to the edge of the direct-light beam in the pupil is 0·25.

The calculation for the boundary-wave image will apply to a plane which intersects the conjugate point and makes the angle of $(0{\cdot}125 + 0{\cdot}025)/200$ radians with the usual image plane. The corresponding phase corrections may thus be computed; their signs will be clear from Figure 9, but it should be noted that the distance $l'$ is greatly exaggerated in the diagram, in comparison with the actual case of calculation.

With regard to the direct light (amplitude $= A_d$ and phase $\phi_{dP}$, say), using the same notation as in equation (10) above, but adding a suffix d to signify the direct light,

$$\begin{matrix} c \\ s \end{matrix} = \int_0^v 2kA_d \begin{matrix} \cos\phi_{dP} \\ \sin\phi_{dP} \end{matrix} \cos(W_R v_P / v_R)\, dv, \qquad \ldots\ldots (12)$$

and in accordance with previous provisions

$$\phi_{Pd} = -\pi v^2/2 - \pi/4.$$

$A_d$ is taken as $\sqrt{2}$, the value of $F_1 F_2$ in the vector diagram.

The relative displacements due to the "direct light" are given in Table 4. The results are corrected so that they have the proper ratio to the figures of Tables 2 and 3.

The results of the numerical calculations are given in Figure 11; the "dark-ground" curve shows the results of the boundary waves (Figure 10) added together with the relevant phase corrections, while the curve marked "aperture" shows the result of adding the direct light; the broken vertical lines at $\omega = \pm\pi$ show the limits of the geometrical image, and it will be obvious that this image, of which the breadth is twice the resolving limit of the objective for self-luminous object points, has no geometrical similarity with the object.

Table 4. Relative Displacements* due to Direct Light ($v = 0$ to $\pm 0{\cdot}25$)

| $W$ | Amplitude | $W$ | Amplitude | $W$ | Amplitude |
|---|---|---|---|---|---|
| 0 | 1·77 | 3·0 | 1·75 | 8·0 | 1·68 |
| 0·25 | 1·77 | 4·0 | 1·74 | 9·0 | 1·66 |
| 0·5 | 1·76 | 5·0 | 1·74 | 10·0 | 1·64 |
| 1·0 | 1·76 | 6·0 | 1·73 | 11·0 | 1·62 |
| 2·0 | 1·76 | 7·0 | 1·71 | 12·0 | 1·60 |

* The variation of the resultant phase angle ($-47°$) is negligible for present purposes. Note that diffraction has spread the illumination beyond the geometrical image.

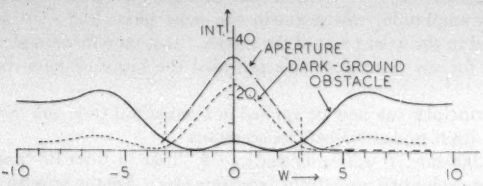


Figure 11.

## § 6. SMALL OBSTACLE

The case of image-formation when the object is a small obstacle obstructing the light is dealt with in a very similar manner. The amplitude in the pupil is represented by the interval $F_1F_2$ between the end points of the Cornu spiral *less* the interval $G_1G_2$, which represents the interval of $v$ corresponding to the obstruction. In the same three cases as before we have

$$(a)\quad F_1F_2 - G_1G_2 = F_1F_2 - (G_1F_2 + F_2G_2);$$
$$(b)\quad = F_1F_2 - (G_1F_1 + F_1F_2 + F_2G_2);$$
$$(c)\quad = F_1F_2 - (G_1F_1 + F_1G_2).$$

These components now represent the direct light amplitude from the whole aperture *minus* the boundary-wave amplitudes of the previous case. We have therefore to add the direct light effect for the full aperture (with the appropriate phases taken into consideration) to the original amplitude contributions taken with reversed signs. According to Lummer's principle, which can be invoked when the aperture is assumed to be unrestricted, the direct light will provide a background image of coherent light of uniform phase; this assumption is not strictly valid in our case, but it may be adopted as a first rough expedient. We will therefore assume that the amplitude (of the background light) is constant and the phase angle is zero (but subject to the above conventional correction of $-\pi/2$). As for the numerical amplitude value of the direct light, it will be of the

same order of magnitude as the values given in Table 4, though not so weakened by diffraction. The exact magnitude need not be calculated for this rough discussion, and we will therefore assume that a likely value is about 4·0.

The remaining curve in Figure 11 shows the bright-field image intensity distributions thus calculated. The edge-diffraction light will cause a series of weak fringes which border the dark image of the obstacle. The dark-field image of the obstacle is identical with that of the narrow aperture, as far as intensity is concerned.

## §7. IMAGE OF PHASE-CONTRAST OBJECT

The effect of passing a plane wave through a phase-changing lamina may be described as composed of "the original wave *plus* the wave due to the object". In Figure 12, if the original wave (amplitude and phase) is represented by OA, and the effect after transmission by the lamina is OB, then the amplitude and phase of the "wave due to the object" is AB.

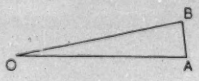


Figure 12.

Table 5

Relative Amplitudes* and Phases in the Image of the Small Aperture

| $\pm W_R$ | 0 | 1 | 2 | 3 | 4 | 5 | 6 | 7 | 8 | 9 | 10 |
|---|---|---|---|---|---|---|---|---|---|---|---|
| Amplitude | 5·82 | 5·04 | 3·90 | 2·36 | 1·02 | 0·14 | 0·62 | 0·45 | 0·14 | 0·25 | 0·22 |
| Phase (deg.) | −96 | −97 | −92 | −89 | −88 | −90 | −69 | −70 | −73 | † | † |

* Intensities are plotted in Figure 11.

† Phase calculation here subject to large uncertainty owing to small values of $\Sigma C$ and $\Sigma S$. The ratio $\Sigma S/\Sigma C$ gives the tangent of the phase angle.

The problem of the image formation of such an object is thus related at once to the problem of the aperture, and this has already been treated in terms of the "boundary waves plus the direct light".

To illustrate the application, let us suppose that the object is a thin uniform lamina of the same size as the aperture and obstacle above, and further, that the retardation is such that AB/OA is 1/5 and that AB then shows retardation of (roughly) $\pi/2$ with respect to OA. We can therefore take one-fifth of the values of the "aperture" amplitudes (Table 5) to represent AB, and the phase angle can be put as roughly 90° throughout, while the relative amplitude and phase of the direct light (assumed uniform) can be taken as (say) 4·0 and zero respectively. Figure 13 shows the resulting curves for ordinary conditions, and also for phase changes of $\pm\pi/2$ for the direct light, to secure positive and negative phase contrast (lower and upper curves respectively). Though the visibility of the "image" of the phase strip is greatly enhanced by the use of phase contrast there is, of course, no particular gain in the rendering of its geometrical form. The case calculated by Françon (1946) is that of a wider object; the edge-haloes which he predicts are comprehensible in terms of the boundary waves.

## §8. EDGE HALOES

We have already noted that cases arise, especially in the case of the microscope, where the object plane contains many small obstacles having sharp boundaries; some may be more or less opaque, and some may be edges of, or steps in, phase-changing laminae. These sharp edges will diffract their pairs of boundary waves into the objective and there will be, in the symmetrical case, a corresponding amplitude distribution of the type of curve 1, Figure 8, in the image plane, in addition to the effect of the direct light, which may be considered to give uniform amplitude. But the relative phase of the direct light will depend on the integration of all the contributions derived from the object-plane, and for various reasons it will not usually be possible to predict it. A variety of bordering fringes may therefore appear according to the relative phases of the boundary wave system and direct light contributions, and some of these are suggested in Figure 14. This argument applies only to cases in which the angular aperture of the illumination is very small.

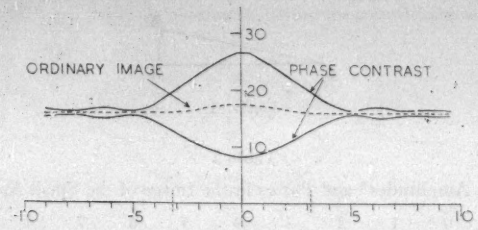


Figure 13.

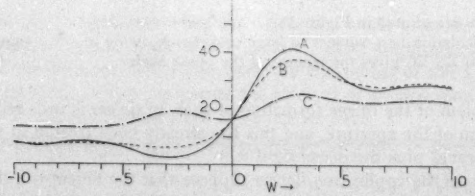


Figure 14. Intensities of edge-halo fringes according to relative phase of background light. A. Retardation 90°. B. Retardation 45°. C. Retardation 0°.

## §9. DIFFRACTION PHOTOGRAPHS

The photographs B (Plate I) and C (Plate II) illustrate the general conclusions for the dark- and light-ground images of apertures and obstacles (slits and wires).

The illumination was from a long-focus collimator. Green light ($\lambda = 0{\cdot}5\mu$ approximately) was used, the width of the slit diaphragm in front of the objective was 4·0 mm., the distance of the object 1,100 mm., and the distance of the image 245 mm.

The images so produced were projected by an eyepiece magnifying $\times 2{\cdot}49$, and the resulting negatives were enlarged with a further magnification of $\times 5{\cdot}70$.

The arrangements are thus fairly near to those of the case for which calculations were made above. In the case of the opaque wire object of diameter 0·262 mm.,

PLATE I.

*To face page* 724

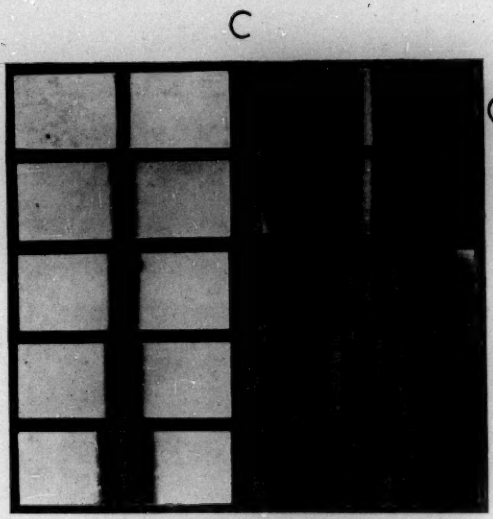


PLATE II.

the illumination in the central part of the image corresponding with the curve of Figure 11 is clearly seen. The image of the aperture of similar size shows no sign of any darkening at the centre, and the bordering fringes are very faint indeed compared with the border fringes in the dark-ground image. The interval corresponding to the "maximum to minimum" of the $(\sin W)/W$ distribution corresponds to 0·148 mm. in the obstacle. The dark-ground images were produced by stopping off the greater part of the direct light by a very narrow wire placed in the principal focus of the objective. It is seen that (as expected) the dark-ground images of wires and slits are indistinguishable. When the size of the object, be it slit or obstacle, is changed, the effects in the dark-ground image can easily be predicted by a corresponding change in the separation of the points $G_1', G_2'$ in the amplitude curves (Figure 10).

Starting with a broad object, the points $G_1', G_2'$ are widely separated, and we see two intensity systems of the type of curve 3 of Figure 8, one corresponding to each edge. As the separation diminishes, however, the nearer bright bands coalesce, and it will be found that the amplitude distribution approximates more and more closely to the type $(\sin W)/W$, the position of the first dark minimum at each side of the central maximum depending only on the aperture of the system; however, the amplitude will fall continuously till the points $G_1'$ and $G_2'$ coincide, when there is, of course, complete extinction both in theory and practice. It is a very interesting thing that the amplitude curves of the type of curve 1 of Figure 8 should have this particular additive property, though of course the "$(\sin W)/W$" type of distribution is predictable from the Cornu diagram.

## § 10. CONCLUSION

The foregoing discussion has been given in the hope that it may afford a starting point in a more suggestive and useful approach to the interpretation of the microscope images of small objects in cases where a severely restricted aperture for the illumination is employed to obtain dark-ground or phase-contrast effects. It has, unfortunately, been considered by some writers that Zernike's (1942) phase vector theory of phase contrast can be applied directly to elicit information about the relative optical thicknesses in the close neighbourhood of loci of phase-change, or even in phase-modulating objects of sizes not much exceeding the ordinary resolving limits. Such information is not likely to be obtained from a static photograph, but it does not appear impossible that a good deal of information about the object can be obtained by controlled variation of the amplitude and phase of the "direct light" and study of the corresponding diffraction effects at the boundary. The discussions in this paper afford no more than a beginning; the results cannot be applied directly, for example, to images secured by means of phase-contrast with ring illuminators and the like, but similar principles can be used, and it is hoped in future to extend the calculations to a greater variety of cases.

## ACKNOWLEDGMENTS

My thanks are due to Miss J. M. Drewitt for assistance with the numerical computations and to Mrs. V. Pawluk for help with the diffraction photographs.

## REFERENCES

Françon, M., 1946, *Revue d'optique*, **25**, 257.
Martin, L. C., 1943, *Proc. Phys. Soc.*, **55**, 104.
Rubinowicz, A., 1917, *Ann. Phys., Lpz.*, **53**, 257.
Zernike, F., 1942, *Physica*, **9**, 686.

# Wave-front Aberrations of Oblique Pencils in a Symmetrical Optical System: Refraction and Transfer Formulae

By W. WEINSTEIN
Technical Optics Section, Imperial College, London

*MS. received 25th February* 1949

*ABSTRACT.* The wave-front aberrations which occur in a pencil traversing a symmetrical optical system at a finite field angle are defined in a new way. Refraction and transfer formulae are derived for all the aberration coefficients up to and including those depending on the fourth power of the aperture of the pencil.

## §1. INTRODUCTION

In a symmetrical optical system the wave-front aberration, or deviation of the wave front from an arbitrarily chosen reference surface, is a function of three variables $\rho_a$, $\phi_a$, $\sigma$ defined as follows:

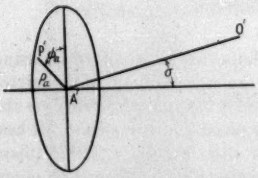


Figure 1.

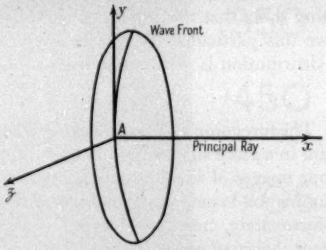


Figure 2.

Let A′ (Figure 1) be the centre of the exit pupil, A′O′ the paraxial principal ray to the Gaussian object point O′, and P′ a point in the exit pupil. Then $\rho_a = A'P'$, $\sigma$ is the angle between A′O′ and the axis, and $\phi_a$ is the azimuth of A′P′ with respect to A′O′, i.e. the angle between the meridian plane and the plane containing P′ and A′O′.

It may be shown (Hamilton 1833) by considerations of symmetry, that the wave-front aberration $W'$ at P′ can be expressed as a power series in which the variables are powers and products of $\rho_a^2$, $\rho_a\sigma\cos\phi_a$, $\sigma^2$. When this is done the terms fall into groups of the fourth, sixth, eighth, ..., degree in $\rho_a$ and $\sigma$, these being the primary or Seidel aberrations, and secondary, tertiary, ..... aberrations. The Seidel aberrations are those terms containing $\rho_a^4$, $\rho_a^3\sigma\cos\phi_a$, $\rho_a^2\sigma^2\cos^2\phi_a$, $\rho_a\sigma^3\cos\phi_a\sigma^4$, i.e. of the fourth degree in $\rho_a$ and $\sigma$.

However, if all the terms of degree 4 or less in $\rho_a$ are considered, irrespective of their degree in $\sigma$, a number of new terms are brought in, containing $\rho_a^3\cos^2\phi_a$, $\rho_a^4\cos^4\phi_a$, $\rho_a^4\cos^2\phi_a$, multiplied by various higher powers of $\sigma$. This means that if the field angle of a pencil is large, aberrations of these types will be appreciable, and since they are only of the third and fourth degree in $\rho$, they will be important

even in pencils of low aperture. Since these are not Seidel or primary aberrations, to obtain their coefficients in the usual way would involve computing secondary, tertiary, and even higher order aberration terms, depending on how important the higher powers of $\sigma$ were in the system concerned. Dr. H. H. Hopkins, to whom the preceding argument is due, has suggested that a better approach would be to suppose that a true principal ray has been traced trigonometrically through the system, with *s*- and *t*-fans, at the desired field angle, and to determine the aberration coefficients up to the fourth power of the aperture of the pencil surrounding this ray. These coefficients would be expressed in terms of the principal ray data, and they would give the wave-front aberration in the form

$$\begin{aligned} W' = {} & B_{22}\rho^2\cos^2\phi + \\ & B_{31}\rho^3\cos\phi + B_{33}\rho^3\cos^3\phi + \\ & B_{40}\rho^4 + B_{42}\rho^4\cos^2\phi + B_{44}\rho^4\cos^4\phi \qquad \ldots\ldots(1) \end{aligned}$$

referred to the sagittal focus. In equation (1) $W'$ is the optical path between the wave front and a spherical surface centred on the sagittal focus and touching the wave front where it meets the principal ray. $W'$ is taken as positive when the wave front is in advance of the sphere; this corresponds to the usual sign convention for longitudinal ray aberration. $B_{22}, B_{31}, \ldots . B_{44}$, are aberration coefficients. $\rho$ and $\phi$ are the aperture radius and azimuth in a plane perpendicular to the principal ray and meeting it at some suitably chosen point, e.g. the intersection with a refracting surface or with the axis of the system.

Of the terms in (1) those containing $B_{22}$, $B_{31}$ and $B_{40}$ are of the same kind as Seidel astigmatism, coma, and spherical aberration respectively but not numerically equal to them, because of the finite field angle, while the remainder are of higher order types, although still only of third or fourth degree in the aperture.

This procedure has the advantage that all variations in the aberrations with the field angle are taken into account, since the principal ray is accurately traced. Thus equation (1) is accurate up to the fourth power of the aperture, no matter how great the field angle may have been. In the usual procedure for studying the aberrations of off-axis pencils at finite field angles, the principal ray is traced, with *s*- and *t*-fans, then a pair of meridian rays at finite distance from the principal ray and possibly also a true sagittal (skew) ray. However, it can be seen that the data thus obtained will not differentiate between coma of the type $\rho^3\cos\phi$ and that of type $\rho^3\cos^3\phi$ since, from (1), the wave-front aberrations due to these two vary in the same way in the meridian and sagittal sections ($\phi = 0$ and $\phi = \pi/2$), and the difference appears only in intermediate azimuths. Similarly no differentiation between types $\rho^4\cos^4\phi$ snd $\rho^4\cos^2\phi$ is possible. On the other hand, if these coefficients could be computed directly, a complete picture of the behaviour of the wave front in all azimuths would be obtained, accurate to the fourth power of the aperture. This was pointed out by Dr. Hopkins. Formulae for the aberration coefficients will be derived in this paper.

## §2. DEFINITION OF THE ABERRATION COEFFICIENTS OF A PENCIL

The term "pencil" is used to denote the ensemble consisting of a true principal ray (not a "paraxial" ray) from an object point at a finite or infinite distance together with all the wave fronts, or surfaces of constant optical path, and all the rays, or wave-front normals, from this point. The aperture is, of course, to be

thought of as limited in extent, but the exact degree of limitation is not material to the discussion. One can then refer without further explanation to the wave front at any point of the principal ray or to the ray from any point on a certain wave front, and so on.

It is convenient to compute aberration coefficients which are simply related to those defined by equation (1).

Take right-handed rectangular axes with the origin at some point of reference A on the principal ray, chosen as in §1, the $x$-axis along the principal ray, and the $y$-axis in the meridian plane (Figure 2). If the principal ray has traversed the system at finite angles of incidence the wave front at any point will have the meridian plane ($x$–$y$ plane) as a plane of symmetry and in general it will have no other kind of symmetry. Hence the equation of the wave front at A may be written

$$x = \frac{1}{2t}y^2 + \frac{1}{2s}z^2 + C_{30}y^3 + C_{12}yz^2 + \left(\frac{1}{8t^3} + C_{40}\right)y^4 + \left(\frac{1}{4t^2s} + C_{22}\right)y^2z^2 + \left(\frac{1}{8s^3} + C_{04}\right)z^4 + \text{terms of degree 5 and higher.} \quad \ldots\ldots(2)$$

In this equation only terms with even powers of $z$ have been included, to give the required symmetry about the $x$–$y$ plane. $t$ and $s$ are the radii of curvature of the wave front in the meridian and sagittal sections, at the origin. In §§4, 5 and 6 below, the origin is taken at the intersection of the principal ray with the refracting surface, and then $t$ and $s$ are equal to the intersection lengths determined by the ordinary formulae for tracing $t$- and $s$-fans. $C_{30}$, $C_{12}$, .... $C_{04}$ are the aberration coefficients which will be determined. The terms in $s$ and $t$ which are included in the coefficients of $y^4, y^2z^2$ and $z^4$ ensure that, when all the $C$'s vanish and $t=s$ the equation will represent a sphere, to the fourth degree in $y$ and $z$. It is not essential to include these terms in $t$ and $s$, since (2) is the Cartesian equation of the wave front, and however the aberration coefficients are defined they must, when substituted in (2), give the actual shape of the wave front; nevertheless, it simplifies the algebra to define them so that there is no aberration when they vanish. Whenever higher order aberrations are defined the definitions are variable to a certain extent. Thus in (2) the coefficient of $y^2z^2$ could be written as $1/(4ts^2)+C'_{22}$ instead of $1/(4t^2s)+C_{22}$, but, as explained above, if $C'_{22}$ were computed instead of $C_{22}$ the actual shape of the wave front would still be known, so that no uncertainty would arise. Such a change from $C_{22}$ to $C'_{22}$ would merely mean that a slightly different definition of primary astigmatism was being tacitly adopted, the difference being in the shape the wave front is assumed to have when only primary astigmatism is present and the fourth power of the aperture is taken into consideration.

To obtain the actual wave-front aberration from (2), referred to any chosen focus, it is simply necessary to subtract from (2) the equation of a sphere centred on that focus and to multiply the result by the refractive index $N$. (Thus a sphere centred on the sagittal focus would be

$$x_0 = \frac{1}{2s}(y^2+z^2) + \frac{1}{8s^3}(y^2+z^2)^2 + \ldots.$$

and the wave-front aberration referred to the sagittal focus would be $N(x-x_0)$, where $N$ is the refractive index.) This gives the aberration as a function of $y$ and $z$, rectangular coordinates in the exit pupil. If the substitution $y=\rho\cos\phi$; $z=\rho\sin\phi$ is made in (2) the right-hand side becomes

$$\frac{1}{2}\left(\frac{1}{t}-\frac{1}{s}\right)\rho^2\cos^2\phi+\frac{1}{2s}\rho^2+(C_{30}-C_{12})\rho^3\cos^3\phi+C_{12}\rho^3\cos\phi$$
$$+\left\{C_{40}-C_{22}+C_{04}+\frac{1}{8}\left(\frac{1}{t^3}-\frac{2}{t^2s}+\frac{1}{s^3}\right)\right\}\rho^4\cos^4\phi$$
$$+\left\{C_{22}-2C_{04}+\frac{1}{4}\left(\frac{1}{t^2s}-\frac{1}{s^3}\right)\right\}\rho^4\cos^2\phi+\left(C_{04}+\frac{1}{8s^3}\right)\rho^4.$$

On subtracting the corresponding expression for $x_0$, multiplying by $N$, and comparing this with (1) it can be seen that

$$\left.\begin{aligned}
&B_{22}=\frac{N}{2}\left(\frac{1}{t}-\frac{1}{s}\right); \qquad B_{31}=NC_{12};\\
&B_{33}=N\{C_{30}-C_{12}\}; \qquad B_{40}=NC_{04};\\
&B_{42}=N\left\{C_{22}-2C_{04}+\frac{1}{4}\left\{\frac{1}{t^2s}-\frac{1}{s^3}\right)\right\};\\
&B_{44}=N\left\{C_{40}-C_{22}+C_{04}+\frac{1}{8}\left(\frac{1}{t^3}-\frac{2}{t^2s}+\frac{1}{s^3}\right)\right\}.
\end{aligned}\right\} \quad \ldots\ldots (3)$$

These equations relate the coefficients defined in (2) to the more usual polar coefficients in (1).

It can be seen that the aberration as defined by $N(x-x_0)$ is an optical path length measured parallel to the principal ray. Aberration is usually thought of as measured either along the ray through the point P or along the normal to the reference sphere, but in the former case the direction would depend on the amount of aberration present and in the latter on the choice of reference sphere. The present definition is independent of these factors. The difference is small with ordinary numerical apertures, but the point must be settled for the definition of higher order aberrations, and for this purpose the choice given here is most convenient.

## § 3. GENERAL METHOD OF DERIVATION OF THE ABERRATION COEFFICIENTS

Methods of deriving aberration coefficients generally depend on the principle of obtaining a quantity which is invariant on refraction, expressing this as a series of powers of some measure of the aperture, the coefficients in the series containing the aberration coefficients, and writing down the equations which state that each term in the series is invariant on refraction. These equations are the refraction formulae for the aberration coefficients. Finally, transfer formulae, for transferring the coefficients from one surface to the next, are found; these are usually fairly simple. The measure of the aperture must be a refraction invariant, and it is usually the central angle or some closely related quantity (von Rohr 1920).

The method used in this paper follows similar lines, and may be described as follows.

Let AP (Figure 3) be a refracting surface, AO the incident principal ray, AO′ the refracted principal ray and AQ the incident wave front at A. The refracted wave front AQ′ can be found in the following way. Let Q, Q′ be chosen so that the normals at these points pass through P and let $N$, $N'$ be the refractive indices of the two media. Then Huygens' construction gives $N'.\,Q'P = N.\,QP$, or, if $Q'P = q'$, $QP = q$,

$$\Delta(Nq) = 0. \qquad \ldots\ldots (4)$$

Part of the refracted wave front at A so constructed is in most cases " virtual" (as in Figure 3), but this is immaterial since the real wave fronts at points further along the refracted principal ray are all derived from it; the aberration coefficients of this wave front will be found, and the refraction invariant * which forms the basis of the method is the quantity $Nq$.

If A is taken as origin, the coordinates of Q will be $(x, y, z)$ where $x$ is given in terms of $y$ and $z$ by equation (2), since Q is on the wave front whose equation is (2). The coordinates of P will be, say $(u, v, w)$, where $u$, $v$, $w$ are functions of $r$,

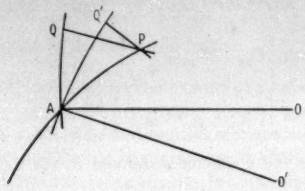


Figure 3.

the radius of the surface, the distance AP, and $\psi$, the angle between the meridian plane and the plane containing P and the normal to the refracting surface†.

A numerical value of $\psi$ is fixed and inserted in the expressions for $u$, $v$ and $w$; in what follows this will be 0, $\pi/4$ or $\pi/2$.

Let $(l, m, n)$ be the direction cosines of the ray through Q; these can be found as functions of $y$ and $z$ from (2), by analytical geometry. Then the fact that the ray through Q passes through P is expressed by the equations

$$u = x + lq, \qquad \ldots\ldots (5\,a)$$

$$v = y + mq, \qquad \ldots\ldots (5\,b)$$

$$w = z + nq, \qquad \ldots\ldots (5\,c)$$

where $x$, $l$, $m$ and $n$ are expressed in terms of $y$ and $z$, and $u$, $v$, $w$ are in terms of AP.

* The reason for using equation (4) is that it is valid for all positions of P, not merely when P is in the meridian plane, and hence it can be used to obtain aberrations in any azimuth. Suppose for the moment that P lies in the meridian plane, and let PQ meet the principal ray in a point $O_1$; then $\Delta N(AO_1 - PO_1)$ is the aberration introduced at the surface, referred to the point $O_1$ as focus, and this expression can be used to obtain all orders of tangential aberrations; but, since there is no intersection point $O_1$ when P does not lie in the meridian plane, this expression is useless for other aberrations. Again, if $O_2$ is the focus for close sagittal rays $\Delta N(AO_2 - PO_2)$ can be used to derive primary aberration expressions (Hopkins unpublished), but at *finite incidence angles* it is not permissible to assume that skew rays pass through the $s$-focus to the required order of accuracy, even for aberrations varying as the third and fourth powers of the aperture.

† The angle $\psi$ is not equal to $\phi$ defined in § 1, unless there is normal incidence.

From these three equations $y$ and $z$ can be eliminated and an expression for $q$ obtained; this will be a power series in AP, and the coefficients will be functions of the principal ray data and the aberration coefficients $C_{30}, \ldots . C_{04}$. This expression for $q$ and a similar one for $q'$ are substituted in (4) and the terms in the successive powers of AP are separately equated to zero, giving explicit expressions for the quantities $\Delta(N \cos IC_{12})$, $\Delta(N \cos {}^3IC_{30})$, etc. These are the refraction formulae (equations (13), (28), (14), (29), (20)).

The incident wave front is a " parallel surface " to the refracted wave front at the previous refracting surface, i.e., it is obtained by laying off a constant distance $D$ along the normal to the refracted wave front. This can be done by analytical geometry, and the result is a set of formulae giving the coefficients of the new wave front (aberration coefficients) in terms of those of the old. These are the transfer formulae (equations (36) to (40)).

## §4. REFRACTION FORMULAE WITH $\psi=0$

This case is the simplest, since the rays all lie in the meridian plane, and the problem is only two dimensional.

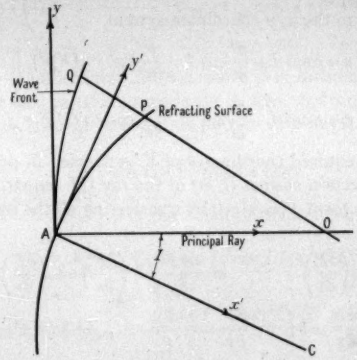


Figure 4.

Let AP (Figure 4) be the meridian section of the refracting surface, AO the incident principal ray, AC the normal to the surface and AQ the meridian section of the incident wave front. Let QPO be the ray of the incident pencil which passes through Q. Let $r$ be the radius of the refracting surface, $I$ the angle of incidence of the principal ray, and $t$ the distance from A to the tangential focus for rays close to the principal ray, so that $t$ is the radius of curvature at A of the curve AQ. Take rectangular axes with origin at A and $x$ axis along AO. Then, from (2), the equation of the curve AQ is

$$x = \frac{1}{2t}y^2 + C_{30}y^3 + \left(\frac{1}{8t^3} + C_{40}\right)y^4 + \text{terms of higher order}, \quad \ldots\ldots (6)$$

the terms in $z$ being omitted since, as stated above, only rays in the meridian plane are considered in this case.

Let AP be denoted by $p$; then the coordinates $(u, v)$ of P are expressed in terms of $p$ as follows:

Take for the moment $x'$, $y'$ axes with origin at A and $x'$ axis along AC, the normal to the circle AP. The equation of this circle is then $x'^2+y'^2=2rx'=p^2$. Hence

$$x'=\frac{1}{2r}p^2; \quad y'^2=p^2-\frac{1}{4r^2}p^4;$$

$$y'=p-\frac{1}{8r^2}p^3+O(p^5),$$

where $O(p^n)$ denotes terms of the $n$th and higher degrees in $p$, the aperture of the pencil. The value of $q$ which is finally obtained as described in § 3 must be correct to the fourth power in $p$, i.e. terms in $q$ which are $O(p^5)$ can be ignored, since aberrations depending on the fourth power of the aperture are being investigated. By following through the algebra the orders of magnitude of the terms in $q$ to which any intermediate expression contributes can be seen, and any non-significant terms in this expression can be dropped. This omission of non-significant terms will usually be carried out without further explanation in the remainder of the paper.

Changing back to the $x, y$ coordinate system,

$$\left.\begin{aligned} u&=p\sin I+\frac{p^2}{2r}\cos I-\frac{p^3}{8r^2}\sin I+O(p^5),\\ v&=p\cos I-\frac{p^2}{2r}\sin I-\frac{p^3}{8r^2}\cos I+O(p^5).\end{aligned}\right\} \quad \ldots\ldots(7)$$

These are the required coordinates of P, expressed in powers of $p$.

To find the direction cosines $(l, m)$ of the ray QP, equation (6) is considered to be written in the form $F(x, y)=0$ by transferring all the terms to the left-hand side. Then

$$l=\frac{\partial F}{\partial x}\Big/\left\{\left(\frac{\partial F}{\partial x}\right)^2+\left(\frac{\partial F}{\partial y}\right)^2\right\}^{\frac{1}{2}}; \qquad m=\frac{\partial F}{\partial y}\Big/\left\{\left(\frac{\partial F}{\partial x}\right)^2+\left(\frac{\partial F}{\partial y}\right)^2\right\}^{\frac{1}{2}}. \quad \ldots\ldots(8)$$

From (6) $\quad \dfrac{\partial F}{\partial x}=1; \qquad \dfrac{\partial F}{\partial y}=-\dfrac{1}{t}y-3C_{30}y^2+O(y^3);$

$$\left(\frac{\partial F}{\partial x}\right)^2+\left(\frac{\partial F}{\partial y}\right)^2=1+\frac{1}{t^2}y^2+\frac{6}{t}C_{30}y^3+O(y^4).$$

Then

$$\left.\begin{aligned} l&=1-\frac{1}{2t^2}y^2-\frac{3}{t}C_{30}y^3+O(y^4),\\ m&=-\frac{1}{t}y-3C_{30}y^2+O(y^3).\end{aligned}\right\} \quad \ldots\ldots(9)$$

These are the required values of the direction cosines, which, with the values of $u$ and $v$ given in (7), are substituted in (5 $a$) and (5 $b$) giving

$$p\sin I+\frac{p^2}{2r}\cos I-\frac{p^3}{8r^2}\sin I=\frac{1}{2t}y^2+C_{30}y^3+\left(\frac{1}{8t^3}+C_{40}\right)y^4 +q\left\{1-\frac{1}{2t^2}y^2-\frac{3}{t}C_{30}y^3\right\}+O(p^5); \quad \ldots\ldots(10\,a)$$

$$p\cos I-\frac{p^2}{2r}\sin I-\frac{p^3}{8r^2}\cos I=y-q\left\{\frac{1}{t}y+3C_{30}y^2\right\}+O(p^4). \quad \ldots\ldots(10\,b)$$

It is next necessary to eliminate $y$ from these equations and solve the result for $q$. From (10*b*), by the usual method of reversion of series,

$$y=p\cos I-\frac{p^2}{2r}\sin I+\frac{pq}{t}\cos I-\frac{p^3}{8r^2}\cos I+\left(3C_{30}\cos^2 I-\frac{1}{2rt}\sin I\right)p^2q$$
$$+\frac{pq^2}{t^2}\cos I+O(p^4). \qquad \ldots\ldots(11)$$

This is substituted in (10*a*) and the resulting equation is solved for $q$, again by reversion of series, giving

$$q=p\sin I+\tfrac{1}{2}\left(\frac{\cos I}{r}-\frac{\cos^2 I}{t}\right)p^2$$
$$+\left\{\frac{1}{2t}\sin I\left(\frac{\cos I}{r}-\frac{\cos^2 I}{t}\right)-\frac{1}{8r^2}\sin I-C_{30}\cos^3 I\right\}p^3$$
$$+\left\{\tfrac{1}{8}\left(\frac{\cos I}{r}-\frac{\cos^2 I}{t}\right)^2+\frac{1}{2t^2}\sin^2 I\left(\frac{\cos I}{r}-\frac{\cos^2 I}{t}\right)-\frac{1}{8r^2t}\sin^2 I\right.$$
$$\left.+\tfrac{3}{2}\sin I\cos I\left(\frac{\cos I}{r}-\frac{2\cos^2 I}{t}\right)C_{30}-C_{40}\cos^4 I\right\}p^4+O(p^5). \qquad \ldots\ldots(12)$$

This value of $q$ is substituted in (4): since $p$ is invariant on refraction the various powers of $p$ can be taken outside the $\Delta$ sign, and since (4) is true for all values of $p$ the coefficients of the various powers of $p$ in (4) must each be zero. This gives

$$\Delta(N\sin I)=0, \text{ Snell's law.}$$

$$\Delta N\left(\frac{\cos I}{r}-\frac{\cos^2 I}{t}\right)=0, \text{ the equation for tracing } t\text{-fans.}$$

$$\Delta(NC_{30}\cos^3 I)=\Delta\left\{\frac{N\sin I}{2t}\left(\frac{\cos I}{r}-\frac{\cos^2 I}{t}\right)\right\}. \qquad \ldots\ldots(13)$$

$$\Delta(NC_{40}\cos^4 I)=\Delta N\left\{\tfrac{3}{2}\sin I\cos I\left(\frac{\cos I}{r}-\frac{\cos^2 I}{t}\right)C_{30}+\frac{1}{8t}\left(\frac{\cos I}{r}-\frac{\cos^2 I}{t}\right)^2\right.$$
$$\left.+\frac{1}{2t^2}\sin^2 I\left(\frac{\cos I}{r}-\frac{\cos^2 I}{t}\right)-\frac{1}{8r^2t}\sin^2 I\right\}. \qquad \ldots\ldots(14)$$

Equations (13) and (14) are the required refraction formulae for $C_{30}$ and $C_{40}$. A result equivalent to (13) was obtained in a different way by Dr. H. H. Hopkins and was communicated privately to the author.

## § 5. REFRACTION FORMULAE WITH $\psi=\pi/2$

The usual coordinate system is taken with the $x$ axis along the principal ray. The point P is taken on the great circle of the refracting surface which is tangent to the $z$ axis at the origin A, i.e. in azimuth $\pi/2$ with respect to the normal to the refracting surface; this great circle lies in a plane inclined at an angle $I$ to the $zx$ plane (see Figure 5), and it can be seen from the figure or from the analysis below that neither P nor Q lies in the $zx$ plane to the order of approximation contemplated. The coordinates of P are

$$u=\frac{p^2}{2r}\cos I; \qquad v=-\frac{p^2}{2r}\sin I; \qquad w=p-\frac{p^3}{8r^2}+O(p^5). \qquad \ldots\ldots(15)$$

The coordinates of Q are $(x, y, z)$, where $x$ is given in terms of $y$ and $z$ by (2), but since $y$ is of the same order of magnitude as $v$, i.e. $y$ is $O(p^2)$, it is permissible to put

$$x = \frac{1}{2s}z^2 + C_{12}yz^2 + \frac{1}{2t}y^2 + \left(\frac{1}{8s^3} + C_{04}\right)z^4 + O(p^5). \quad \ldots\ldots(16)$$

As in §4

$$l, m, n = \left(\frac{\partial F}{\partial x}, \frac{\partial F}{\partial y}, \frac{\partial F}{\partial z}\right) \Big/ \left\{\left(\frac{\partial F}{\partial x}\right)^2 + \left(\frac{\partial F}{\partial y}\right)^2 + \left(\frac{\partial F}{\partial z}\right)^2\right\}^{\frac{1}{2}},$$

so that

$$\left.\begin{aligned} l &= 1 - \frac{1}{2s^2}z^2 + O(p^4), \\ m &= O(p^2), \\ n &= -\frac{1}{s}z + O(p^3). \end{aligned}\right\} \quad \ldots\ldots(17)$$

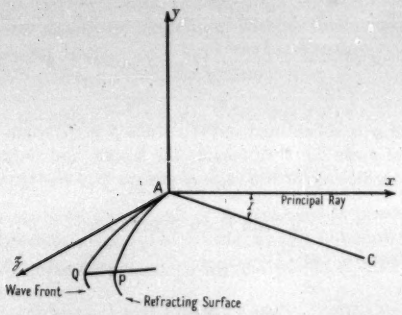


Figure 5.

Substituting from (15), (16) and (17) in (5 *a*), (5 *b*) and (5 *c*),

$$\frac{p^2}{2r}\cos I = \frac{1}{2s}z^2 + C_{12}yz^2 + \frac{1}{2t}y^2 + \left(\frac{1}{8s^3} + C_{04}\right)z^4 + q\left(1 - \frac{1}{2s^2}z^2\right) + O(p^5), \quad \ldots\ldots(18\,a)$$

$$-\frac{p^2}{2r}\sin I = y + O(p^4), \quad \ldots\ldots(18\,b)$$

$$p - \frac{p^3}{8r^2} = z - \frac{1}{s}zq + O(p^5). \quad \ldots\ldots(18\,c)$$

In these equations $q$ is taken as $O(p^2)$; this follows from (19) below.

Substituting for $y$ and $z$ from (18 *b*) and (18 *c*) in (18 *a*) and solving for $q$ by reversion of series,

$$q = \tfrac{1}{2}\left(\frac{\cos I}{r} - \frac{1}{s}\right)p^2 + \left\{\frac{1}{8s}\left(\frac{\cos I}{r} - \frac{1}{s}\right)^2 + \frac{1}{8r^2}\sin^2 I\left(\frac{1}{s} - \frac{1}{t}\right) + \frac{C_{12}}{2r}\sin I - C_{04}\right\}p^4 + O(p^6). \quad \ldots\ldots(19)$$

Applying (4), the successive terms give

$$\Delta N\left(\frac{\cos I}{r}-\frac{1}{s}\right)=0, \text{ the equation for tracing } s\text{-fans, and}$$

$$\Delta(NC_{04})=\Delta N\left\{\frac{C_{12}}{2r}\sin I+\frac{1}{8s}\left(\frac{\cos I}{r}-\frac{1}{s}\right)^2+\frac{1}{8r^2}\sin^2 I\left(\frac{1}{s}-\frac{1}{t}\right)\right\}. \quad \ldots\ldots (20)$$

Equation (20) is the refraction formula for $C_{04}$; it involves the values of $C_{12}$ before and after refraction, as might be expected, and the refraction formula for this coefficient will be obtained in the next section.

## § 6. REFRACTION FORMULAE WITH $\psi=\pi/4$

In this case P is taken on the great circle through A, the plane of which is in azimuth $\pi/4$ with respect to the normal to the refracting surface (Figure 6).

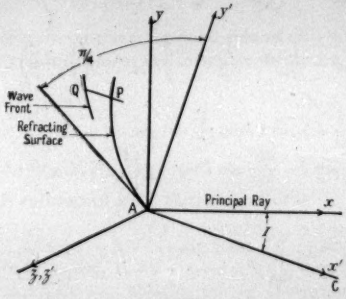


Figure 6.

The coordinates of P can be found as in § 4, by means of the auxiliary axes $Ax', y', z'$. For typographical convenience put $a=1/\sqrt{2}$. Then the $x', y', z'$ coordinates of P are

$$\frac{1}{2r}p^2,\ ap-\frac{a}{8r^2}p^3,\ ap-\frac{a}{8r^2}p^3,\ +O(p^5).$$

Hence in the $x, y, z$ system,

$$\left.\begin{aligned} u&=ap\sin I+\frac{p^2}{2r}\cos I-\frac{ap^3}{8r^2}\sin I+O(p^5),\\ v&=ap\cos I-\frac{p^2}{2r}\sin I-\frac{ap^3}{8r^2}\cos I+O(p^5),\\ w&=ap-\frac{a}{8r^2}p^3+O(p^5). \end{aligned}\right\} \quad \ldots\ldots (21)$$

The equation of the wave front must now be taken as in equation (2), since all the terms given there are of significant orders of magnitude. The direction cosines of the ray QP are, retaining all significant terms:

$$\left.\begin{aligned} l &= 1 - \frac{1}{2t^2}y^2 - \frac{1}{2s^2}z^2 - \frac{3}{t}C_{30}y^3 - \left(\frac{1}{t}+\frac{2}{s}\right)C_{12}yz^2 + O(p^4), \\ m &= -\frac{1}{t}y - 3C_{30}y^2 - C_{12}z^2 + O(p^3), \\ n &= -\frac{1}{s}z - 2C_{12}yz + O(p^3). \end{aligned}\right\} \quad \ldots\ldots(22)$$

Substituting from (2), (21) and (22) in (5 *a*), (5 *b*), (5 *c*),

$$\begin{aligned} ap\sin I + \frac{p^2}{2r}\cos I - \frac{ap^3}{8r^2}\sin I &= \frac{1}{2t}y^2 + \frac{1}{2s}z^2 + C_{30}y^3 \\ &\quad + C_{12}yz^2 + \left(\frac{1}{8t^3}+C_{40}\right)y^4 + \left(\frac{1}{4t^2s}+C_{22}\right)y^2z^2 + \left(\frac{1}{8s^3}+C_{04}\right)z^4 \\ &\quad + q\left\{1 - \frac{1}{2t^2}y^2 - \frac{1}{2s^2}z^2 - \frac{3}{t}C_{30}y^3 - \left(\frac{1}{t}+\frac{2}{s}\right)C_{12}yz^2\right\} + O(p^5), \end{aligned} \quad \ldots\ldots(23\,a)$$

$$ap\cos I - \frac{p^2}{2r}\sin I - \frac{ap^3}{8r^2}\cos I = y - q\left\{\frac{1}{t}y + 3C_{30}y^2 + C_{12}z^2\right\} + O(p^4), \quad \ldots\ldots(23\,b)$$

$$ap - \frac{a}{8r^2}p^3 = z - q\left\{\frac{1}{s}z + 2C_{12}yz\right\} + O(p^4). \quad \ldots\ldots(23\,c)$$

As before, $y$ and $z$ must be eliminated from these equations, and the result solved for $q$ in terms of $p$. It can be seen from the diagram or from (25) and (26) below that

$$\therefore \quad y = ap\cos I + O(p^2), \qquad q = ap\sin I + O(p^2),$$

so that in the highest degree terms which are significant in any equation it is permissible to put $y = ap\cos I$, $q = ap\sin I$. Using these, it is found that

$$z = ap + \frac{a}{s}pq + \left\{\frac{a}{2s^2}\sin^2 I - \frac{a}{8r^2} + aC_{12}\sin I\cos I\right\}p^3 + O(p^4), \quad \ldots\ldots(24)$$

$$\begin{aligned} y = ap\cos I - \frac{p^2}{2r}\sin I + \frac{a}{t}pq\cos I + \Big\{&\frac{a}{2t^2}\sin^2 I\cos I - \frac{a}{8r^2}\cos I \\ &- \frac{a}{2rt}\sin^2 I + \frac{3a}{2}C_{30}\sin I\cos^2 I + \frac{a}{2}C_{12}\sin I\Big\}p^3 + O(p^4). \end{aligned} \quad \ldots\ldots(25)$$

The values of $y$ and $z$ from (24) and (25) are then substituted in (23$a$), neglecting terms which are $O(p^5)$, and the result is solved for $q$, giving

$$\begin{aligned} q = ap\sin I &+ \left\{\frac{\cos I}{2r} - \frac{\cos^2 I}{4t} - \frac{1}{4s}\right\} p^2 + \left\{\frac{a}{2rt}\cos I \sin I - \frac{a}{8r^2}\sin I \right. \\ &- \frac{a}{4t^2}\cos^2 I \sin I - \frac{a}{4s^2}\sin I - \frac{a}{2}C_{30}\cos^3 I - \frac{a}{2}C_{12}\cos I\Big\} p^3 \\ &+ \left\{\frac{1}{32t^3}\cos^4 I - \frac{1}{8t^3}\cos^2 I \sin^2 I - \frac{1}{8rt^2}\cos^3 I + \frac{1}{4rt^2}\cos I \sin^2 I \right. \\ &+ \frac{1}{16r^2t}\cos^2 I - \frac{1}{8r^2t}\sin^2 I + \frac{1}{32s^3} - \frac{1}{8s^3}\sin^2 I - \frac{1}{8rs^2}\cos I + \frac{1}{16r^2s} \\ &+ \frac{1}{16s^2t}\cos^2 I + \tfrac{3}{4}\sin I \cos I\left(\frac{\cos I}{r} - \frac{\cos^2 I}{t}\right) C_{30} \\ &+ \tfrac{1}{4}\sin I\left(\frac{1}{r} - \frac{2\cos I}{s} - \frac{\cos I}{t}\right) C_{12} - \tfrac{1}{4}C_{40}\cos^4 I \\ &\left. - \tfrac{1}{4}C_{22}\cos^2 I - \tfrac{1}{4}C_{04}\right\} p^4 + O(p^5). \qquad \ldots\ldots (26) \end{aligned}$$

Using (4), the first term on the right hand side of (26) gives Snell's law, and the second is a linear combination of the formulae for tracing $s$- and $t$-foci. The third term gives

$$\Delta N\left\{C_{30}\cos^3 I + C_{12}\cos I + \frac{1}{2s^2}\sin I + \frac{1}{2t^2}\cos^2 I \sin I - \frac{1}{rt}\cos I \sin I\right\} = 0. \qquad \ldots\ldots (27)$$

If equation (13) is subtracted from this, the result is

$$\Delta(C_{12}N\cos I) = \Delta N\left\{\frac{1}{2rt}\sin I \cos I - \frac{1}{2s^2}\sin I\right\}. \qquad \ldots\ldots (28)$$

Equation (28) is the refraction formula for the aberration coefficient $C_{12}$.

The term in $p^4$ in (26) gives in a similar way, on using (24) and (20) to eliminate $C_{40}$ and $C_{04}$,

$$\begin{aligned} \Delta(C_{12}N\cos^2 I) = \Delta N &\left\{\tfrac{1}{2}\sin I\left(\frac{1}{r} - \frac{2\cos I}{t} - \frac{4\cos I}{s}\right) C_{12} \right. \\ &- \frac{3}{2r}C_{30}\sin I \cos^2 I + \frac{1}{2rt^2}\cos I \sin^2 I - \frac{1}{4rt^2}\cos^3 I - \frac{1}{4r^2t}\sin^2 I \\ &\left. + \frac{1}{8r^3}\cos I - \frac{1}{2s^3}\sin^2 I - \frac{1}{4rs^2}\cos I + \frac{1}{4s^2t}\cos^2 I\right\}. \qquad \ldots\ldots (29) \end{aligned}$$

This is the refraction formula for $C_{22}$, the last to be found.

## § 7. TRANSFER FORMULAE FOR THE ABERRATION COEFFICIENTS

All that now remains to be done is to find transfer formulae giving the values of the aberration coefficients before the pencil is refracted at a surface in terms of their values immediately after refraction at the previous surface, as explained in § 3.

Suppose that the equation of the wave front immediately after refraction at a certain surface is

$$x' = \frac{1}{2t'}y'^2 + \frac{1}{2s'}z'^2 + C'_{30}y'^3 + C'_{12}y'z'^2 + \left(\frac{1}{8t'^3} + C'_{40}\right)y'^4 + \left(\frac{1}{4t'^2s'} + C'_{22}\right)y'^2z'^2 + \left(\frac{1}{8s'^3} + C'_{04}\right)z'^4 + \ldots \quad \ldots\ldots(30)$$

and let the equation of the wave front immediately before refraction at the next surface be (2), i.e. the same as (30), but with the primes omitted. Let the distance along the principal ray from the first surface to the second be $D'$; then if points are taken at a constant distance $D'$ from the surface (30) along its normals, the locus of such points will be the surface (2) (Figure 7).

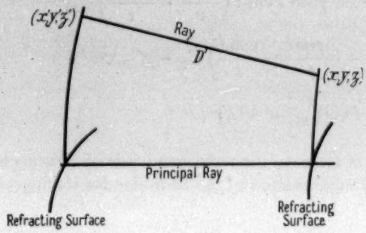


Figure 7.

If the normal to (30) has the direction cosines $(l', m', n')$ the points concerned will have coordinates $x, y, z$ given by

$$\left.\begin{aligned} x &= x' + (l'-1)D', \\ y &= y' + m'D', \\ z &= z' + n'D'. \end{aligned}\right\} \quad \ldots\ldots(31)$$

But since the two surfaces have a common normal, $l'$, $m'$ and $n'$ in (31) may be replaced by $l, m, n$, the direction cosines of the normal to (2), giving

$$\left.\begin{aligned} x' &= x - (l-1)D', \\ y' &= y - mD', \\ z' &= z - nD'. \end{aligned}\right\} \quad \ldots\ldots(32)$$

When these values of $x'$, $y'$ and $z'$ are substituted in (30) and $x, l, m, n$, are expressed in terms of $y$ and $z$ the result must be an identity in $y$ and $z$,

$$\begin{aligned} x - (l-1)D' = {} & \frac{1}{2t'}(y-mD')^2 + \frac{1}{2s'}(z-nD')^2 + C'_{30}(y-mD')^3 \\ & + C'_{12}(y-mD')(z-nD')^2 + \left(\frac{1}{8t'^3} + C'_{40}\right)(y-mD')^4 \\ & + \left(\frac{1}{4t'^2s'} + C'_{22}\right)(y-mD')^2(z-nD')^2 \\ & + \left(\frac{1}{8s'^3} + C'_{04}\right)(z-nD')^4 + \ldots. \end{aligned} \quad \ldots\ldots(33)$$

When the coefficients of the various powers of $y$ and $z$ in this identity are separately equated to zero, a set of relations between the primed and unprimed aberration coefficients is obtained, and these give the required transfer formulae.

The direction cosines $(l, m, n)$ are obtained as in § 6, but the values are required to a higher order of accuracy; equation (33) must be correct to $O(p^4)$, where $p$ is of the same order of magnitude as $y$ and $z$; hence $l$ must be correct to $O(p^4)$ and $m$ and $n$ to $O(p^3)$, since $D'$ is $O(p^0)$. It is found that

$$\left.\begin{aligned} l-1 = &-\left\{\frac{1}{2t^2}y^2+\frac{1}{2s^2}z^2+\frac{3}{t}C_{30}y^3+\left(\frac{1}{t}+\frac{2}{s}\right)C_{12}yz^2+\left(\frac{4}{t}C_{40}+\frac{9}{2}C_{30}^2+\frac{1}{8t^4}\right)y^4\right.\\ &+\left(2\left(\frac{1}{t}+\frac{1}{s}\right)C_{22}+3C_{30}C_{12}+2C_{12}^2+\frac{1}{2t^3s}-\frac{1}{4t^2s^2}\right)y^2z^2\\ &\left.+\left(\frac{4}{s}C_{04}+\tfrac{1}{2}C_{12}^2+\frac{1}{8s^4}\right)z^4\right\}+O(p^5),\\ m = &-\left\{\frac{1}{t}y+3C_{30}y^2+C_{12}z^2+4C_{40}y^3+\left(2C_{22}-\frac{1}{2ts^2}+\frac{1}{2t^2s}\right)yz^2\right\}+O(p^4),\\ n = &-\left\{\frac{1}{s}z+2C_{12}yz+2C_{22}y^2z+4C_{04}z^3\right\}+O(p^4). \end{aligned}\right\} \quad \ldots\ldots(34)$$

Hence, since $t=t'-D'$, $s=s'-D'$, it follows that

$$\begin{aligned} y-mD' = &\frac{t'}{t}y+3D'C_{30}y^2+D'C_{12}z^2+4D'C_{40}y^3\\ &+D'\left(2C_{22}-\frac{1}{2ts^2}+\frac{1}{2t^2s}\right)yz^2+O(p^4),\\ z-nD' = &\frac{s'}{s}z+2D'C_{12}yz+2D'C_{22}y^2z+4D'C_{04}z^3+O(p^4). \end{aligned}$$

On substituting these and the value of $x$ from (2) in (33) the identity in $y$ and $z$ is obtained; equating the coefficients of $y^2$ and $z^2$ to zero gives the obvious relations

$$t=t'-D'; \qquad s=s'-D'. \qquad \ldots\ldots(35)$$

From the coefficients of $y^3$ and $yz^2$ the following are obtained, after some simplification:

$$C_{30}=\left(\frac{t'}{t}\right)^3 C'_{30}; \qquad \ldots\ldots(36)$$

$$C_{12}=\frac{t'}{t}\left(\frac{s'}{s}\right)^2 C'_{12}. \qquad \ldots\ldots(37)$$

From the coefficients of $y^4$, $y^2z^2$ and $z^4$, after simplification including the use of (36) and (37),

$$C_{40}=\left(\frac{t'}{t}\right)^4\left\{C'_{40}+\frac{9}{2}\frac{Dt'}{t}C'^2_{30}\right\}, \qquad \ldots\ldots(38)$$

$$C_{22}=\left(\frac{t's'}{ts}\right)^2\left\{C'_{22}+3\frac{D't'}{t}C'_{12}C'_{30}+2\frac{D's'}{s}C'^2_{12}\right\}, \qquad \ldots\ldots(39)$$

$$C_{04}=\left(\frac{s'}{s}\right)^4\left\{C'_{04}+\tfrac{1}{2}\frac{D't'}{t}C'^2_{12}\right\}. \qquad \ldots\ldots(40)$$

Equations (36) to (40) are the transfer formulae for the aberration coefficients.

## §8. DISCUSSION OF THE RESULTS

**The refraction and transfer formulae may be collected together as follows:**

| Coefficient | $C_{30}$ | $C_{12}$ | $C_{40}$ | $C_{22}$ | $C_{04}$ |
|---|---|---|---|---|---|
| Refraction formula equation no. | (13) | (28) | (14) | (29) | (20) |
| Transfer formula equation no. | (36) | (37) | (38) | (39) | (40) |

It will be seen that the formulae for the fourth power coefficients $C_{40}$, $C_{22}$, $C_{04}$ contain one or both of the third power coefficients $C_{30}$, $C_{12}$. In the case of the refraction formulae this means that the amount of fourth power aberration introduced on refraction at a surface depends on the amount of third power aberration present in the incident wave front*.

From the transfer formulae it can be seen that the wave front aberrations change in type as the wave front travels along the principal ray. For example, equation (40) shows that a wave front having primary coma ($C_{12}$) will, after travelling some distance, also have some primary spherical aberration ($C_{04}$). This effect is usually quite small, but it may reach considerable proportions in a system with large separations between surfaces. By a similar argument to that in the last paragraph it can be shown that the change on transfer of an $n$th degree coefficient ($C_{ij}$, where $i+j=n$) involves coefficients of the $n-1$th degree.

The formulae as given above are probably in the best form for exhibiting the relationships of the aberration coefficients to each other and to the data of the principal ray trace, and in this paper they will be left in this form. In a subsequent paper they will be put into forms more suitable for numerical computation and numerical examples will be given to show how closely the aberration coefficients reproduce the actual aberrations of a system, as determined by ray-tracing. Further work to be published includes formulae showing the effect of shifting the stop position, generalizations of the formulae for non-spherical surfaces, and formulae for the chromatic variations of the aberrations.

## ACKNOWLEDGMENTS

This work is part of a programme undertaken for the Ministry of Supply, to whom thanks are due for permission to publish it. The author is grateful to Professor L. C. Martin and to Dr. H. H. Hopkins for advice and criticism; Dr. Hopkins suggested the investigation of the aberration of a pencil at finite field angles as part of the programme of work.

## REFERENCES

HAMILTON, W. R., 1833, *British Association Report*, p. 360.

VON ROHR, M., 1920, *The Formation of Images in Optical Instruments* (London: H.M. Stationery Office), §129.

* There is a similar effect for all higher degree aberration terms. Suppose that the aberration coefficient $C_{ij}$ from the term $y^i z^j$ in (2) is being investigated, where $i+j>4$, so that quantities which are $O(p^{i+j})$ must be retained in the expression for $q$; since $q$ is usually $O(p)$, (unless $i=0$, when $\psi$ is taken as $\pi/2$ as in §5 and $q$ is $O(p^2)$) equation (5$a$) shows that terms in $l$ which are $O(p^{i+j-1})$ must be retained, and from the method of evaluating $l$ (see §5) it is clear that coefficients of terms in $x$ which are $O(p^{i+j-1})$ will enter into such terms in $l$. That is, in the refraction formula for $C_{ij}$, coefficients of degree one lower, such as $C_{i-1,j}$, $C_{i+1,j-2}$ etc., will occur. In the case where $i=0$, so that $q$ is $O(p^2)$, this is still true, since $y$ is $O(p^2)$ and the term in $x$ containing $C_{1,j-2}$ in equation (5$a$) is $O(p^j)$; thus $C_{1,j-2}$ occurs in the coefficient of $p^j$ in the final expression for $q$. For example, if $C_{06}$ were being evaluated, $C_{14}$ would be involved, and so on.

# The Temperature Variation of the Long-Wave Limit of Infra-Red Photoconductivity in Lead Sulphide and Similar Substances

By T. S. MOSS*

Physics Department, Telecommunications Research Establishment, Malvern

*Communicated by R. A. Smith; MS. received 13th May 1949*

*ABSTRACT.* Measurements have been carried out on the spectral distribution of the photoconductive effect in layers of lead sulphide, selenide and telluride, at temperatures ranging from room temperature to that of liquid hydrogen. It is shown that cooling has a marked effect on the long-wave limit of sensitivity, which increases by as much as two microns on cooling with liquid hydrogen.

Brief descriptions of spectral measurements on these materials have already been published by the author. It is shown that depopulation of energy levels due to thermal activation of electrons is not responsible for the shift of spectral sensitivity. The suggestion is made that the shift may be related to the variation of dielectric constant with temperature.

## §1. INTRODUCTION

A CONSIDERABLE number of materials, mainly oxides and sulphides or related types, are now known which exhibit photoconductivity on irradiation by light in the visible or near infra-red region. Examples are HgS, CdS, CdSe, CdTe, S, Se, $MoS_2$, $Sb_2S_3$, $Bi_2S_3$, ZnS, $Ag_2S$, $Cu_2O$, PbS, PbSe, PbTe, $PbCrO_4$, and a few mixed crystals.

For stibnite, $Sb_2S_3$, Elliot found that the wavelength of peak sensitivity was reduced from $0{\cdot}76\,\mu$ at $-20°$ c. to $0{\cdot}68\,\mu$ at $-190°$ c. (Elliot 1915).

For acanthite, $Ag_2S$ (Coblentz 1919), it was found that the wavelength of peak sensitivity decreased from $1{\cdot}5\,\mu$ to $1{\cdot}3\,\mu$ on cooling from 22° c. to $-158°$ c. Similar results were obtained for argentite—an alternative crystalline form of $Ag_2S$.

For stephanite (Barish 1935) a progressive reduction in the threshold wavelength from $0{\cdot}8\,\mu$ to $0{\cdot}74\,\mu$ takes place as the temperature is reduced from 21° c. to $-125°$ c.

The absorption edge of $MoS_2$ moves from $0{\cdot}7\,\mu$ at room temperature to $0{\cdot}66\,\mu$ at $-190°$ c. (Coblentz 1919).

Frerichs (1947) showed that for CdS there was a linear relation between the temperature and the threshold wavelength which varied from $0{\cdot}58\,\mu$ at 500° c. to $0{\cdot}49\,\mu$ at $-183°$ c.

For the substances PbS, PbSe, PbTe, which show conductivity at longer wavelengths than the substances mentioned above, the threshold wavelength *increases* with cooling. Experiments on this effect are described in the following section.

## §2. EXPERIMENTAL RESULTS

The material used for the measurements of spectral sensitivity was in the form of microcrystalline layers deposited on the inner walls of small evacuated Dewar vessels. The PbS layers used were chemically deposited, and subsequently sensitized by heating in oxygen.

* Now attached to the Department of Colloid Science, Cambridge.

The PbSe and PbTe layers were made by evaporation *in vacuo* of appropriate quantities of the bulk compounds. These compounds were prepared by heating the constituent elements together in evacuated quartz tubes for some hours at 1000° c. Both the PbSe and PbTe were made with an initial excess of Se (or Te) of 5% over the stoichiometric composition, and then purified by vacuum sublimation.

The material was sensitized by heating at low pressure (about $10^{-5}$ mm. Hg) at a temperature just below the sublimation temperature for the compound, for periods varying from one to twenty hours. The final layer was then formed by evaporating the film by a blowtorch flame whilst the electrode surface was water-cooled.

It was necessary to provide the cells with windows capable of transmitting the range of wavelengths required. For PbS, the window was an "infra-red glass" of the soda–zinc-oxide–silicate type. The transmission of the window was measured after the other measurements on the layer were completed. It was found that the transmission was more than 70% between 1·0 and 4·2 $\mu$, falling to 25% at 4·5 $\mu$. The spectral sensitivity curves were corrected for this loss.

For the PbSe and PbTe cells, the window material was KRS 5 (a mixture of thallium bromide and iodide) which had 65% transmission from 1 to 35 $\mu$. Plates of this material were fixed to the cell envelopes by vacuum wax. Thus the envelopes could not be heated during the sensitizing process. Two means of overcoming this difficulty were evolved:

(*a*) The window was kept cool by immersion in water, whilst the layer (deposited on the inner wall) was heated by filling the inside of the cell with a low melting point alloy, maintained at the requisite temperature of about 400° c. by a small electric heater.

(*b*) The envelope was made with an elongated neck to which the window was attached. The envelope was then mounted on the vacuum system with the window protruding through the base of an oven, so that it could again be watercooled.

No measurements of the reflection or absorption of the layers were made. However, it is known (Mellor 1923) that the reflection coefficient of PbS is constant at 31% over the wavelength range of 1 to 10 $\mu$. For PbSe the reflection coefficient for red light is 40% (Schneiderhohn 1931) and it will probably stay constant at about this value in a like manner to that of PbS. Similar behaviour would be expected for PbTe.

To overcome the difficulty of the absorption varying with wavelength, the layers were made relatively thick, so that there would be almost no transmission at all wavelengths used. Then, with the reflection coefficient roughly constant, the energy absorbed would be proportional to the incident radiation.

Measurements on PbS films* at room temperature have shown that the absorption varies only gradually from 1 $\mu$ to 4 $\mu$. Similar results have been obtained (Simpson and Daly, unpublished data) for PbTe, where a layer about 0·2 $\mu$ thick had 80% absorption in the near infra-red, falling to 50% at longer wavelengths.

The thicknesses of the layers used by the author were estimated by weighing the films after the rest of the measurements were completed. The values obtained were: PbS 1·8 $\mu$, PbSe 1·2 $\mu$, PbTe 1·0 $\mu$ (approximately).

The spectrometer used in these measurements was a double monochromator with lithium fluoride prisms and having a high degree of freedom from scatter.

* Unpublished experiments carried out by E. J. Harris at T.R.E. in 1945.

Radiation from a Nernst source was interrupted by a motor driven chopper disc at 800 c/s. before entering the spectrometer. The resultant signal from the cell was fed into a high gain amplifier tuned to 800 c/s., the output from which was read on an A.C. meter.

A Hilger thermopile was used to measure the energy emerging from the spectrometer.

The sensitivity figures for an equal-energy spectrum could then readily be found by virtue of the fact that, for the intensities used, the signal from the layer

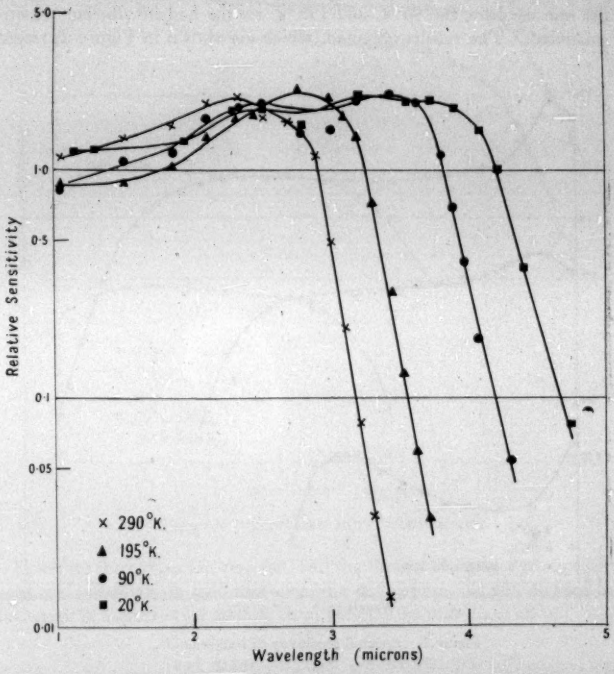


Figure 1. Spectral sensitivity of lead sulphide. Scales adjusted to make peak sensitivities equal.

was proportional to the incident radiation. It may be noted that, due to the manufacturing difficulties caused by the use of windows which could not be heated, these layers were not of optimum sensitivity. For such layers the linearity law holds up to higher intensities.

### § 3. MEASUREMENTS ON PbS, PbSe, PbTe

For lead sulphide, measurements were carried out at room temperature, and when cooled by solid carbon dioxide in acetone, liquid oxygen and liquid hydrogen. The results (referred to an equal-energy spectrum) are shown in Figure 1.

It will be observed that the curves are comparatively flat at the shorter wavelengths, but that as the wavelength is increased, a "threshold" is reached beyond which the sensitivity decays rapidly in an approximately exponential manner. This point extends to longer wavelengths as the temperature is lowered. Defining the "threshold" as the wavelength at which the sensitivity has fallen to 50% of its peak value, we see that cooling has increased this wavelength from 2·9 to 4·2 microns.

For the PbSe layers sensitivity measurements were made at 290° K., 195° K. and 90° K. The room temperature measurements were made on a different layer, since the one used for the 90° K. and 195° K. results had insufficient sensitivity when uncooled. The results obtained, which are shown in Figure 2, resemble

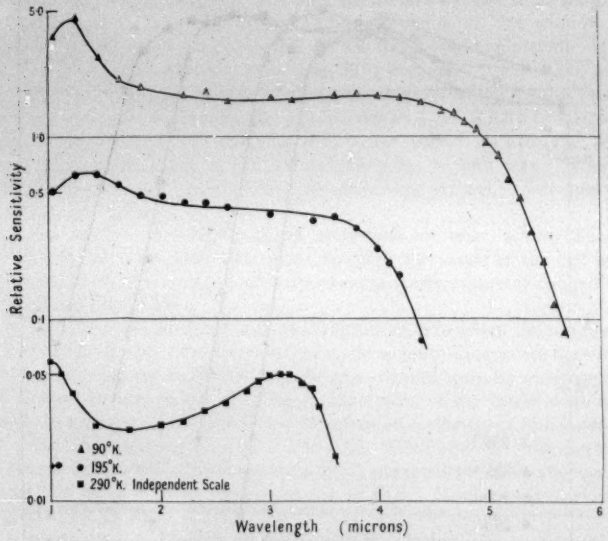


Figure 2. Spectral sensitivity of lead selenide.

those for the sulphide. As the curves are flat over a considerable range of wavelengths, it is convenient to take the threshold where the sensitivity has dropped to 50% of its value at some point on the flat part of the curve, say 3·0 $\mu$. With this definition, it is seen that the threshold is extended from about 3·5 $\mu$ to 5·0 $\mu$ on cooling to 90° K.

For PbTe, experiments were carried out at temperatures of 20° K., 77° K., 90° K., 195° K. and 234° K. This latter temperature, the melting point of mercury, is the highest temperature at which any of the PbTe layers yet made had adequate sensitivity to enable a spectral measurement to be made. Even so, the sensitivity at both 234° K. and 195° K. was poor, with consequent loss of accuracy—particularly at the longer wavelengths. The experimental results are plotted in Figure 3.

The measurements at 20° K. did not cover the complete wavelength range due to the fact that the design of the cell envelope was unsatisfactory for use with liquid hydrogen, which evaporated so rapidly that only a small number of points could be plotted. These were accordingly taken over the threshold region.

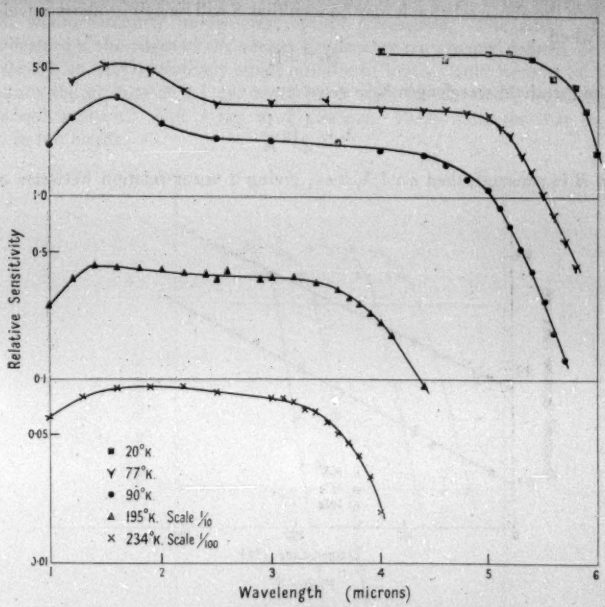


Figure 3. Spectral sensitivity of lead telluride.

As before the curves are very flat, and the threshold wavelength is again taken where the sensitivity is half that over the flat region. It will be seen that this wavelength is increased by cooling from below 4·0 $\mu$ to 6·0 $\mu$ at 20° K.

## §4. DISCUSSION OF RESULTS

It has been found for all three types of layer, that if the quantum value appropriate to the threshold wavelength is plotted against the temperature, the points fall on a straight line. Such plots are shown in Figure 4. The PbS results are shown on the top line, while those for PbSe and PbTe lie on the same (lower) line.

The threshold quantum value $\epsilon_T$ may be expressed as $\epsilon_T = \epsilon_0 + \alpha T$, where $\alpha$ has a similar value for all three materials. Any of the family of PbS spectral sensitivity curves can be represented by an empirical formula of the type $S = A/[1 + B e^{a\lambda}]$ where $\lambda$ is in microns. $a$ is determined from the slope of the curve beyond the "threshold", $B$ is adjusted to give the threshold at the correct wavelength, and $A$ is merely a scale factor for the absolute sensitivity.

$B$ is independent of temperature and has the value $e^{-29}$, while $a$ varies with temperature as follows:

| $T$(° K.) | 290 | 195 | 90 | 20 |
|---|---|---|---|---|
| $a$ | 9·92 | 8·90 | 7·62 | 6·85 |

From the above relation it may be seen that $S$ will be half its short-wavelength value when

$$Be^{a\lambda}=1,$$

i. e. the threshold wavelength $\lambda_T$ is given by

$$\lambda_T=\frac{1}{a}\ln\frac{1}{B}.$$

Since $B$ is constant, then $a\propto 1/\lambda_T\propto\epsilon_T$, giving a linear relation between $a$ and

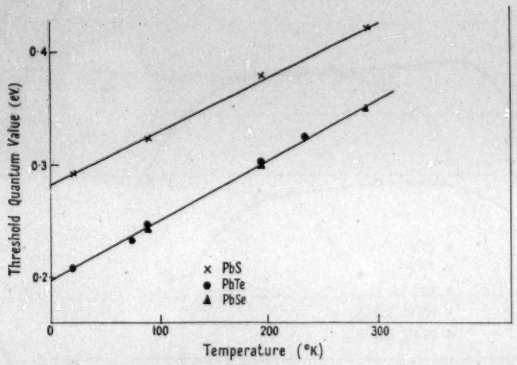


Figure 4.

the temperature which is found to be $a=(575+T)/87$. Thus the whole family of spectral sensitivity curves for PbS may be expressed as

$$S_\lambda\propto\frac{1}{1+\exp[\lambda(575+T)/87-29]}.$$

This function is plotted in Figure 5 for comparison with the experimental curves.

The PbSe and PbTe results may be expressed by a similar formula, i.e.

$$S_\lambda\propto\frac{1}{1+\exp[\lambda(388+T)/125-19]}.$$

In this case, however, the agreement is inferior to that for PbS.

## §5. POSSIBLE CAUSES OF SPECTRAL SHIFT

So far there is no general theory of photoconductivity in semiconductors, and the factors determining the threshold wavelength and its temperature dependence are not yet fully understood.

One factor which it was thought might contribute to the shift of threshold wavelength is the varying density of conduction electrons in the material as the temperature changes. On the band theory of solids, increasing numbers of

electrons will be raised from the full band to the conduction band of energy levels as the temperature is raised. It is possible that these electrons could fill the lower levels in the conduction band to such an extent that the optical transitions giving rise to the photoconductivity could only take place to levels somewhat above the bottom of the conduction band. Depopulation of the levels at the top of the filled band would similarly modify the optical transitions. The effect would be emphasized if the edges of the energy bands were not sharply defined, but tailed off slowly, so that a relatively small number of levels would have to be filled to produce the change of 0·1 ev. required to shift the threshold wavelength the observed amount. Soft x-ray work (Skinner 1938) indicates that there are tails to the bands.

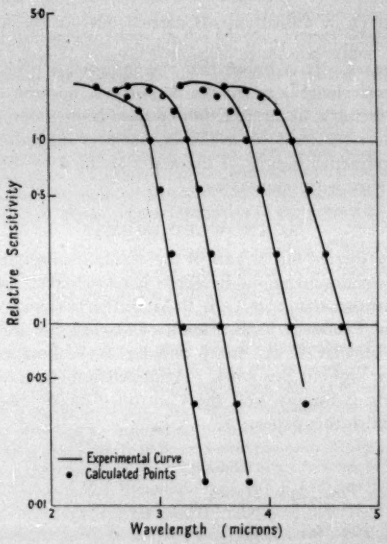


Figure 5.

The mechanism suggested could be checked experimentally by using a strong light to produce the high density of conduction electrons, whilst maintaining the temperature constant. Accordingly, the spectral sensitivity was measured for a PbS layer at room temperature and then at liquid oxygen temperature, with a steady illumination on the layer such that the conductivity was almost restored to its original room temperature value. It was found that the usual large shift occurred on cooling, and that the application of the light had a negligible effect.

Another mechanism which may contribute to the shift of the spectral sensitivity curves is change of the refractive index of the material. If the photo-effect does not take place equally at all lattice points but occurs only at privileged positions where the periodicity of the lattice is disturbed by either interstitial ions, vacant lattice sites, or cracks, then these centres will be somewhat similar to

isolated atoms except that they are immersed in a medium of dielectric constant equal to that of the bulk material. The energy levels of the centres will then be reduced in the ratio $1/K^2$, where K is the effective dielectric constant of the material in the neighbourhood of the centre. The threshold of the photoconductive effect will then depend on the dielectric constant, any temperature variation of which will cause a spectral shift.

According to Mott and Gurney (1940) this dielectric constant will be nearly that of the material at optical frequencies—i.e. (refractive index)$^2$.

Unfortunately no data are at present available on the temperature variation of the refractive index of the PbS series with which to test this hypothesis.*

## § 6. CONCLUSIONS

Results are given of measurements carried out on the spectral distribution of infra-red photoconductivity in lead sulphide, selenide, and telluride layers at various temperatures. It is found that the long-wave threshold of sensitivity moves to longer wavelengths as the temperature is reduced, the quantum value of the threshold being a linear function of the absolute temperature. No full explanation of these results is yet available, but it is suggested that temperature variation of the refractive indices of the materials may be the cause of the shift of spectral sensitivity with temperature.

## ACKNOWLEDGMENTS

This work was carried out as part of the research programme of the Physics Department, Telecommunications Research Establishment, Ministry of Supply.

The author wishes to thank Dr. G. B. B. M. Sutherland and Mr. D. E. Blackwell of Cambridge and Professor F. E. Simon of Oxford for arranging supplies of liquid hydrogen, and Dr. R. A. Smith and Dr. F. E. Jones of T.R.E. for their encouragement throughout this work. Acknowledgment is made to the Chief Scientist, Ministry of Supply, and the Controller, H.M. Stationery Office, for permission to publish this paper.

## REFERENCES

Barish, J., 1935, *Ann. Phys., Lpz.*, **21**, 804.
Coblentz, W. W., 1919, *Bull. Bur. Stds., Wash.*, **15**, 121, 231.
Elliot, D. S., 1915, *Phys. Rev.*, **5**, 53.
Frerichs, R., 1947, *Phys. Rev.*, **72**, 594.
Mellor, J. W., 1923, *Inorganic and Theoretical Chemistry* (London : Longmans, Green).
Moss, T. S., 1947, *Nature, Lond.*, **159**, 467 ; 1948, *Ibid.*, **161**, 776.
Mott, N. F., and Gurney, R. W., 1940, *Electronic Processes in Ionic Crystals* (Oxford : University Press).
Schneiderhohn, H., 1931, *Lehrbuch der Erzmikroskopie*, Vol. 2 (Berlin : Borntraeger).
Skinner, H. W. B., 1938, *Rep. Prog. Phys.*, **5**, 257 (London : Physical Society).

* A further article on the theory underlying these measurements is to be published.

# REVIEWS OF BOOKS

*Mercury Arcs*, by F. J. TEAGO and J. F. GILL. Pp. viii + 107. Methuen's Monographs on Physical Subjects. 2nd (revised) Edition. (London: Methuen, 1949.) 6*s.* 6*d.*

The mercury arc rectifier is the most common form of gas-filled valve, and is of great interest to the modern electrical engineer. The control of very high currents, voltage regulation, frequency changers and speed control of heavy A.C. motors, are just a few of the modern applications which have now developed into an important branch of electrical engineering.

This type of rectifier operates in virtue of the copious production of electrons at local regions of the cathode, which is a pool of mercury; the electrons produced ionize the vapour through which a low-voltage arc passes to the anode. Voltage drop is practically independent of the current passed. Vapour is supplied by the evaporation of the cathode, and mercury has the advantage that this loss due to evaporation is made good by the return of the liquid condensed from the vapour at the cool walls of the containing vessel. If no electrons can be produced at the other electrode (the anode) then no current passes when the applied voltage is reversed, and perfect rectification takes place. On the other hand, if for some reason the anode develops electron-emitting regions, then a glow discharge, which possibly leads to an arc, can take place on the reverse phase, and rectification is reduced; when a full arc (back-fire) occurs there is complete failure of the rectifying action. Thus the mercury arc rectifier depends for its action on the asymmetry of the properties of the cathode and anode.

Now the operation of such a rectifier presents a number of fundamental problems of great interest to the physicist. In the first place, there is the important problem of the mechanism of electron production at the cathode hot-spot, and various mechanisms have been suggested :—local thermionic emission; cold emission in the field set up by the positive ion space charge near the cathde hot-spot; microscopic oscillation of the mercury surface, set up by fluctuations in the surface, leading to sharp projections of mercury from which emission then occurs due to the intensified field; but the full explanation has yet to be given. In fact, considerable doubt exists concerning the actual state of matter in the microscopic region near the surface of the hot-spot. Moreover, the development of electron emitting regions in the anode presents an interesting problem to the physicist. Consequently, a modern book on mercury arcs is likely to be read with great interest by the research physicist and electrical engineer alike, to see what discussion is given to these fundamental problems.

*Mercury Arcs* by Professor F. J. Teago and the late J. F. Gill was first published in 1936, but a second edition, revised, has been issued this year. It has the object of outlining the "more important aspects of the arc from the electrical, mechanical, and operation standpoints; .... and fine detail has purposely been omitted in order that the essential principles may stand out clearly".

The book has 11 chapters and an appendix. The first chapter, of 12 pages, covers the theory of the rectifier, including cathode processes and back-fires. Chapter 2, of 15 pages, gives constructional details of a high-output tank rectifier, together with some observations on high vacua, including diffusion pumps, McLeod and Pirani gauges. The rest of this book of 104 pages is taken up with what may be called circuit analysis, as indicated by the chapter titles: Grid control of voltage; Grid control of current; Voltage regulation; Current-voltage characteristics; Rectification, inversion and regeneration; Wave-form analysis; Transformer ratings; Power factor; Mathematics of mercury arcs; Appendix, The Pirani gauge. The chapter on the mathematics of mercury arcs has nothing at all to do with the mechanism of the arc itself; it does not discuss the diffusion of ions and electrons, recombination, and ion-bombardment of electrodes, but gives analyses of transformer circuits containing ideal rectifiers.

It should thus be clear that the title of the book is misleading; a more appropriate title would have been Mercury Arc Circuit Analysis. Considered as a book on Mercury Arcs, it fails in the aim stated in the Preface, viz. to make essential principles stand out clearly. The inadequate treatment of the physics of mercury arcs is the more unfortunate as the

book appears in Methuen's Series of Monographs on Physical Subjects. The brief discussion given on the mechanism of the arc, which is the subject of greatest interest to the physicist, contains some questionable statements. For instance, the rectifying action does not as is stated (page 1) depend upon the unilateral conductivity of an ionized vapour. In the discussion (pages 4 to 6) of the cathode hot-spot, the impression is given that electron production at the cathode is accounted for by thermionic emission, although experiments are quoted from which the authors conclude (page 8) that it is doubtful if the hot-spot temperature ever reaches 1000° C. Again, the mechanism of back-fire is treated very briefly for so important a subject, and the practical problem of commutation oscillations is not dealt with at all. Considering the inadequate treatment of these fundamental problems of the mercury arc rectifier, it is difficult to find justification for the inclusion of an appendix entitled the Pirani Gauge, which in fact gives the well-known theory of the unbalanced Wheatstone bridge and nothing else. It appears that the book is likely to be of more interest to the circuit engineer than to the physicist. F. LLEWELLYN JONES.

---

# CONTENTS FOR SECTION A

PAGE

Prof. W. HEITLER and Prof. L. JÁNOSSY. On the Size–Frequency Distribution of Penetrating Showers . . . . . 669

Dr. A. DUPERIER. The Meson Intensity at the Surface of the Earth and the Temperature at the Production Level . . . . . 684

Mr. C. B. VAN WYK. On the Decay of $\tau$-Mesons . . . . . 697

Miss J. JACOBS. Excited Electronic Levels in Conjugated Molecules—III: Energy States of Naphthalene . . . . . 710

Dr. H. G. WOLFHARD and Dr. W. G. PARKER. A New Technique for the Spectroscopic Examination of Flames at Normal Pressures . . . . . 722

Dr. G. F. J. GARLICK and Mr. A. F. GIBSON. Dielectric Changes in Phosphors containing more than One Activator . . . . . 731

Prof. A. RUBINOWICZ. Eigenfunctions following from Sommerfeld's Polynomial Method . . . . . 736

Letters to the Editor:

Mr. B. V. THOSAR. Origin of Low-Energy Electron Lines in the $\beta$-spectrum of $^{198}$Au . . . . . 739

Mr. B. EISLER and Dr. R. F. BARROW. The Ultra-Violet Absorption Spectrum of SnO . . . . . 740

Mr. W. H. HALL. X-Ray Line Broadening in Metals . . . . . 741

Dr. R. STREET and Mr. J. C. WOOLLEY. Magnetic Viscosity in Mn–Zn Ferrite . . . . . 743

Reviews of Books . . . . . 745

Corrigendum . . . . . 746

Contents for Section B . . . . . 747

Abstracts for Section B . . . . . 747

# ABSTRACTS FOR SECTION A

*On the Size–Frequency Distribution of Penetrating Showers*, by W. HEITLER and L. JÁNOSSY.

*ABSTRACT.* We have calculated the relative number of showers containing $n$ mesons when a fast primary nucleon hits a compound nucleus on the assumption that in a single nucleon–nucleon collision only one meson is produced (pure plural production). The cross section for meson production is assumed to have the form $\Phi(\epsilon/E)\,d\epsilon/E$, where $E$ is the energy of the primary and $\epsilon$ the energy lost by it, but the absolute value of $\Phi$ and its dependence on $\epsilon/E$ are left open. The fluctuations of the shower size are duly taken into account. For comparison with experiments it is assumed that about half the number of fast shower particles are fast protons as suggested by the positive excess of penetrating shower particles. The theoretical results depend on two constants, the total cross section and some weighted average over the energy distribution $\Phi(\epsilon/E)$. Choosing these suitably, the results are in good agreement with the relevant data within the experimental statistical errors, and the agreement extends also to the " large showers " with 20 or so thin tracks. The values of the constants thus determined are physically reasonable. It is concluded that the size–frequency distribution of penetrating showers can be fully understood on the basis of pure plural production, but some—small or large—contribution from multiple processes cannot be excluded.

*The Meson Intensity at the Surface of the Earth and the Temperature at the Production Level*, by A. DUPERIER.

*ABSTRACT.* Meson intensity has been recorded by using a triple-coincidence arrangement with a lead absorber 25 cm. thick between the counters. The comparison of daily mean values with the height of a number of pressure-levels has led us to take into consideration the temperature of the air layer between 200 and 100 mb. The results show that this temperature appears to be a factor closely controlling the meson intensity at the surface of the earth; the intensity increases with increasing temperature at the rate of 0·12% per °c.

Other factors in determining the intensity are the mass of air and the height of the 100 mb. level over the station. The corresponding coefficients of absorption and decay prove to be comparable with those obtained from other measurements for mesons of the same momentum. It has also been found that the coexistence of the three effects permits explanation of the variability exhibited by the barometric coefficient when evaluated from short periods of observations.

These results may therefore be taken as evidence that the bulk of mesons is produced at the height of 100 mb.

If the positive effect of temperature is interpreted as the result of processes of decay and interactions with air nuclei of $\pi$-mesons at the production level, then the coefficient 0·12% per °c. leads to a value of $4{\cdot}9\times10^{-8}$ sec. for the upper limit of the mean life of $\pi$-mesons.

*On the Decay of $\tau$-Mesons*, by C. B. VAN WYK.

*ABSTRACT.* The production of $\tau$-mesons (mass about 900 electron masses) by cosmic rays in rather thin layers of air in the upper atmosphere seems to indicate that the nucleon $\tau$-meson coupling constant is not very small. The Berkeley experiments show that this is also true for the nucleon–$\pi$-meson coupling constant. Consequently the decay of a charged $\tau$-meson into a photon and a charged $\pi$-meson by means of virtual creation and annihilation of nucleons ought to be fairly probable. In this paper this decay process, with the emission of one photon, is studied for the various types of $\tau$- and $\pi$-mesons. Unless both mesons have zero spin, the matrix elements, and therefore the lifetimes, are found to be of the same order of magnitude, and the $\tau$-meson turns out to be too short-lived to be observed photographically.

If both mesons have zero spin the emission of only one photon is forbidden. The detailed discussion of higher order decay processes in this case is reserved for a later paper.

*Excited Electronic Levels in Conjugated Molecules—III: Energy States of Naphthalene*, by J. JACOBS

*ABSTRACT.* The electronic states of naphthalene are determined using antisymmetrized molecular orbitals, which are based on wave functions given by the simple molecular orbital theory. This method allows the electronic interaction term to be included explicitly in the Hamiltonian for the system. A clear distinction is made between electronic configurations determined with these wave functions and the actual states of the molecule: states arise from a superposition of configurations of the same symmetry. The ground state becomes considerably stabilized by this configurational interaction, to which even highly excited levels contribute. Calculated energy values for some of the lower transitions agree well with ultra-violet spectral data, as do the newly derived oscillator strengths. A tentative assignment is made regarding the polarization of the electronic transitions in the region of 30,000—55,000 $cm^{-1}$.

*A New Technique for the Spectroscopic Examination of Flames at Normal Pressures*, by H. G. WOLFHARD and W. G. PARKER.

*ABSTRACT.* Up to the present spectroscopic studies of flames supported on a tube have been limited by the geometry of the flame. Thus the important reaction zone presents a three-dimensional problem in which it is impossible to locate the emitters exactly. Moreover this zone is so thin in premixed gas flames that intermediate products cannot be determined from absorption studies. To overcome these difficulties the authors have constructed a burner with a two-dimensional diffusion flame in which the reaction zone at ordinary pressures is 5–10 mm. thick and has an optical depth of 5 cm. or more. With this flame many of the reacting molecules can be located through either their emission or absorption spectra or both. The value of the new technique in the elucidation of combustion processes is demonstrated with reference to $NH_3$–$O_2$ and $H_2$–$O_2$ flames, and mention is made of its application to hydrocarbon flames.

*Dielectric Changes in Phosphors containing more than One Activator*, by G. F. J. GARLICK and A. F. GIBSON.

*ABSTRACT.* It is well known that some luminescent materials, notably zinc sulphide, show marked changes in dielectric constant and dielectric loss when excited. Recent work by the authors has established that the changes are due to the filling of electron traps, which have large effective diameter and high polarizability.

The present paper describes measurements of the dielectric changes in phosphors containing two or more luminescence activators. Assuming that the dielectric changes are due to electron trapping, it is possible to derive information regarding the nature of electron traps and in particular their apparent association with the luminescence centres. The results support the contention that the introduction of the activating impurity into phosphors produces trapping states for excited electrons and that each trap forms part of a complex which includes the luminescence centre.

*Eigenfunctions following from Sommerfeld's Polynomial Method*, by A. RUBINOWICZ.

*ABSTRACT.* The eigenfunctions following from Sommerfeld's polynomial method were determined in the general case. They are products of a convergence factor $E$ and a polynomial $P$ given by a hypergeometric series. The form of $E$ depends upon whether $P$ is expressible by the ordinary or the confluent hypergeometric series.

---

## CORRIGENDUM

"The Physical Basis of Life", by J. D. BERNAL (*Proc. Phys. Soc.* B, 1949, **62**, 597).

Page 600, last clause of footnote, viz.*: "and secondly, they must originate and develop out of some pre-existing system, or, in plain English, they must work and they must have got there in the first place" *should occur* in the text immediately after the words "dynamic stability" (line 22).